Instituto de Neurociencias

Consejo Superior de Investigaciones Científicas

Universidad Miguel Hernández

Blood Oxygenated Level Dependent functional Magnetic Resonance Imaging (BOLD fMRI) and Local Field Potentials in the hippocampus of mice lacking IP_3-dependent calcium signalling in astrocytes

Doctoral Thesis presented by:

Pierrick Jego

Director:

Dr.Santiago Canals

Sant Joan d' Alacant, 2014

INSTITUTO DE NEUROCIENCIAS

Consejo Superior de Investigaciones Científicas
Universidad Miguel Hernández
Instituto de Neurociencias

A QUIEN CORRESPONDA,

Dr Santiago Canals Garmendia, Director del Instituto Neurociencias, centro mixto de la Universidad Miguel Hernández (UMH) y la Agencia Estatal Consejo Superior de Investigaciones Científicas (CSIC)

CERTIFICA,

Que la Tesis Doctoral "*Blood Oxygenated Level Dependent functional Magnetic Resonance Imaging (BOLD fMRI) and Local Field Potentials in the hippocampus of mice lacking IP3-dependent calcium signalling in astrocytes*" ha sido realizada por D. Pierrick Jego, Licenciado en Neurociencias, bajo su dirección.

Que ha revisado los contenidos científicos y los aspectos formales del trabajo y da su conformidad para que sea presentada a la Comisión de Doctorado de la Universidad Miguel Hernández.

Para que así conste, y a los efectos oportunos, expide y firma el presente Certificado en San Juan de Alicante a 21 de mayo de 2014.

Fdo. Santiago Canals

[illegible]

INSTITUTO DE NEUROCIENCIAS

Consejo Superior de Investigaciones Científicas
Universidad Miguel Hernández
Instituto de Neurociencias

A QUIEN CORRESPONDA,

Prof. Juan Lerma Gómez, Director del Instituto Neurociencias, centro mixto de la Universidad Miguel Hernández (UMH) y la Agencia Estatal Consejo Superior de Investigaciones Científicas (CSIC)

CERTIFICA,

Que la Tesis Doctoral "*Blood Oxygenated Level Dependent functional Magnetic Resonance Imaging (BOLD fMRI) and Local Field Potentials in the hippocampus of mice lacking IP3-dependent calcium signalling in astrocytes*" ha sido realizada por D. Pierrick Jego, Licenciado en Neurociencias, bajo la dirección del Dr. Santiago Canals Gamoneda, y da su conformidad para que sea presentada a la Comisión de Doctorado de la Universidad Miguel Hernández.

Para que así conste, y a los efectos oportunos, expide y firma el presente Certificado en San Juan de Alicante a 21 de mayo de 2014.

Fdo. Juan Lerma
Director

INSTITUTO DE NEUROCIENCIAS
CSIC

[illegible]
[illegible]
www.in.umh.es

Tel: +34 965 9 9221 (c)
+34 965-919230 (s)
Fax: +34 965 919561

Av. Ramón y Cajal s/n
Campus de San Juan
03550 SAN JUAN DE ALICANTE - ESPAÑA

Acknowledgment

I would like to first thank Santiago Canals, who gave me the opportunity to achieve this PhD, which by the way permitted me to discover an extremely interesting field. I benefit from the opportunity to thanks Alfonso Araque, who gave me my main material for work, and Gertrudis Perea, for her help, her advices and her motivation. I also thank my labmates Carlos, Andrea, Begoña. I want to specially acknowledge Feliberto for his friendship and being a great guide in his country, and Efren for his collaboration, his calm and open minded spirit (and all his "I am sorry").Great acknowledgments will be for Jesus Pacheco that more than of course be my main collaborator there, downstairs, helped me to write, correct and think this project, and made me discover a new passion, climbing. I also would like to thanks Antonio Caller, from the INA, for having made me try rugby and for having taken care of my animals and plants when I couldn't.

I would like to show my gratitude to the coordinators of the SyMBad Marie Curie program: Dr Christophe Mulle and Dr Antonella Caminiti for the organization of this great European PhD program that led me to see and met great researchers in plenty of different fields.

In general, I thank all the friendly people that I met here, from squash players to beer partners passing by dinner preparators. I particularly would like to thanks Zeus and Gabriele, friend/flatmate/squatter, I don't know, and all the other italians…that made me discover the art of eating pasta and pizza, and that olive oil can substitute water, and Wil for sharing beer and sports, since 5 years now. I don't forget my friends from Bordeaux, who with I started neuroscience in extremely serious conditions: Mehdi, Jojo, Julien, Till and Wil again, the "external ones, world citizens" that made me change my mind when necessary Hugo, Xavier, Max, and Matthieu, my brother.

I want to finish my acknowledgements with what I think to be the most important, my parents, that always did the best they could for me, helped me by facts and words, and showed all their comprehension when I was still a unruly young man. Of course, for finish, I don't want to "thank" because the word is too weak, but all my thoughts go to Letizia, for the person she is, and the person she made of me. I came here alone and I am now leaving with two new families, hers and ours. I am proud to bring her back with me (with a little "something"…).

Index

Abstract *13*

Resumen *15*

1 - Preface **17**

2 - Abbreviations **21**

3 - Introduction **25**

3.1 - Neurovascular coupling 29

Cellular and molecular origins of neurovascular coupling 33

Local Field Potentials and neurovascular coupling 34

Spatial coupling between neural activity and the vascular response 36

Temporal coupling between neural activity and the vascular response 36

Amplitude coupling between neural activity and the vascular response 37

3.2 - Functional Magnetic Resonance Imaging and Blood Oxygenated Level Dependent signal 37

Tissue contrast and relaxation 39

Blood Oxygenated Level Dependent contrast 39

The Positive BOLD response 42

Metabolic attenuation of the metabolic BOLD response 44

fMRI acquisition 45

3.3 - Astrocytes 45

General characteristics 45

Astrocytes location and neurovascular coupling 47

Astrocytic calcium signaling 48

Astrocytic control of blood flow 51

In vitro/in vivo 52

3.4 - Summary 52

4 - Aims **55**

5 - Material and Methods **59**

5.1 - Animals 61

IP_3R2 KO mice generation 61

5.2 - Anesthesia 62

5.3 - Surgery 63
Electrodes positioning 65
5.4 - Local Field Potentials recordings 66
Population Spike and Excitatory Post Synaptic Potential 66
Trisynaptic loop of the hippocampus 67
Intensity/Responses - Input / Output 68
5.5 - Set up of the fMRI stimulation protocols 69
Brief and long 10 hertz train stimulation protocols 69
fMRI 70
5.6 - Behavioral tests 72
Open Field 72
Novel Object Recognition 72
5.7 - Statistical analysis 73
6 - Results **75**
6.1 - Behavioral results 77
Open field 77
Novel Object Recognition 78
6.2 - Set up of anesthesia and stimulation protocol 79
Anesthesia 79
fMRI protocols 81
6.3 - Electrophysiology and BOLD fMRI signals 83
Electrophysiology 83
Brief stimulation of the PP and initiation of the BOLD signal 84
Long stimulation of the PP and maintenance of the BOLD signal 89
Local Field Potentials recording in the CA1 region of the hippocampus 93
7 - Discussion **97**
7.1 - fMRI set up 99
7.2 - Neurovascular coupling 100
7.3 - Electrophysiology 102
7.4 - Behavior 105
7.5 - Perspectives and conclusion 105
8 – Conclusions (y conclusiones) **107 - 111**
9 - Bibliography **115**
10 - Annex **127**

Abstract

Non-invasive brain imaging techniques, as functional magnetic resonance imaging (fMRI), allow us to study cognitive functions in humans, but at the same time, they are emerging as powerful diagnostic tools for neurological and psychiatric disorders. Despite their importance, the physiological and cellular mechanisms underlying fMRI signal generation are not well understood. Astrocytes are well known since Santiago Ramón y Cajal's work to be located in tight contact between neurons and brain blood vessels and due to its strategic positioning they were consider as putative transductors of neuronal activity into vascular responses. With the concept of the tripartite synapse at the end of the 90's a renewed interest emerged on understanding the contribution of astrocytes to neurotransmission and synaptic plasticity (Araque et al.,1999). Proportionally less attention has received its role in regulating vascular responses to neuronal activity, the so called neuro-vascular coupling. In 2003, Zonta et al., showed in vitro that after synaptic activation astrocytes uptake extracellular glutamate initiating calcium signaling cascade that finally translated into arteriole dilation. In 2006, Metea and Newman showed that an inositol-1,4,5-triphosphate (IP_3) injection into astrocytes, that mobilize calcium from intracellular stores, is enough to dilate artificially constricted vessels in retina slices. These findings, together with previous evidence demonstrating the important role of IP_3-dependent calcium signaling in astrocytes for neuronal transmission and plasticity, supported the hypothesis that astrocytes, indeed, were playing a key role in neurovascular coupling. An important caveat of these studies, however, is that they were mainly performed in vitro, experimental conditions in which the energy metabolic substrates are provided ad libitum in the artificial cerebrospinal fluid and the vascular system is devoid of pressure and function. Consequently, it appears necessary to study neuro-glio-vascular coupling in vivo. To this end, genetically modified mice for the subtype 2 of the IP_3 receptor (specific for astrocytes) have been created.

We used fMRI and Blood Oxygenated Level Dependent (BOLD) signal, which permits to visualize neuronal activation through local hyperemia, during electrical Perforant Path stimulation. In parallel, we measure Local Field Potential within the hippocampus during the very same stimulation. We found that IP_3 dependent calcium waves in astrocytes are not necessary to neurovascular coupling, nor to initiate the vasodilation neither to maintain it. More surprisingly, we found that synaptic transmission in IP_3R2 KO mice hippocampus is slightly weaken during a long stimulation. These results suggest that neurovascular coupling

is mediated by a mechanism independent of astrocyte internal calcium stores *in vivo*. These same calcium stores probably play a role in synaptic strength, maybe by decreasing uptake and/or release of neuro or gliotransmitters.

Key words: neurovascular coupling, astrocytes, fMRI, Inositol triphosphate, Local Field Potentials

Resumen

Técnicas de imagen cerebral no invasivas, como la resonancia magnética funcional (fMRI), nos permiten estudiar las funciones cognitivas en los seres humanos, pero al mismo tiempo, están surgiendo como potentes herramientas de diagnóstico para los trastornos neurológicos y psiquiátricos. A pesar de su importancia, los mecanismos fisiológicos y celulares que subyacen a la generación de señales de resonancia magnética funcional no se conocen bien. Los astrocitos son bien conocidos desde la obra de Santiago Ramón y Cajal. Se encuentran en estrecho contacto entre las neuronas y los vasos sanguíneos del cerebro y debido a su posición estratégica se consideran como transductores putativos de la actividad neuronal en las respuestas vasculares. Con el concepto de la sinapsis tripartita al final de la década de los 90, un renovado interés surgido en la comprensión de la contribución de los astrocitos con la neurotransmisión y la plasticidad sináptica (Araque et al., 1999). Proporcionalmente menos atención ha recibido su papel en la regulación de las respuestas vasculares a la actividad neuronal, llamado "acoplamiento neurovascular". En 2003, Zonta et al., mostró *in vitro* que después de la activación sináptica los astrocitos captaban el glutamato extracelular iniciando cascada de señalización de calcio que finalmente se tradujo en la dilatación de las arteriolas. En 2006, Metea y Newman mostraron que una inyección de inositol-1,4,5- trifosfato (IP_3) la en los astrocitos , que moviliza las reservas de calcio intracelular, es suficiente para dilatar los vasos artificialmente estrechados en secciones de retina. Estos hallazgos, junto con la evidencia previa que demuestra el importante papel de las olas de calcio IP_3-dependientes en los astrocitos para la transmisión neuronal y la plasticidad, apoyaron la hipótesis de que los astrocitos, de hecho, estaban jugando un papel clave en el acoplamiento neurovascular. Una advertencia importante de estos estudios, sin embargo, es que se llevaron a cabo principalmente in vitro, las condiciones experimentales en las que los sustratos metabólicos de energía se proporcionaron *ad libitum* en el líquido cefalorraquídeo artificial y el sistema vascular es desprovisto de la presión. Por tanto, parece necesario estudiar el acoplamiento neuro-glio-vascular *in vivo*. Para este fin, ratones modificado genéticamente para el subtipo 2 del receptor de IP_3 (específico para astrocitos) han sido creados.

Se utilizó fMRI y la sangre oxigenada Nivel de señal dependiente (BOLD), que permite visualizar la activación neuronal a través de la hiperemia local durante la estimulación eléctrica de la Vía Perforante. En paralelo, se mide Potenciales Campos Locales en el

hipocampo durante el mismo estímulo. Se encontró que el IP_3 ondas de calcio dependientes en los astrocitos no son necesarios para el acoplamiento neurovascular , ni para iniciar la vasodilatación ni para mantenerla. Más sorprendentemente, se encontró que la transmisión sináptica en el hipocampo ratones KO IP_3R2 se debilita ligeramente durante un largo estimulación. Estos resultados sugieren que el acoplamiento neurovascular está mediada por un mecanismo independiente de astrocitos tiendas de calcio interno in vivo. Estas mismas reservas de calcio probablemente juegan un papel en la fuerza sináptica, tal vez por la disminución de la absorción y / o liberación de neuro o gliotransmisores .

Palabras clave: acoplamiento neurovascular, astrocitos, fMRI, inositol trifosfato, Potenciales de campo locales

1 - Preface

This work will be presented under the form of a publication (*in preparation*) for Brief communication in Journal of Cerebral Blood Flow and Metabolism:

Functional MRI in mice lacking IP3 dependent calcium signalling in astrocytes

Pierrick Jego[a], Jesús Pacheco [a], Alfonso Araque, and Santiago Canals[a,*]

[a]Instituto de Neurociencias, Consejo Superior de Investigaciones Científicas & Universidad Miguel Hernández, Sant Joan d'Alacant 03550, Spain.

Corresponding author: Santiago Canals (scanals@umh.es)
Dr. Santiago Canals
Instituto de Neurociencias CSIC-UMH

Acknowledgements: We are grateful to Begoña Fernández for excellent technical assistance. Research at S.C. lab is supported by grants from the Spanish MINECO (BFU2012-39958 and PIM2010ERN-00679 as part of the Era-Net NEURON TRANSALC project). PJ has been supported by the "Symbad" Marie Curie ITN program.

Running title: Functional MRI in mice lacking IP3 dependent calcium signalling in astrocytes

2 - Abbreviations

AA: arachidonic acid

AP: Antero Posterior

ATP: Adenosine Tri Phosphate

BOLD: Blood Oxygenated Level dependent

CA, **CA3**: AMON CORN 1 and 3 (of the hippocampus)

Ca^{2+}(i): intracellular calcium

CBF: Cerebral Blood Flow

CBV: Cerebral Blood Volume

CMRO2: Cerebral Metabolic Rate of Oxygen

CNS: Central Nervous System

CO2: Carbon dioxyde

COX: Cyclo-oxygenase

DAG: diacyl glycerol

DG: Dentate Gyrus

dHb: desoxyHaemoglobine

DI: Discrimination Index

DV: Dorso Ventral

EC: Entorhinal Cortex

EET: epoxyeicosatrienoic acid

EPSP: Excitatory Post synaptic Potential

fMRI: functional Magnetic Resonance Imaging

GE-EPI: Gradient Echo Echo Planar Imaging

I/O: Input / Output

IP3: Inositol 1,4,5-trisphosphate

IP3R2: IP3 receptor 2nd subtype

K+: Potassium

KO: Knock Out

LFP: Local Field Potential

LTP: Long Term Potentiation

ME: Multi Electrode

mGluR: metabotropic glutamate receptor

ML: Medio Lateral

MR: Magnetic Resonance

NMR: Nuclear Magnetic Resonance

NO: Nitric Oxyde

NOR: Novel Object Recognition

OF: Open Field

PET: Positon Emission Tomography

PIP2: phosphatidylinositol 4,5-bisphosphate

PLA and PLC: phospholipase A and phospholipase C

PP: Perforant Pathway

PS: Population Spike

TE: Echo time

TR: Relaxation Time

3 - Introduction

At the end of the nineteenth century, the first evidence in support of coordination between brain work and energy supply was provided. Mosso, by measuring brain pulsations over the right prefrontal cortex in a subject with abnormally thinned skull, reported increased pulsations when the subject performed a mathematical task. In 1890, Sherrington, directly measuring blood variations applying a self-made device (Figure 1) on the brain surface, showed that stimulation of the sensory nerves, in the medulla oblongata, produced an increase in brain blood pressure (Roy & Sherrington 1890).

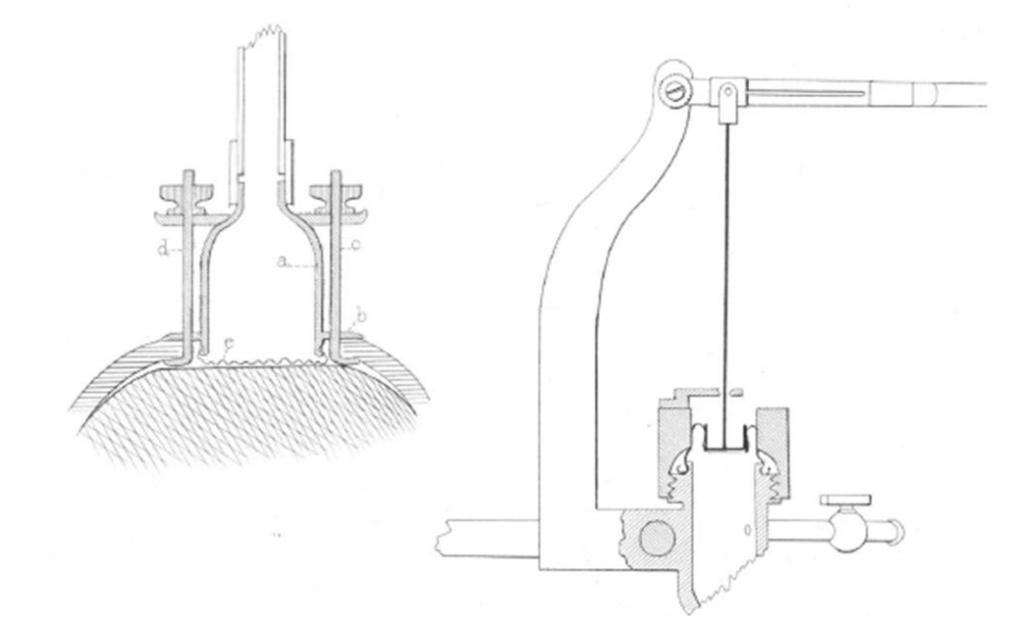

Figure 1: **The shape of the capsule from the selfmade device, and its fixation.**
Adapted from "Roy and Sherrington 1890: *ON THE REGULATION OF THE BLOOD-SUPPLY OF THE BRAIN*".

This hemodynamic response that accompanies brain activation was later found to also exist in pathological situations such as ischemia (Ames et al 1968). The vascular response was interpreted as a compensatory mechanism that fuels the brain either during increased energy expenditure or during restriction of metabolic substrate delivery. This phenomenon has been called neurovascular coupling, defining the correlation between neuronal activity and blood vessel diameter modulation: in response to performing physical activities, and in case of any dysfunction, the body must adjust its blood flow in order to deliver nutrients such as oxygen and glucose to stressed tissues and allow them to function (Iadecola 2004, Iadecola & Gorelick 2004). Since higher processes in the brain occur almost constantly, cerebral blood

flow (CBF) is essential for the maintenance of neurons, astrocytes, and other cells of the brain (Iadecola et al 1990, Iadecola & Reis 1990).

Groups of neurons (and their associated astrocytes) are functionally coupled to smooth muscle cells and endothelial cells of the capillaries, thereby regulating their blood supply. These functional units are called neurovascular units (Figure 2, (Harder et al 2002)).

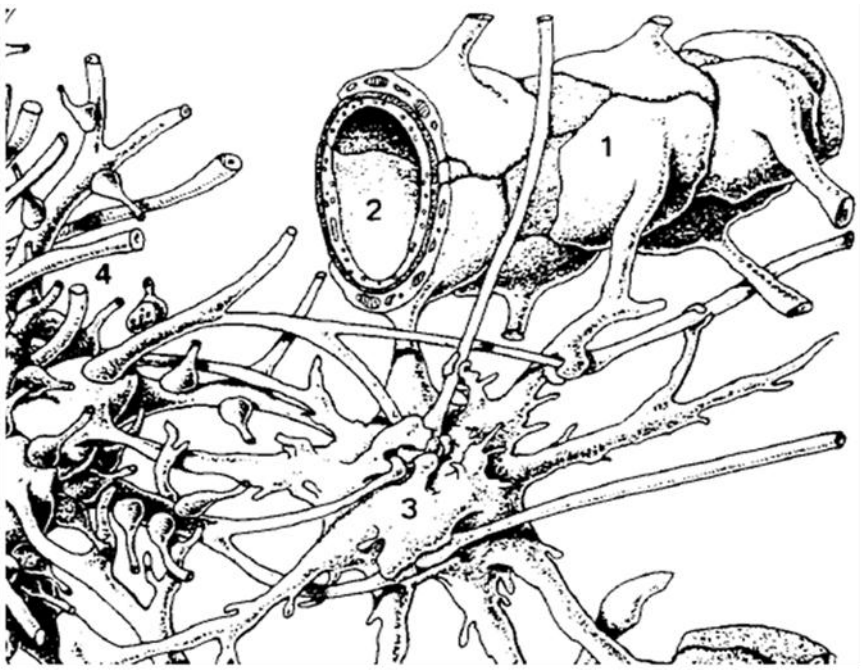

Figure 2: Astrocytic foot processes (adapted from Kandel « Principles of neural science»). Astrocytes (3) are juxtaposed between neurons (4) and cerebral arterioles (2). Astrocytic foot processes (1) contact and completely envelope arterioles in the cerebral circulation.

All along the 20th century, the development of technologies, particularly in fields such as physics or chemistry, led to the creation of brain imaging techniques which revolutionized neuroscience. For the first time, it allowed measurements of human brain function using vascular signals, and thus, indirect measure of neuronal activity. Functional Magnetic Resonance Imaging (fMRI), based on the magnetic properties of hemoglobin, enabled to visualize neuronal activity in live patients or animals, in a non-intrusive way. However, although regularly used in human medicine and neuroscience research, the molecular and physiological mechanisms underlying these variations of hemodynamic responses is still unclear and its origin unknown.

3.1 - Neurovascular coupling

Neurovascular coupling refers to the relationship between local neural activity and subsequent changes in CBF. The magnitude and spatial location of blood flow changes are tightly linked to changes in neural activity through a hypothetical complex sequence of coordinated events involving neurons, glia, and vascular cells. Many vascular-based functional brain imaging techniques, such as fMRI, rely on this coupling to infer changes in neural activity. However, despite the spatio-temporal correlation between neuronal activity and vascular responses, the precise quantitative relation between both magnitudes is not fully understood.

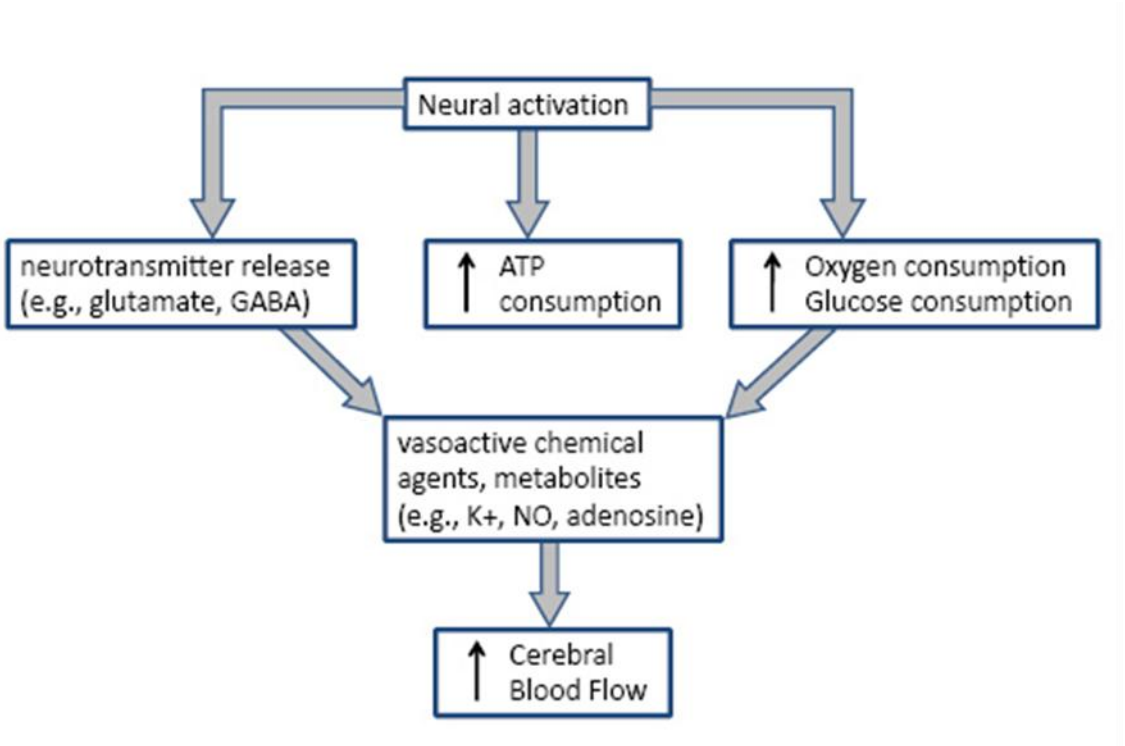

Figure 3: Neural basis of Neurovascular coupling.

Neural activation in a defined brain region leads to neurotransmitter releases in parallel to an increase in ATP, oxygen and glucose consumption in this region. Consequently, through still unclear pathways and mechanisms, an increase of CBF is observed. The phenomenon is called neurovascular coupling.

Brain activation is accompanied by a complex sequence of cellular, metabolic, and vascular processes partially developed below. Although the mechanisms linking these events are still under investigation, the basic sequence can be summarized as shown in Figure 3. To summarize, various cellular processes of neurons, such as the restoration of ionic gradients and neurotransmitter recycling or firing of action potentials, require energy in the form of adenosine triphosphate (ATP). ATP is synthesized first by glycolysis, which is anaerobic and produces a small amount of ATP, and then by oxidative glucose metabolism, which requires oxygen and produces a large amount of ATP. In the brain, about 90% of glucose is metabolized by the latter mechanism, i.e., aerobically. Cerebral metabolism thus depends on a constant supply of both glucose and oxygen. A continuous supply of these two energy substrates is maintained by CBF, which delivers glucose and oxygen to neural tissue through the complex web of blood vessels in the brain's vascular system (Figure 4). The whole brain is irrigated by a large and complex vasculature. Blood flow to the brain is provided by extra cerebral and intracerebral arteries and arterioles. Large arteries supply branching pial arterioles that dive deeper into the brain. In general, extracerebral vessels are innervated by peripheral nerves, while intracerebral microvessels are regulated by local interneurons and central neuronal terminals (Rancillac et al 2006). Arteries and arterioles consist of an endothelial cell layer, smooth muscle cells. The penetrating arteriole is surrounded by an invagination of the pia mater, which forms a perivascular space (Virchow–Robin space). When the basement membranes of the pia and the penetrating arteriole coalesce, the space disappears and the vessel becomes a capillary. Large arteries divide in thinner superficial and perforating arterioles providing irrigation to both surface and depth of cerebral tissues, and then diving through the meninges as capillaries ensuring vascularization to the whole brain. Moreover, the complex functions of the brain are linked with highly sensitive electrochemical and biochemical processes that can occur only in a homeostatic medium free from any variations. In addition, as a central command for the whole body, the brain needs to be kept away from toxins or other pathogenic agents. On this purpose, the circuitry of cerebral blood vessels in vertebrates presents, by comparison with peripheral vessels, large structural and functional differences (Bundgaard & Abbott 2008). It results in a clear separation between the brain and its surrounding medium: the blood-brain barrier. This barrier consists of endothelial cells, surrounding vessels, tightly attached by gap junctions, and therefore isolates the brain from the external environment. This highly impermeable membrane is also composed by two other types of cell, pericytes and astrocytes, constituting altogether the so-called blood brain barrier, acting as a protective filter between blood and neurons. Pericytes function as

contractile cells that wrap around the endothelium of capillaries. Astrocytes as their name suggests, are characteristically star-shaped and are the most abundant cell of the human brain performing many functions.

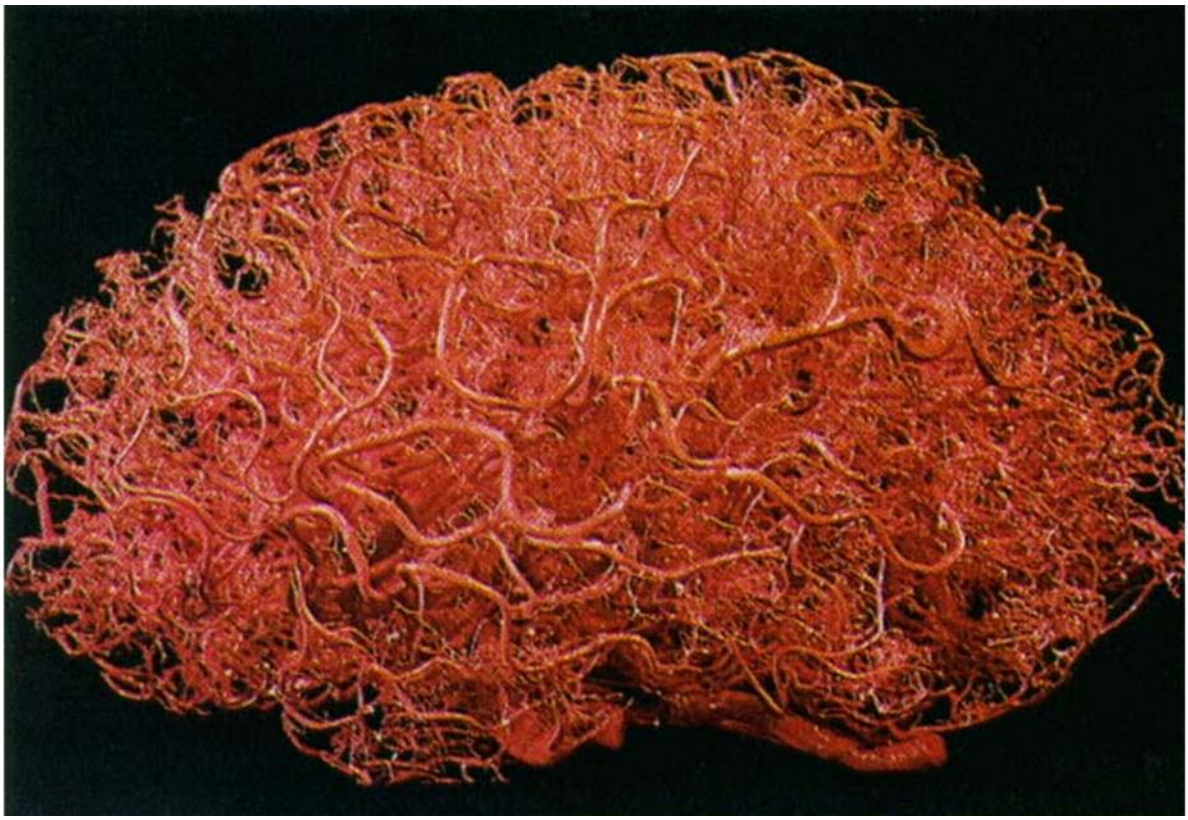

Figure 4: Complex blood irrigation in human brain.

Blood flow to the brain is provided by extra cerebral and intracerebral arterioles and capillaries. Large arteries divide in branching pial arterioles, and then capillaries, that dive deeper into the brain to supply neurons and glial cells in energy substrates.

Accordingly, during neural activity, increases in oxygen and glucose consumption are followed by an increase in CBF. Whereas the fractional increases in CBF and glucose consumption are similar in magnitude, oxygen consumption increases much less than CBF, leading to a clear increase in the amount of oxygen present in the blood and tissue. This oversupply of oxygen due to the mismatch between CBF and oxygen consumption is the basis of blood-oxygenation level dependent (BOLD) fMRI, which detects alterations in levels of deoxygenated hemoglobin and cerebral blood volume (CBV) (Figure 5). While it is

view supports a feed-back mechanism where the byproducts due to energy uses act as signaling molecules to increase blood supply and restore energy buffers. But, although intuitive, the idea that energy supply (i.e., local blood flow) is controlled directly by energy demand (i.e., metabolic activity) appears to be oversimplified. In a more recent view, an alternative possibility is that local blood flow is directly controlled by a feed-forward mechanism involving neuronal signaling via neurotransmitters (Attwell & Iadecola 2002, Lauritzen 2005). A lot of recent data, mainly from *in-vitro* preparations, go in favor of the feed-forward model (Attwell et al 2010, Petzold & Murthy 2011) (Figure 6). Both models, however, are probably non-exclusive and coexist in specific physiological states (Moreno et al 2013).

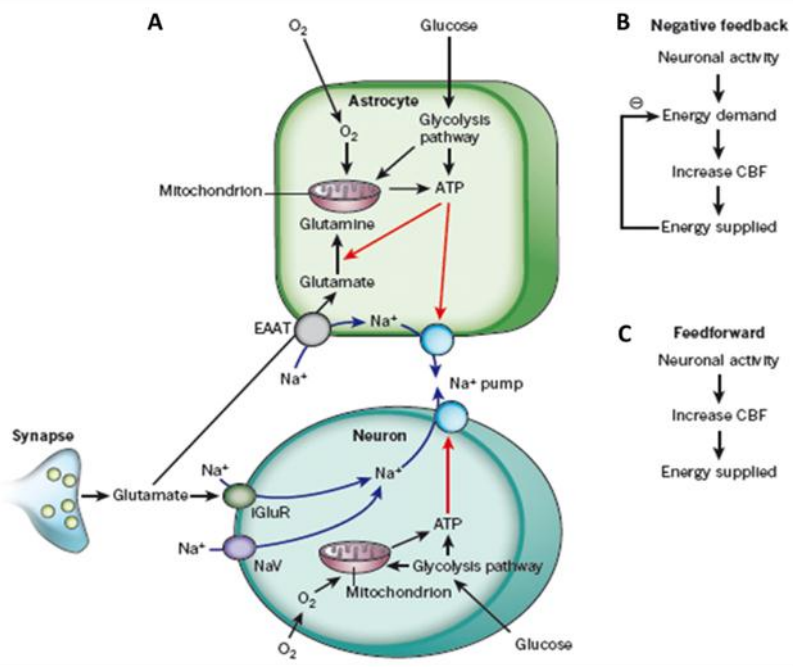

Figure 6: Energy supply, usage and blood flow regulation in the brain.

A, ATP is generated from glycolysis and mitochondrial oxidative phosphorylation in neurons and glia. ATP is mainly consumed (red arrows) by ion pumping in neurons, to maintain the ion gradients underlying synaptic and action potentials, following Na+ entry (blue arrows) through ionotropic glutamate receptors (iGluR) and voltage-gated Na+ channels (NaV). It is also used in glia for Na+-coupled neurotransmitter uptake by xcitatory amino acid transporters (EAAT) and for metabolic processing (shown for conversion of glutamate to glutamine), and on maintaining the cells' resting potentials. B, The negative-feedback control hypothesis for vascular energy supply, in which a fall in energy level induces an increased

CBF. C, The feedforward regulation hypothesis for vascular energy supply (from Attwell et al., 2010).

Cellular and molecular origins of neurovascular coupling

Recent evidences for this mechanism suggest that astrocytes may play an important role in linking neurotransmitter activity to vascular response (Harder et al 1998, Pellerin & Magistretti 2004). Astrocytes are a critical component for glutamate recycling. A cascade of chemical events within the astrocyte may then link the rate of glutamate cycling to the production of vasoactive chemical agents (Raichle & Mintun 2006). In this view, neurovascular coupling is mediated by neuronal signaling mechanisms via glial pathways, rather than by mechanisms that sense energy consumption (feedforward theory). In addition, neurovascular coupling might be mediated by diffusion of products of neuronal activity without the involvement of glial cells (Attwell & Iadecola 2002). In the cerebral cortex, dopamine (Krimer et al 1998), noradrenaline (Raichle et al 1975) and serotonin (Cohen et al 1996) are present in neurons innervating microvessels and produce vasoconstriction. Finally, there is evidence that direct neuronal innervation of smooth muscle cells can also control blood flow (Hamel 2004, Iadecola 2004, Iadecola & Gorelick 2004). Ultimately, it is likely that multiple mechanisms, both feedforward and feedback, function to mediate neurovascular coupling (Attwell & Iadecola 2002, Lauritzen 2005, Moreno et al 2013, Uludag et al 2004). Finally, it has also been proposed that the disproportional increase in glucose use comparing to oxygen consumption in fMRI is due to the stimulation of anaerobic glycolysis in astrocytes, which serves as a fast energy source for the astrocytic uptake of glutamate and its enzymatic conversion to glutamine and provides lactate as a preferred metabolic substrate for neurons (Magistretti & Pellerin 1999).

It is important to note that neurovascular coupling must provide for continuous brain function which requires metabolic nutrients and the elimination of waste products such as CO2 and excessive heat. The fact that this process occurs on a fine spatio-temporal scale provides the basis for many powerful neuroimaging techniques. Although neural activity and blood flow are closely coupled, it is important to understand which aspects of neural activity drive the vascular response. Synaptic transmission and action potentials represent two different aspects of neural activity, each with their own molecular basis and energy requirements. Synaptic activity is reflected in the Local Field Potential (LFP) and can be considered as the input to the neuron, while action potentials (spikes) are the output signal. Altogether, they permit communication between neurons.

Local Field Potentials and neurovascular coupling

In many cases, LFPs and spikes are highly correlated and will therefore both correlate with the vascular response. This is likely to be the case in most studies of bottom-up sensory processing where both efferent and afferent activity increase proportionally (Logothetis & Wandell 2004). It has been shown that functional hyperemia is highly correlated with LFPs (Canals et al 2009, Canals et al 2008, Logothetis et al 2001, Mathiesen et al 1998, Mathiesen et al 2000, Thomsen et al 2004).

However, there are many situations where spikes and subthreshold responses are dissociated and several experimental investigations have noted dissociations between LFPs and spikes. For instance, higher level brain areas may be subject to feedback and neuromodulatory signals that alter subthreshold membrane potential but do not elicit spikes. Evidence for this is as follows:

• In cerebellar cortex, electrical stimulation of parallel fibers inhibits Purkinje cell spiking, but increases overall synaptic activity. LFPs and CBF both increased, whereas spiking activity was eliminated (Mathiesen et al 1998).

• Adaptation to sustained visual stimulation decreases spike rate in many V1 neurons, while LFP and BOLD responses remain elevated (Logothetis et al 2001).

• Visual stimuli presented at high flicker rates elicit LFP but not spiking activity in primary visual cortex. Strong coupling between LFP and vascular responses was observed even in the absence of spikes (Viswanathan & Freeman 2007).

• Attentional modulation of activity in V1 is observed with fMRI (Gandhi et al 1999), but not with neurophysiological recordings of spike activity. The vascular response observed with fMRI may therefore reflect increased subthreshold depolarizations that do not elicit spikes, but do drive the vascular response (Yoshor et al 2007).

• Injection of a serotonin agonist in V1 reduced multi-unit spiking activity with no effect on LFP or BOLD (Rauch et al 2008).

In summary, existing data suggest that when afferent and efferent activities are correlated, the vascular response can be considered to reflect both spike rate and synaptic activity. However, when the two are dissociated, the vascular response more closely reflects synaptic activity and may not serve as an indicator of spike rate in the local neural population.

The use of vascular responses to infer neural activity requires an understanding of how these two signals are coupled in space (volume of tissue engaged in the process), time (delay of activation), and amplitude (correlation between intensity of neural activation and vascular changes).

Spatial coupling between neural activity and the vascular response

An important question for the application of neuroimaging techniques is to know how well-localized the vascular response is when a limited population of neurons is activated. Spatial resolution of the vascular response depends in large part on what component of the vascular system is considered. The dense network of capillaries penetrating the gray matter affords the highest spatial resolution, with an inter-vessel distance of ~25um, while the larger compartments of arteries and veins are much sparser and less confined to individual functional modules (Pawlik et al 1981). Thus, it has been shown, using different imaging modalities, that maps can be obtained by enhancing signal from the capillary component while minimizing contributions from large vessels (Vanzetta et al 2004, Yacoub et al 2007). There are a few reports of a submillimeter vascular point spread function (Duong et al 2001, Harel et al 2006), while other estimates are on the order of 1-2mm (Thompson et al 2005), 2mm (Shmuel et al 2007), or 3.5mm (Parkes et al 2005). Overall, this estimate depends on the magnetic field (e.g., 1.5 Tesla vs. 7 Tesla), technique (spin echo vs. gradient echo BOLD fMRI), species (e.g., cat vs. human), and brain region (e.g., thalamus vs. cortex). Therefore, most successful high resolution studies have relied on a differential mapping approach, whereby two orthogonal conditions are compared in order to suppress spatially non-specific components of the signal (Grinvald et al 2000). Use of the early metabolic response (i.e., "initial dip") may provide improved localization and the ability to generate single condition functional maps (Frostig et al 1990), but practical use of the initial dip for functional mapping is severely limited by poor Signal-to-Noise Ratio and brief duration. Continued optimization of imaging techniques to selectively enhance capillary CBF responses may permit routine acquisition of single condition map at high spatial resolution.

Temporal coupling between neural activity and the vascular response

A severe experimental limitation imposed by neurovascular coupling is the lack of temporal information in the vascular response. The CBF response to a brief period of neural activation is typically delayed by 2-3 seconds and peaks 4-6 seconds after the neural response.

Because of this temporal filter, fast modulation of neural activity is unlikely to be reflected in the vascular response. The delay of CBF relative to neuronal activity is probably not due to slow reaction of smooth muscle cells. Instead, the delay is probably related to the slow diffusion and uptake of neurovascular mediators. In spite of this slow process, several studies suggest that the temporal fidelity of the vascular response (i.e., how accurately it reflects neuronal timing) may be fine enough to encode temporal differences in neuronal activity on the order of seconds (Kellman et al 2003).

Amplitude coupling between neural activity and the vascular response

In general, fMRI studies are based on amplitude changes. The relationship between neural activity and vascular response appears to be largely linear, making the interpretation of neuroimaging studies much easier, at least for stimulus durations larger than 4s (Li & Freeman 2007, Logothetis et al 2001). However, various nonlinearities have been reported: for instance, neural responses below certain amplitude may not evoke a CBF response, or neural responses may saturate, while vascular responses continue to increase (Sheth et al 2004). Nevertheless, in most of cases, there is a large range over which neural and vascular responses maintain a linear relationship.

In conclusion, the cellular mechanisms of neurovascular coupling have been proposed and continue to be investigated (Harder et al 1998, Harder et al 2000, Harder et al 2002, Metea & Newman 2006). On one hand, the phenomenon responsible for hyperemia is still a matter of controversy and could be a mix between the so called feed forward and feedback theories. On the other hand, hyperemia can be triggered by different mechanisms that can be envisaged to work partly in parallel in a dependent manner as well as independently. In any case, as it will be more developed below, astrocytes seem to play a crucial role in neurovascular coupling. Different tools such as a pharmacological approach, KO mice and so on are available to understand hyperemia. Despite some spatial and temporal limits explained above, the applications of those tools in experiments combining fMRI and electrophysiological recordings of brain activity have the potential to uncover the physiological underpinning of the BOLD signal.

3.2 - Functional Magnetic Resonance Imaging and Blood Oxygenated Level Dependent signal

The blood-oxygen-level-dependent (BOLD) magnetic resonance signal used in functional imaging of the brain reflects the loss of oxygen from haemoglobin, causing its iron to become paramagnetic, which influences the magnetic field experienced by protons in surrounding water molecules (Ogawa et al 1990). It is based on principles of Nuclear Magnetic Resonance (NMR). NMR was first described and measured in molecular beams by Isidor Rabi in 1938, being awarded by the Nobel Prize in physics in 1944 for his work. In 1946, working independently, Felix Bloch and Edward Mills Purcell expanded the technique for use on liquids and solids, for which they shared the Nobel Prize in Physics in 1952.
Nevertheless, it was not until 1971 when Raymond Damadian observed that the relaxation times of healthy and tumoral tissue were different. From that moment, the use of Magnetic Resonance (MR) to study diseases was considered. Like many developments in science, these early suggestions were considered esoteric and it took almost a decade before industry recognized their diagnostic potential. In 1973, Paul Lauterbur use back projection techniques similar to those used in computed tomography to generate the first *in-vitro* MR image. In 1975, Richard Ernst proposed the use of phase and frequency phase encoding and the Fourier transform to generate MR images. This technique is the actual basis for Magnetic Resonance Imaging (MRI). For that discovery, he received the Nobel Prize in Chemistry in 1991. Over the last two decades, MRI has matured into a versatile diagnostic imaging modality within radiology, and is accepted as the gold-standard in several areas by virtue of its exquisite anatomical depiction of soft tissue. Furthermore, in 2003 Sir Peter Mansfield and Paul Lauterbur were awarded by the Nobel Prize in Medicine and Physiology for their development of the Echo-Planar Imaging (EPI), setting the basis of the actual fMRI.

The term magnetic resonance (MR) is shorthand for nuclear magnetic resonance (NMR). The word “nuclear” is frequently dropped, particularly in medical applications, because of its inappropriate connotations of high-energy processes such as fission (splitting of nuclei) and radioactivity (decay of unstable nuclei). MR is unrelated to either of these processes, and is actually a very low-energy phenomenon, involving the absorption and emission of radio frequency waves. At the intensities used in MR scanners, there is no study reporting any risk to humans or animals. MRI depicts a series of characteristics that make this

technique very popular for both clinic and research applications: noninvasiveness, the use of non-ionizing radiation, clinical availability etc. A major strength of MRI is its sensitivity to a plethora of physiological factors. This makes MRI extraordinarily versatile, and provides a fertile ground for innovative academic research into novel applications. It is important to emphasize the ability to provide information regarding the "functional status" of tissue by using endogenous contrast mechanisms. Also, it is possible to combine MRI with the use exogenous contrast material to extract information regarding the spatial distribution, tissue function, metabolic activity, or monitoring gene expression.

Tissue contrast and relaxation

In NMR, the process called relaxation refers to nuclei that return to the thermodynamic equilibrium state after being excited in the magnet.

This process is known as T1 or "longitudinal magnetic" relaxation. T1 refers to the mean time for an individual nucleus to return to its thermal equilibrium state of the spins. Once the nuclear spin population is relaxed, it can be probed again, since it is in the initial, equilibrium (mixed) state. This process involved the emission of energy. The processing nuclei can also fall out of alignment with each other (returning the net magnetization vector to a non-processing field) and stop producing a signal. This is called T2 or transverse relaxation. This process does not involve the energy interchange. Because of the difference in the actual relaxation mechanisms involved (for example, inter-molecular vs. intra-molecular magnetic dipole-dipole interactions), T1 is usually longer than T2. In practice, the value of T2*, which is the actually observed decay time of the observed NMR signal, or free induction decay, also depends on the static magnetic field inhomogeneity, which is quite significant. The origin of these inhomogeneities could be due to intrinsic defects of the magnet field or distortion in the external magnet field originated by the tissue magnetic susceptibility. Both T1 and T2 depend on the rate of molecular motions as well as the gyromagnetic ratios of both the resonating and their strongly interacting, next-neighbor nuclei that are not at resonance.

Different tissues in the head have different NMR relaxation times. It is possible to exploit these differences in order to provide image contrast that is derived from differences in T1, T2 or T2*. These are known as T1-weighted, T2-weighted and T2*-weighted images, respectively. Relaxation time contrast is most easily achieved by altering two of the fundamental sequence timing parameters: the repeat time between subsequent radiofrequency excitation pulses (TR), and the time to echo following the excitation pulse (TE).

The most basic underlying source of image contrast in MRI is spin density contrast. For this contrast the image intensity is simply proportional to the local number density of

spins contributing signal. Since almost all human MRI scans map the distribution of the single proton nucleus of hydrogen, this is often referred to as proton density contrast. In biomedical imaging, most of the proton signal comes from water which is bound in the tissue (Figure 7).

Blood Oxygenation Level Dependent (BOLD) contrast

The blood oxygen level-dependent (BOLD) response is a sensitive indicator of where neural activity has acutely changed in response to a transient stimulus. Activation of neurons and establishment of the ion potentials in the cells of the brain all require a supply of energy**,** supplied in the form of ATP generated in the mitochondria. ATP formation via glucose consumption requires oxygen, provided by blood perfusing the tissue.

Water content of various tissues in the human body

Tissue	Water content (%)
Brain Grey/White average	77,4
Cerebro Spinal Fluid	97,5
Skeletal muscle	79,2
Heart	80
Bone	12,2

Figure 7: Water content in human body. Adapted from Mansfield P. (1988).

Oxygen is not very soluble in blood so it is transported bound to the large iron containing molecule, haemoglobin. The presence of the iron atoms in the molecule mean that haemoglobin has magnetic properties, which in analogy to the contrast agents mentioned above, reduce the relaxation time of the blood. The location of the oxygen binding sites on haemoglobin mean that, when oxygen is bound, the molecule alters from being paramagnetic (having a significant magnetic effect on its environment) to being diamagnetic (having little effect). Such oxygen dependence makes haemoglobin a sensitive magnetic marker to the level of blood oxygenation and consequently to neuronal activity. If the oxygenation level of the blood decreases (or more specifically, if the level of deoxyhaemoglobin increases), it causes the T2* of blood, and to a lesser extent the T2 of blood, to decrease also, resulting in slightly

lower signal in a T2*-weighted image. Conversely, if the blood oxygenation level rises then the T2* value increases, resulting in higher signal in a T2*-weighted image. One important feature of the BOLD effect is that the signal seen in MR images upon neuronal activation is a positive signal change, representing a decrease in the concentration of deoxyhaemoglobin.

This rather indirect coupling between neuronal activity and BOLD signal change in MRI has several significant features. First, since the signal change observed is as a result of a perfusion increase that is local to the tissue of interest but is generally on a larger spatial scale than the electrical activity, the site of the activation on an image may be somewhat larger than and distant from the site of the neural activity.

Second, the delay in the onset of signal change as the blood flow and blood volume increase mean that, although it is possible to obtain MR images as fast as 10 frames per second, the actual temporal resolution of the BOLD haemodynamic response is somewhat poorer. For example, a brief burst of neural activity lasting only tens of milliseconds will result in a BOLD signal change that peaks after about 6 seconds, and does not return to baseline completely for approximately 12 seconds. That said, by approximating the BOLD signal change relative to the neuronal activity as a linear response function, deconvolution methods have been able to distinguish events that are as short as several hundred milliseconds apart.

The typical fMRI BOLD response is schematically divided into three phases, as shown in figure 8. First, immediately after electrical activity commences there may be a brief period of approximately 0.5–1 s during which the MRI signal decreases slightly below baseline (~0.5 per cent). This is a very subtle effect and is often not seen at conventional magnetic field strengths. This first phase has become known as the ‘initial dip’. This event, reported in both human and animal fMRI studies, corresponds to an apparent surge in tissue deoxyhaemoglobin (dHb) levels, occurring immediately following onset of stimulation. This dHb surge has been attributed to an immediate, stimulus-driven increase in oxygen consumption accompanied by a slight latency in the circulatory response. This phenomenon puts in evidence the delay of vasodilation following neuronal activity, highlighting the physiological answer of the brain. It has also been suggested that BOLD functional MRI based solely on detection of the initial negative dip may offer more precise spatial localization of neuronal electrical activity (than detection of the larger positive response). Subsequently, the BOLD response increases, yielding a robust ‘positive BOLD response’ which peaks 4–6 s after the stimulus commences. This is the positive BOLD response commonly used by fMRI researchers. Finally, upon cessation of the stimulus, there is a return of the BOLD response to

baseline, often accompanied by a 'post stimulus undershoot', during which the response passes through baseline and remains negative for several tens of seconds. Eventually, the response returns to baseline. The figure also shows an 'overshoot' period during the early positive BOLD response, which is another feature sometimes observed in fMRI experiments. During the first phase a small negative 'initial dip' may be observed. Subsequently, a more robust 'positive BOLD response' is observed. Following cessation of the stimulus a return to baseline accompanied by a 'post-stimulus undershoot' often seen.

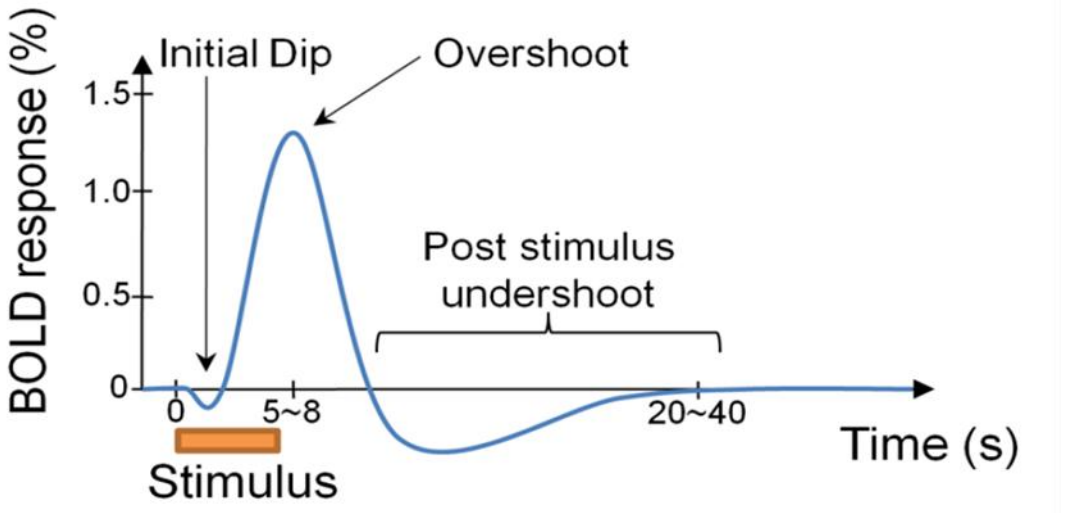

Figure 8: Schematic representation of the common features of the fMRI BOLD response to a period of neuronal stimulation.

The positive BOLD response

In humans, Positron Emission Tomography (PET) measurements shown that when an individual is passively lying in the imager under quiet, visually neutral conditions, the baseline rate of blood flow through a typical 100 grams sample of cortical tissue in the brain is in the neighborhood of 50 ml/min (Matthew et al 1993). Initiation of intense stimulation, such as rapid flashing of high contrast visual patterns, can increase perfusion rates in affected brain areas by 50–70 per cent (at locations that process visual input, in this case) (Fox & Henson 1986). These flow increases elevate capillary blood oxygenation, accelerating the delivery of oxygen across the capillary wall and lowering venous dHb levels. Since dHb decreases the MR signal in T2*-weighted images, activation-induced reductions in the tissue concentration of this compound lead to positive signal changes, which are usually around 2–3 per cent of the baseline signal level (at 1.5 Tesla). These blood oxygenation level dependent

signal changes are the basis for most MRI-based functional brain mapping. While the magnitude of the blood flow response to a given stimulus is a basic physiological property of brain tissue, the size of the BOLD response depends on both the biological response and on the physics of the magnetic resonance imaging process.

In general, both the amplitude and the shape of the response waveform can vary. Obviously, the amplitude of the response will be zero in regions of the brain that are not affected by a particular stimulus. Also, response amplitudes (for both flow and oxygenation) may be diminished when the behavioral or psychophysical contrast between the baseline state and the activation condition of interest is reduced. Although short, impulsive stimuli have been found to produce response waveforms in both flow and BOLD with a relatively invariant form (Burock et al 1998), the shape of the response waveforms to a step input (onset of sustained stimulation) is somewhat variable (Hoge et al 1999).

Although a pronounced positive response overshoot is often accompanied by a similarly large post-stimulus undershoot, the size of such transient signal features relative to the steady-state segment is highly variable and in some cases there is no discernible overshoot (or undershoot).

Both extremes (pronounced or no overshoot) may be observed in a single cortical location during different types of stimulation, and there is no general correlation between overall response magnitude and the presence or absence of overshoot. When present, the positive response overshoot appears to be much more pronounced in the BOLD signal than in the flow response waveforms. This observation suggests that some physical mechanism is probably amplifying the sensitivity of the BOLD signal to blood flow transients in the early phases following changes in stimulation state. One candidate for this amplifying influence, observed by Mandeville et al. during forepaw stimulation in rats, is the slow adjustment of CBV, which weights the amount of deoxyhaemoglobin in the tissues) during changes in stimulation state (Mandeville et al 1999).The elevated CBV levels associated with sustained stimulation may take up to a minute to evolve, leading to a reduction in BOLD signal that is only significant in the late, steady-state phase. The reverse occurs upon stimulus cessation; when the elevated CBV levels (and accompanying BOLD signal reduction) persist briefly even as blood flow falls dramatically, contributing to a negative post-stimulus undershoot in the signal (Figure 9).

In general, the BOLD signal curve obtained after fMRI acquisition and analysis is simplified by not considering the initial dip, the positive response overshoot and negative post-stimulus undershoot. In this way, the main quantifiable parameters of the fMRI response

function are, first of all, the amplitude of the BOLD signal, measured as a percentage of variation of the signal from the baseline, the latency of appearance of the signal as well as its length (from the fMRI maps get from the analysis, the number of voxels can also be taken into account to estimate the spatial repartition of the activation.).

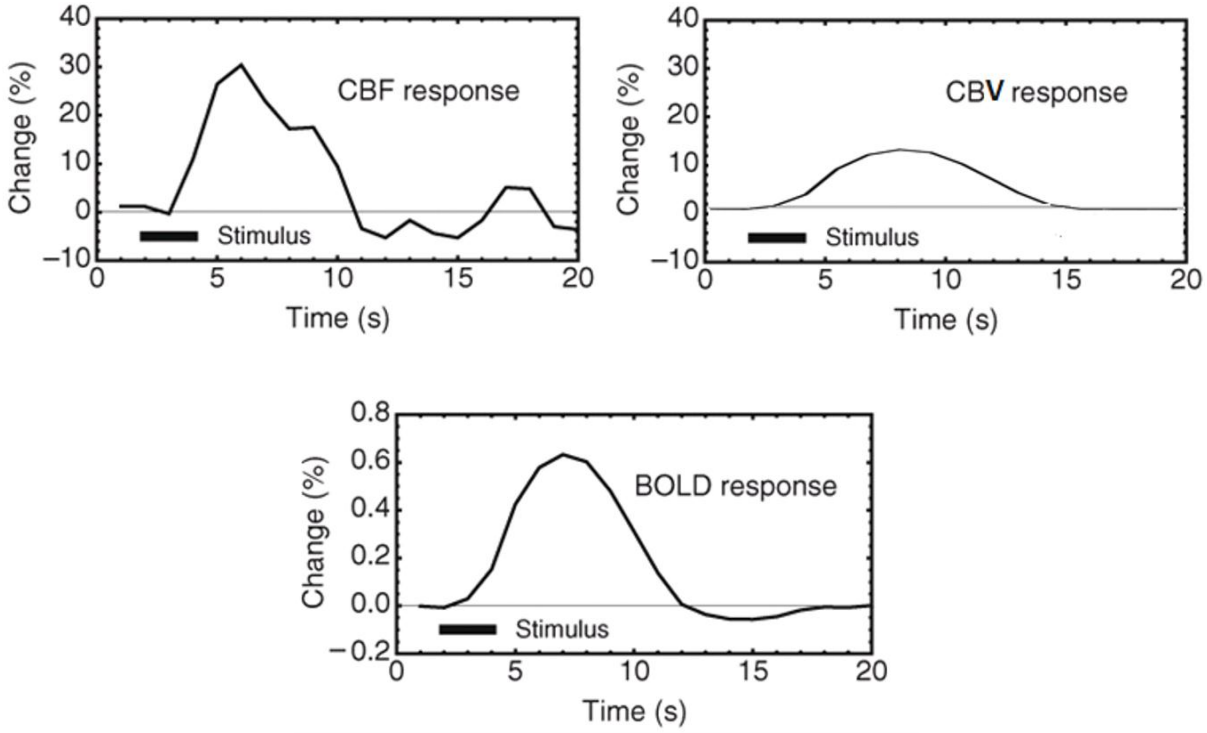

Figure 9: Cerebral Blood Flow (CBF), Blood Volume (CBV) signals and respective BOLD response.

Blood flow exhibits an abrupt jump to its elevated level during stimulation, while blood volume adjusts gradually. Upon cessation of stimulation, blood volume returns slowly to its baseline value.

Metabolic attenuation of the positive BOLD response

The observations, described above, of a negative signal dip in the first second of stimulation illustrate the effect of a BOLD signal reduction caused by an increase in cerebral metabolic rate of oxygen (CMRO2). While this negative dip is rapidly obliterated by the closely trailing CBF response, it is likely that CMRO2 continues to increase during at least the first ten seconds of stimulation. This would suggest that the late-phase positive BOLD

response is subject to considerable attenuation due to increased oxygen consumption by activated tissues. By comparing BOLD signals observed during elevation of perfusion rates to specific levels with either neural stimulation or CO2induced vasodilation, it is possible to isolate the effect of metabolic deoxyhaemoglobin production, providing a relatively direct demonstration of increased steady-state oxygen consumption by activated neurons.

fMRI acquisition

During fMRI acquisition, the first few seconds of acquisition are used to establish the baseline of the CBF at a resting state. It permits to eliminate the intrinsic variations of the blood flow as well as the small movements of the brain. It is later necessary to statistically estimate the CBF variations due to the transient stimulus. The acquisition is done by volume, corresponding to the RT (2 sec in general). The start of the stimulus will then trigger the BOLD signal as described above. The statistical analysis will aim at comparing images acquired during the stimulus to resting state images, voxels per voxels. A correlation between the CBF changes and the stimulus is calculated (Figure 10).

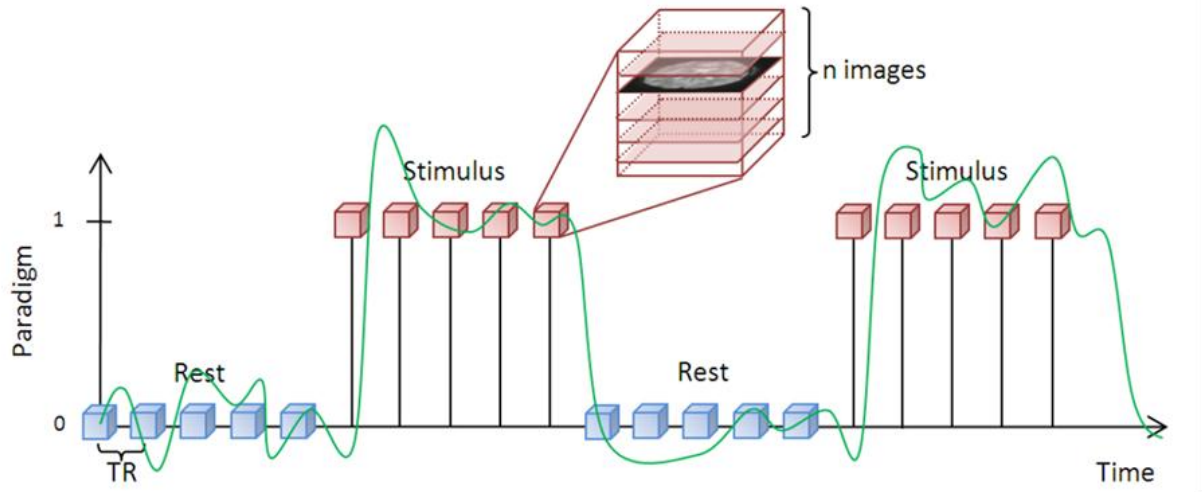

Figure 10: Schematic of the fMRI data structure and its acquisition process.

At each time-point, depending on the relaxation time (TR), a volume (cubes) of n images are taken. A stimulus (sensitive, visual or electrical) is applied (red cubes) and the images are compared with the ones got during the resting time. In green, a classical hypothetical relative BOLD signal curve matching with the protocol.

3.3 - Astrocytes

General characteristics

The term “glia” encompasses in the Central Nervous System (CNS) 3 subpopulations of glial cells: astrocyte, microglia and oligodendrocyte (equivalent to Schwann cells in the PNS). They represent a huge part of the brain in terms of mass and number, although their relative proportion is still very controversial. The famous scientist Erik Kandel estimates in his widely used *The Principles of Neural Science*, that: “Glial cells far outnumber neurons. There are between 10 and 50 times more glia than neurons in the CNS of vertebrates.”, (Kandel ER, “Principles of Neural Science”) when for instance, some other teams defend a ratio of 1:1 (Herculano-Houzel & Lent 2005).

Glial cells were originally described by Virchow (1846) as non-neuronal cells constituting the ‘‘glue’’ of the brain. Later studies classified glial cells in the CNS as astrocytes, oligodendrocytes, and microglia, each of which has different histological characteristics and functions, described by Ramon y Cajal in 1911. Once thought to be merely supportive elements, maybe due to the fact that they are non-excitable cells, glial cells have made the big leap toward the center of attention (Hertz & Zielke 2004). The big part of the change in their status can be attributed to the findings that glia, particularly astrocytes, can integrate neuronal inputs and modulate synaptic activity (Araque et al 1999).

Beyond the 3 types of glial cells, astrocytes appear to largely outnumber the others. They are cells characterized by small somata (< 10 um) and numerous highly branched processes. The astrocytic process is in close contact with both pre- and postsynaptic terminals. It is estimated that one single astrocyte is in contact with 100,000 synapses, which suggests their important role in synaptic regulation. Interestingly, each astrocyte “covered” a defined area of synapses and vessels and its expansions do not overlap with that of others. In parallel, researchers realized that the ratio of astrocytes to neurons varies from one brain region to another, sometimes dramatically. Several early studies found for example a astrocyte to neuron ratio of about 1:1 in the cortex, and 17 to 1 in the thalamus (Pakkenberg & Gundersen 1988). Moreover, astrocytes, in addition to form diversity, present a large heterogeneity of function (Oberheim et al 2012). A lot of studies focusing on different aspects of astrocytes are reviewed, highlighting the multitude of roles and the importance of these cells in the CNS. These foundings are well described since a decade in high quality publications and reviews. They included Ca2+ homeostasis and signaling, receptor distribution (Barres 1991a, Barres

1991b, Porter & McCarthy 1997, Verkhratsky & Kettenmann 1996), metabolic support for neurons (Coles & Abbott 1996, Tsacopoulos & Magistretti 1996), the clearance of extracellular ions (Newman & Reichenbach 1996) and neurotransmitters (Mennerick & Zorumski 1994, Nicholls & Attwell 1990), and the role of astrocytes in synaptogenesis (Pfrieger & Barres 1996, Pfrieger & Barres 1997).

Astrocytes location and neurovascular coupling

Classically, astrocytes are known to have high K+ permeability and to be important in regulating extracellular K+ necessary for maintaining neuronal excitability. In addition, they can also maintain external medium around the active neurons by regulating extracellular K+ concentration, volume, osmolarity, pH, and concentration of neurotransmitters, particularly glutamate and γ-aminobutyric acid (GABA) at the synaptic cleft. Astrocytes are in close association with neurons, can enwrap synaptic terminals (Ventura & Harris 1999), and have foot processes ensheathing the capillaries. Because of their anatomical location, they were thought for a long time to have an intermediary role in matching neuronal activity to CBF and metabolism. In 1885, Golgi first described the contact of astrocytic foot processes with arterioles and capillaries. By sending specialized processes to both the vasculature and synaptic contacts, astrocytes have a unique anatomical position between neurons and arterioles to couple neuronal activity to blood supply. On their other side, astrocytes sense synaptic activity and their role as an active element of the synapse together with pre- and postsynaptic terminals has led to the term ‘‘tripartite synapse’’ [(Araque et al 1999), Figure 11].

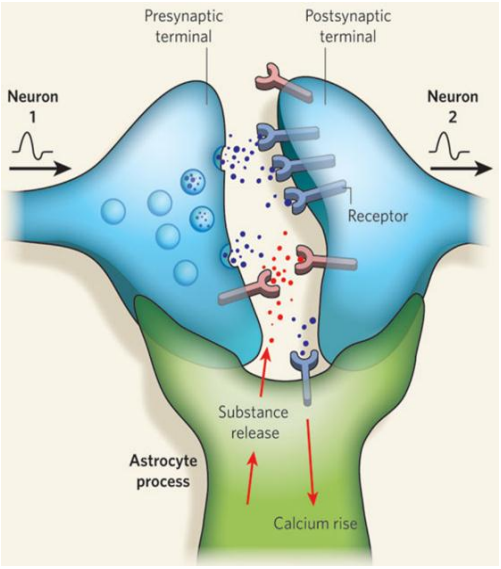

Figure 11: Scheme of the tripartite synapse. Defined in 1999 by A. Araque, it consists in the enwraping of the neuronal synapse by an astrocyte extension. Astrocytes are now known to capture synaptic neurotransmitters, then triggering calcium mediated pathways within the astrocyte leading to the release in the synaptic cleft «gliotransmitters», that in turns modulate neuronal activity but also reach neighboring astrocytes, introducing an «inter-astrocyte communication» (from N.J. Allen and B.A. Barres Nature 2009).

They release a variety of vasoactive molecules such as glutamate, ATP, NO, prostaglandin, epoxyeicosatrienoic acid (EETs), and D-serine (Petzold & Murthy 2011).

Astrocytic Calcium (Ca^{2+}(i)) Signaling

A major step in understanding the active role played by astrocytes in several brain functions has been achieved by demonstrating that calcium signaling is an important feature in astrocyte physiology and represents a form of cell excitability (Verkhratsky & Toescu 1998). Indeed, these cells can sense, integrate, and respond to external stimuli released by neurons through changes in intracellular calcium concentration Ca^{2+}(i). Since astrocytes do not generate action potentials and are devoid of synaptic contacts between each other, the existence of an elaborate Ca^{2+}(i) signaling mechanism may allow these cells to communicate. This concept is based on the pioneering observations of Ca^{2+}(i) signaling in astrocytes and the concept of a glial long-range signaling system (Cornell-Bell et al 1990). Several studies have demonstrated that gap junction channels and/or the release of an active factor in the extracellular space are involved in the propagation of astrocytic Ca^{2+}(i) signaling. The source of Ca^{2+} for astrocytic Ca^{2+} surges is predominantly, but not exclusively, internal stores such as the endoplasmic reticulum. The activation of inositol trisphosphate receptor subtype 2 (IP_3R2), an IP_3 receptor type specifically expressed in astrocytes in the CNS (Holtzclaw et al 2002), is critical for astrocytic Ca^{2+}(i) surges in the hippocampus (Petravicz et al 2008) and cerebral cortex (Takata et al 2011). Mechanisms of Ca^{2+}(i) wave propagation include diffusion of Ca^{2+}(i) ions within the cell but also of Inositol 1,4,5-trisphosphate (IP_3) through gap junctions and extracellular ATP signalling. These called "Ca^{2+}(i) waves" are properly IP_3 waves, which diffuse further than Ca^{2+} ions (Allbritton et al 1992) (Figure 12).

Stimulation of glutamate metabotropic receptors (Group I mGluR), present on astrocyte synaptic endfoot at the synapse, causes the associated enzyme phospholipase C (PLC) to hydrolyze phospholipids from the plasma membrane. The hydrolysis of phosphatidylinositol 4,5-bisphosphate (PIP2) leads to the formation of $IP_3$and diacyl glycerol (DAG). Due to its hydrophilic character, IP_3can travel to the endoplasmic reticulum, the Ca^{2+}(i) tank of the cell, where it binds its receptor. There, the opening of calcium channels frees Ca^{2+} ions, increasing in this way the cytosolic Ca^{2+}(i) concentrations. The Ca^{2+}(i) dependent PLC is re-activated and produces more IP_3. IP_3will diffuse to neighboring astrocytes until its quantity is not enough to raise Ca^{2+}(i) to a limit of PLC activation (Hofer et al 2002). The lipophilic DAG remains in the membrane, acting as a cofactor for the activation of protein kinase C.

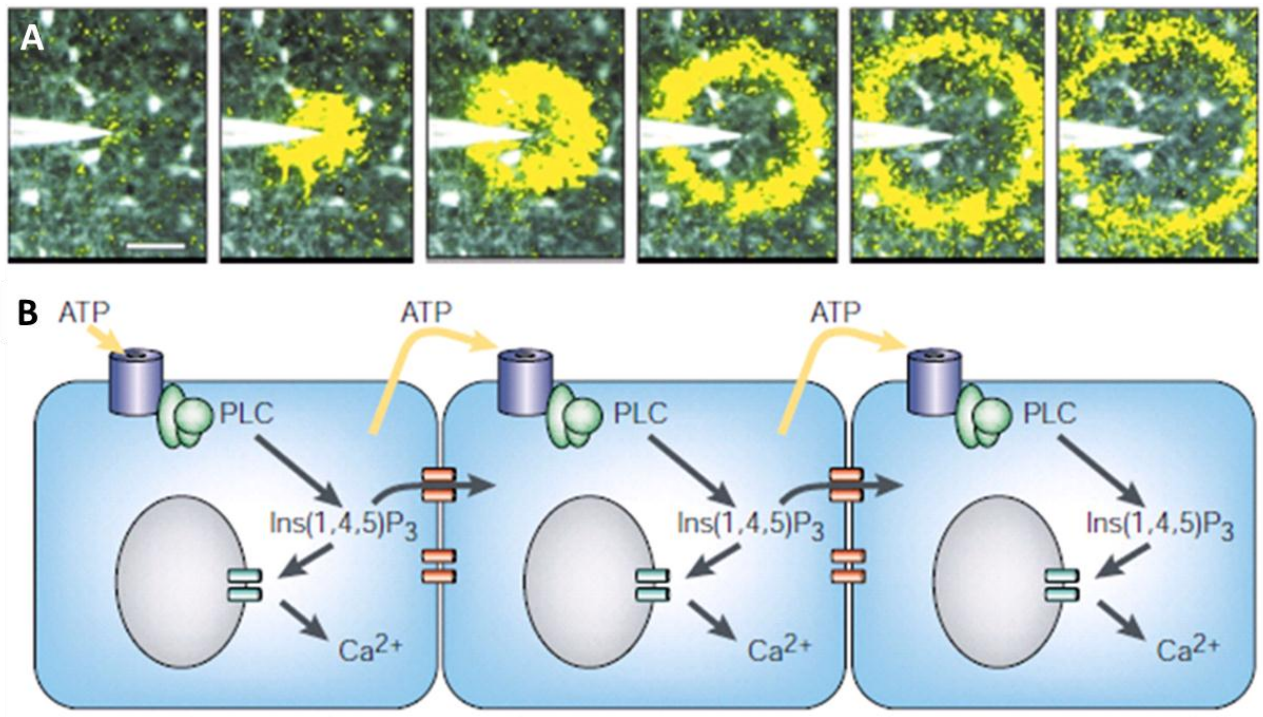

Figure 12: Stimulation of glial cells from the retina evokes a radially propagating wave of elevated calcium.

A. Calcium waves evoked by mechanical stimulation of a glial cell. B. Proposed mechanisms for propagation of calcium waves. IP3, generated by the active phopholipase C pathway, would diffuse to nearby glia, release Ca^{2+}(i)from their internal stores. The release of ATP, which can cause further generation of IP3 and release of ATP of nearby cells, could explain longer signaling (from Haydon, 2001).

The uptaking of glutamate by astrocytes during synaptic activity leads to intercellular communication, but also to the activation of many intra-astrocyte pathways (Figure 13). Some of these pathways are Ca^{2+}(i)-dependent and could be involved in the vascular response after neuronal activation. For instance, AA creates sub products such as EETs and prostaglandins, both with strong vasodilator properties. Moreover, Ca^{2+}(i) can activates calcium dependent K+ channel. This increases extracellular K+ concentration with vasodilation effects.

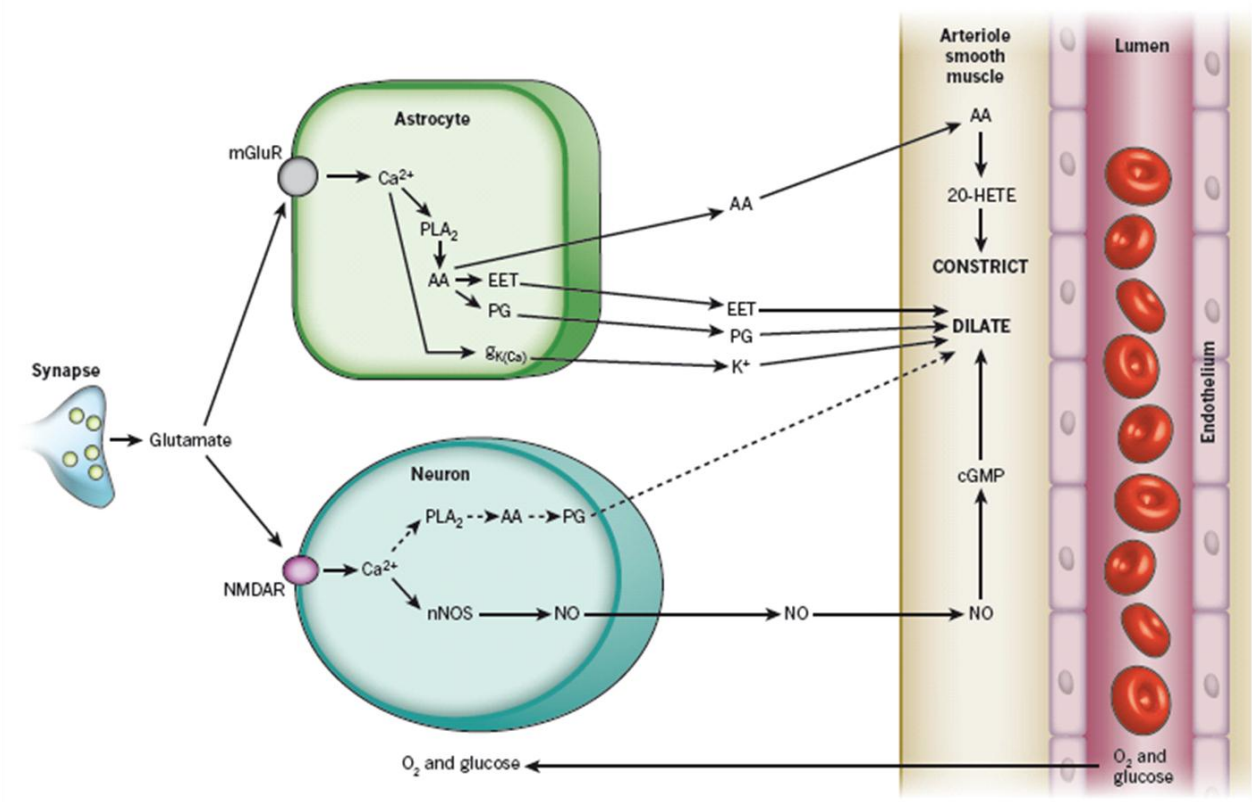

Figure 13: Major pathways by which glutamate regulates cerebral blood flow.

Pathways from astrocytes and neurons (left) that regulate blood flow by sending messengers (arrows) to influence the smooth muscle around the arterioles that supply oxygen and glucose to the cells (right, shown as the vessel lumen surrounded by endothelial cells and smooth muscle). In neurons, synaptically released glutamate acts on N-methyl-d-aspartate receptors (NMDAR) to raise $[Ca^{2+}]i$, causing neuronal NO synthase to release NO, which activates smooth muscle guanylate cyclase. This generates cGMP to dilate vessels. Raised $[Ca^{2+}]i$ may also generate AA from phospholipase A2 (PLA2), which is converted by cyclo-oxygenase 2 (COX2) to prostaglandins (PG) that dilate vessels. Glutamate raises $[Ca^{2+}]i$ in astrocytes by activating mGluRs, generating AA and thus three types of metabolite: prostaglandins (by COX1/3, and COX2 in pathological situations) and EETs (by P450 epoxygenase) in astrocytes, which dilate vessels, and 20-HETE (by ω-hydroxylase) in smooth muscle, which constricts vessels. A rise of $[Ca^{2+}]I$ in astrocyte endfeet may activate Ca^{2+}-gated K+ channels (gK(Ca)), releasing K+, which also dilates vessels (from Attwell et al.,2010).

Astrocytic control of cerebral blood flow

Accordingly with their key position, emerging evidence shows that neuronal activity can control microcirculation using astrocytes as a mediator. In 2003, Zonta et al., showed *in vitro* that after synaptic activation, astrocytes uptake extracellular glutamate initiating Ca^{2+}(i) signaling cascade that finally translated into arteriole dilation (Zonta et al 2003). In other words, they show that the dilation of arterioles triggered by neuronal activity is dependent on glutamate-mediated Ca $^{2+}$ i oscillations in astrocytes. Moreover, inhibition of these Ca^{2+}(i) responses resulted in the impairment of activity-dependent vasodilation, whereas selective activation of single astrocytes that were in contact with arterioles triggered vessel relaxation and they found that a cyclooxygenase product is centrally involved in this astrocyte-mediated control of arterioles. *In vivo* blockade of glutamate-mediated Ca^{2+}(i) elevations in astrocytes reduced without deleted the blood flow increase in the somatosensory cortex during contralateral forepaw stimulation. In 2006, Metea and Newman showed that IP_3 injection into astrocytes, that mobilize Ca2+ from intracellular stores, is enough to dilate artificially constricted vessels in retina slices (Metea & Newman 2006). They also show that glial-evoked vasodilations were blocked by inhibitors of cytochrome P450 epoxygenase, the synthetic enzyme for EETs, and that NO could influence vasodilation in response of glial stimulation. Taken together, these findings indicate that astrocytic pathways and metabolites are actively contributing to neurovascular coupling and suggest that regulation of blood flow involve Ca^{2+}(i) dependent astrocytic pathways.

An interesting feature emerges from the previous studies done on CBF regulation. A fraction of the CBF response remained unresponsive to mGluR or COX inhibition. The CBF regulation can drastically decrease without totally blocked hyperemia, highlighting the fact that several parallel pathways are involved in neurovascular coupling (Shi et al 2008).

It is important to notice that functional hyperemia occurs less than 2 sec after the onset of the stimulation, whereas astrocytic Ca^{2+} elevation is slower, typically delayed by more than 2–3 sec (Schummers et al 2008, Wang et al 2009). Based on this finding it was suggested that the astrocyte-Ca^{2+} response might be more important for sustaining the vasodilation during prolonged activation rather than as an initiating signal (Koehler et al 2009).

However, the observation that astrocyte are crucial in trigger functional hyperemia have been only done *in vitro*, and there is no evidence yet to affirm that this occurs also *in vivo*. Indeed, many important differences exist between the two systems.

In vitro / in vivo

Studying vascular regulation in slices has significant advantages, including the exquisite control over cellular elements. However, an inherent and critical limitation of studies in brain slices is that blood vessels in these preparations lack perfusion and, therefore, are maximally dilated, because myogenic tone induced by intraluminal pressure is missing. Preconstriction of vessels in slices, as well as large changes in the oxygen tension, can result in the conversion of arteriolar constriction into dilation (Gordon et al 2008, Mulligan & MacVicar 2004). This conversion has been suggested to underlie competing roles of astrocytes during different states of brain activation, but it is difficult to decide what is more physiological or at least less artificial: preconstriction of vessels by pharmacologically blocking the production of important signaling molecules such as NO (Zonta et al 2003), leaving vessels untreated and, thus, maximally dilated (Mulligan & MacVicar 2004), or inducing variations of tissue oxygen tension (Gordon et al 2008) that are larger than those measured in the intact brain during physiological activation (Ances et al 2001, Offenhauser et al 2005). Another important point to consider is how slice stimulation protocols relate to typical physiological sensory stimulation (Anderson & Nedergaard 2003). It is also difficult to speculate whether the very slow time scale at which vessel tone changed in some studies (Gordon et al 2008, Zonta et al 2003) is an effect of slice temperature, maximally dilated vessels, or lack of perfusion. For all these reasons, any result got *in vitro* has to be considered with precaution, and an *in vivo* equivalent experiment is not only recommendable but absolutely necessary, for a complete understanding of the role of astrocytes in neurovascular coupling.

4 - Summary

In summary, neurovascular coupling, or functional hyperemia, is a complex physiological phenomenon which permit oxygen and glucose supply after energy expenditure by neuronal activity. Both the initial event triggering it and the metabolic pathways responsible of it remain unclear. The triggering event could be an energy consumption dependent feedback mechanism or a feed forward mechanism originated by synaptic activity (Attwell et al 2010), although these two events are physiologically linked, as energy

expenditure due to action potentials propagation will lead to neurotransmitters release. While data do not exclude the possibility that multiple factors and signaling pathways, including the direct innervation of vessels, contribute to functional hyperemia, they show that the activation of astrocytes is centrally involved in this neurovascular coupling. Many metabolic pathways are activated within astrocytes, and many metabolites deriving from astrocytic metabolism, have been show to play a part in neurovascular coupling.

Here, we will study the functional hyperemia *in vivo*, in IP_3R2 Knock Out (KO) mice, to remove the artefacts induced by *in vitro* preparation. These mice do not express IP_3 receptors on the endoplasmic reticulum and consequently lack intra and inter cellular calcium signaling, a key mechanism in astrocytes. In this way, we expect to largely decrease inter astrocytes communication as well as to partially block astrocytes metabolism. fMRI, and particularly BOLD signal fMRI, appears to be a good tool to deepen functional hyperemia mechanism.

4 - Aims

In our study, we want to deepen the understanding of the importance of Ca^{2+}(i) signaling, that should trigger most of the astrocytic signaling pathways, in neurovascular coupling *in vivo*. For this purpose, we have at our disposal IP_3R2 KO mice, which do not present astrocytic intracellular releases of Ca^{2+}(i). As most of the signaling pathway triggering hyperhemia through astrocytes are supposed to be Ca^{2+}(i) dependent, we expect from these mice to present a deficit in functional hyperhemia.

1. Our main objective is to highlight the role of Ca^{2+}(i) signaling in neurovascular coupling thanks to BOLD signal in functional Magnetic Resonance Imaging, after a Perforant Pathway electrical stimulation. We expect to observe a decrease or even a suppression of the BOLD signal in the hippocampus.

2. In parallel, we want to record Local Field Potentials in the hippocampus during the same stimulation protocol, in order to investigate a potential role of Ca^{2+}(i) signaling in synaptic transmission at a network scale.

3. We want to check these two parameters (neurovascular coupling and LFP) first during a short stimulation, but also during a long lasting stimulation, to deepen the role of IP_3 dependent Ca^{2+}(i) signaling in astrocytes not only in neurovascular coupling ignition but in its maintenance

4. We will control that these mutant mice are not phenotypically impaired with wild type ones, in terms of memory and recognition.

5 - Materials and methods

5.1 - Animals

All animal procedures were approved by the corresponding ethical committee (IN-CSIC) and were performed in accordance with Spanish (law 32/2007) and European regulations (EU directive 86/609, EU decree 2001-486).

Four months old male C57Bl6/J mice were housed in cage of 4 animals, with a 12-hour diurnal light cycle with food and water ad libitum. Each animal was about 35g at the date of the experiment.

IP3R2 KO mice generation

The IP_3R2 KO mice were generously donated by Dr Alfonso Araque. The IP_3R2 genomic DNA was isolated from a 129SVJ mouse genomic library (Stratagene) and used to construct the IP_3R2 targeting vector by standard techniques (Figure 1). Briefly, 2 fragments of the IP_3R2 gene were cloned into a targeting vector that contained a neomycin selection cassette flanked by FRT sites. A 539-bp fragment containing exon 3 of IP_3R2 (116 bp) was inserted into 2 flanking LoxP sites. The targeting vector was linearized with NotI and subsequently electroporated into R1 embryonic stem (ES) cells. G418-resistant ES clones (480 clones) were screened for homologous recombination by DNA blot analysis, as described below. Two independent homologous recombinant ES clones were microinjected into blastocysts from C57BL/6J mice to generate male chimeras. Male chimeras were bred with female Black Swiss mice to generate germline transmitted floxed heterozygous mice ($IP_3R2^{+/flox}$). $IP_3R2^{+/flox}$ mice were subsequently intercrossed and crossed with Pro-Cre mice, which restricted Cre expression to male germ cells undergoing spermatogenesis, to generate mice which were doubly heterozygous for IP_3R2 floxed allele and Pro-Cre allele (Pro-Cre, $IP_3R2^{+/flox}$). Pro-Cre, $IP_3R2^{+/flox}$ males were crossed to female breeders to generate germline heterozygous null mutant offsprings ($IP_3R2^{+/-}$). Intercrosses of the $IP_3R2^{+/-}$ were used to generate homozygous null mutant mice ($IP_3R2^{-/-}$).

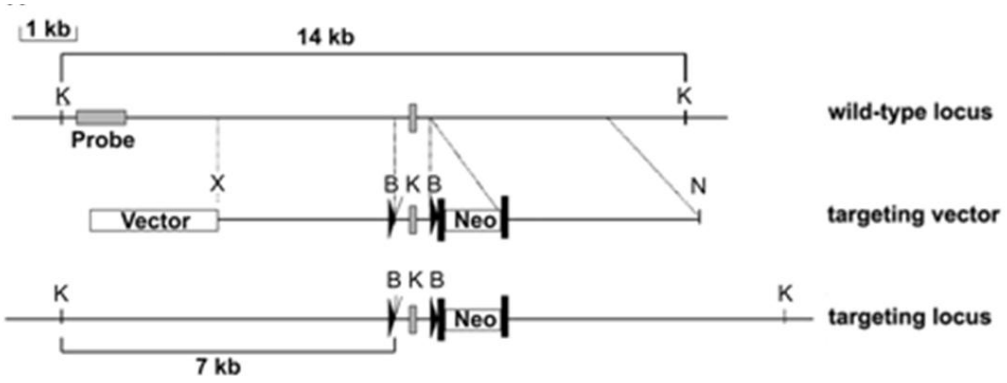

Figure 1: Targeting strategy, restriction map of the relevant genomic gene of IP3R2.
The targeting construct is shown in the center, and the mutated locus after recombination is shown at the bottom. The targeting construct was generated by flanking exon 3 of IP3R2 with 2 loxP sites and flanking the neo-cassette by frt sites. B indicates BamHI; K, KpnI; N, NotI, Neo represents neomycin resistance gene; arrowheads represent LoxP sites; and the long boxes represent frt sites (from Targeted generation of IP3R2-deficient mice from Li X, Zima A. V, Sheikh F, Blatter L. A, Chen J. Endothelin-1-induced arrhythmogenic Ca2+signaling is abolished in atrial myocytes of inositol-1,4,5-trisphosphate (IP3)-receptor type 2-deficient mice. Circ Res. 2005;96:1274–1280).

5.2 - Anesthesia

Different anesthetics have different side effects on both neuronal and vascular sides. Therefore we first tested three different anesthetics with different mechanisms of action.

Urethane (Sigma): Urethane modestly affects multiple neurotransmitter systems at an anesthetic concentration (Hara & Harris 2002). Urethane anesthesia was optimized for mice. A intra peritoneal injection of urethane in saline at 1.7g/kg resulted optimal, inhibiting reflexes to tail and hind paw pinch and keeping heart rate (390 beat per minute (bpm) +/- 5%) and breathing rate (110bpm +/- 10%) under physiological limits. If necessary, the animal was re-injected at 10% of the initial dose. For fMRI data acquisition no additional urethane supplements were required.

Isoflurane (Esteve): Under the form of a volatile gas, it would inhibit NMDA receptor's activity together with K+ channels. It is also supposed to activate ATPase and to decrease mitochondrial oxidative respiration. Finally, it generates a global decrease of neuronal activity, although the precise effects are not perfectly known. It has a strong vasodilator power that can complicate fMRI results interpretation. The induction of anesthesia was done at 5% of isoflurane for 10 minutes, then the animal was placed on the stereotaxic apparatus and the isoflurane level was slowly lowed until to 1-1,5%. It was then maintained all along the surgery as low as possible, around 1%. The vital parameters were as follow: heart rate 300 bpm, breathing rate 60-100 bpm. During the fMRI acquisition, anesthesia was maintained at the minimum necessary to keep the animal anesthetized (not higher than 0.75 %).

(D-) Medetomidine ((Dex) Domitor Esteve 0.5mg/mL): it is a synthetic drug, an alpha 2 agonist, used as both a surgical anesthetic and analgesic. Based on the literature (Adamczak et al 2010), we administered an initial sub cutaneous bolus at 0.4mg/kg followed by a perfusion at 0.8mg/kg/h. We obtained a good anesthetic level during approximately 90 minutes that was long enough to perform the fMRI experiments. The original marketed product is a racemic mixture of 2 stereoisomers: L- and D-medetomidine. As the L- isomer has shown very low effect, dexmedetomidine (D-medetomidine) is now largely preferred. D-medetomidine has a potentiated effect compared with Medetomidine (Domitor Esteve 1mg/mL) (Burnside et al 2013), so that we switched to it, following by the way the very same protocol.

5.3 - Surgery

Anesthetized animals were placed on the stereotaxic apparatus. Isoflurane was required during surgery (2hours +/- 30 minutes) to compensate the relative short duration of dexmedetomidine anesthesia. Body temperature was continuously monitored with a rectal probe and maintained at 37.0 ± 0.5 °C with in-house feedback controlled water (during fMRI experiments) or electrical (during surgery and electrophysiological recordings) blankets. The vital parameters (Heart rate, breathing rate and 0_2 blood saturation) were monitored. The depth of anesthesia was checked by testing the mouse's reflexes by tail and toe pinching. The

animal was supplied in oxygen at 0.4 L/min. After a local subcutaneous anesthetic injection (bupivacaïne, B.Braun 0.5%), the scalp was incised, and small burr holes were made in the skull above the hippocampus for the insertion of a recording electrode (from bregma in millimeters: anteroposterior (AP) −2, mediolateral (ML) 1.2), and above the perforant pathway (PP) (from lambda in millimeters: AP 0, ML 2.6) (Figure 2). After the electrophysiological recordings, the recording electrode was removed and the stimulation electrode was fixed with dental cement (Palacos-R, Hereaus). For these experiments, surgery was performed under isoflurane as described above and then the anesthesia was switched to dexmedetomidine once the animal was located in the scanner. The transition from isoflurane to dexmedetomidine anethesia was performed by decreasing slowly the isoflurane level while injecting the initial bolus of dexmedetomidine. When the respiration rate decreased until 50 bpm in the first 3 min after bolus administration, isoflurane was discontinued faster. When isoflurane was discontinued, all animals showed an increase in respiratory rate, which stabilized approximately 20 min after the initial dexmedetomidine bolus. Immediately after bolus administration, a subcutaneous perfusion of dexmedetomidine at 0.8mg/kg/h was started until the end of the fMRI experiment (Adamczak et al 2010). Before sacrificing the animal by cervical dislocation, it was deeply anesthetized again with isoflurane at 5%.

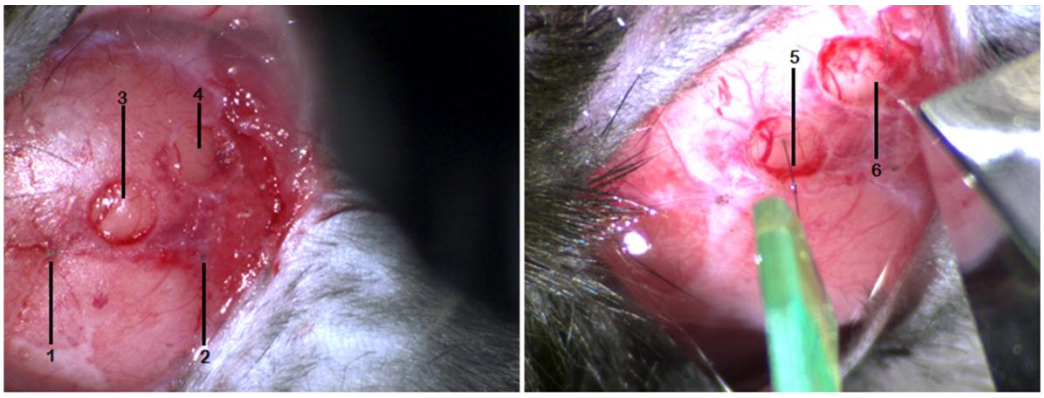

Figure 2: Surgery and electrodes positioning.

With references bregma (1) and lambda (2), holes were drilled through the skull following Watson and Paxinos coordinates above the hippocampus (3) and the Perforant Path (4). A LFPs recording Multi Electrode Array (5) and a monopolar stimulating electrode (6) were placed thanks to a stereotaxic frame.

Electrodes positioning

Electrodes were stereotaxically implanted according to Paxinos and Watson atlas (Figure 3C). On the right side of the animal's skull, LFPs were recorded with a Multi Electrode (ME) (NeuroNexus Ann Harbor, MI, USA) placed through the hippocampus (AP: -2mm from bregma ; ML : 1.2mm ; DV : 2.2 mm) in order to pass through the dentate gyrus (DG) and Amon Corn 1 (CA1) (Figure 3B). A stimulating monopolar electrode was preferred to a bipolar electrode in order to avoid tissue damaging during long stimulation (Temel et al 2004). It consisted in the welding of two Iridum-Platinium wire (A-M systems, cat 776000 bare 0.002'', coated 0.004'', Sequim, WA,USA) and was positioned on the Perforant Path, following the Paxinos and Watson coordinates (AP : 0 from lambda ; ML : 2.5mm ; DV : 1.5 mm +- 0.2 mm, with an angle of 10 degres).

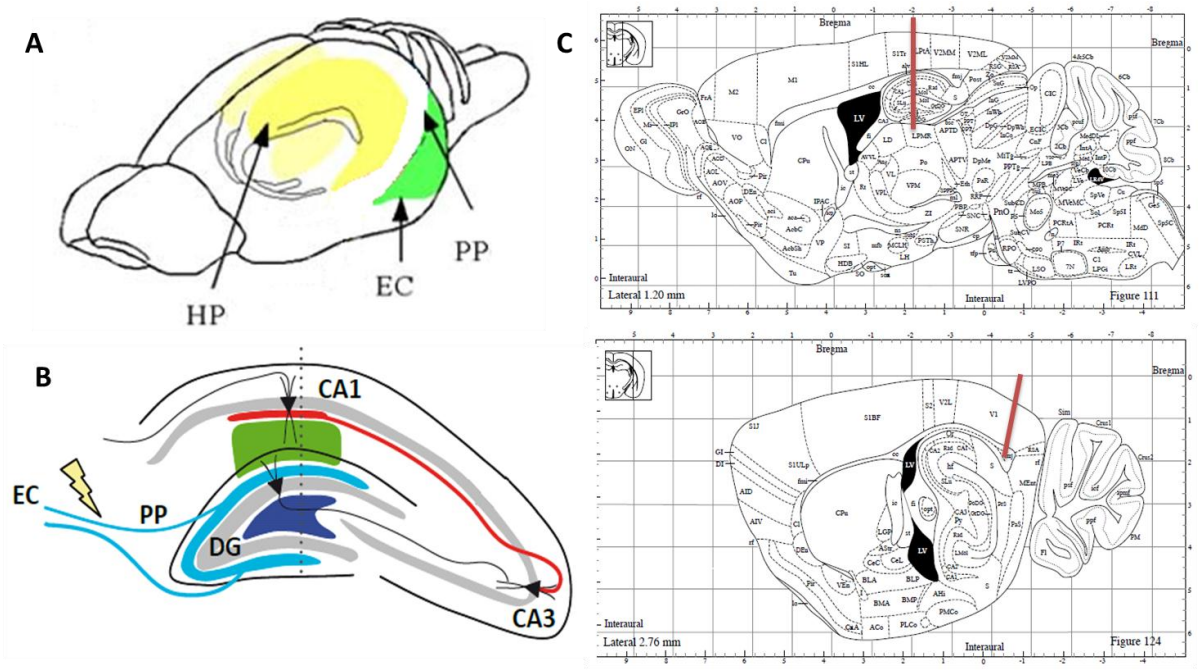

Figure 3: Electrophysiological stimulation and recordings.

A, Morphologic positioning of the Perforant Path (PP), the Entorhinal Cortex (EC) and the Hippocampus (HP) in the mouse brain. B, Iridium electrode stimulating (lightning) the PP, projections from the entorhinal cortex (EC) to the hippocampus. The recording electrode (dotted) was positionned through the whole hippocampus to record LFPs in the DG and CA1. C, Stereotaxic position of the recording (up) and stimulating (bottom) electrodes.

The ME was first used to confirm the right positioning of the stimulating electrode. The final positions of both recording and stimulating electrodes were optimized based on the spatial profile of the stereotypic evoked potentials, and later on confirmed in anatomical MRI scans. In order to limit the artifact due to the metallic component of the electrode and to get nicer images in the magnet, two types of electrodes have been used during the study: an Iridium-Platinium electrode and carbon fiber one, producing the same fMRI results (but different image artefact). The carbon electrode were produced in the lab following the protocol set up by Jeff F. Dunn and colleagues (Dunn et al 2009) (Figure 4). Its electrical characteristics (conductance and resistance) were identical to the iridium ones.

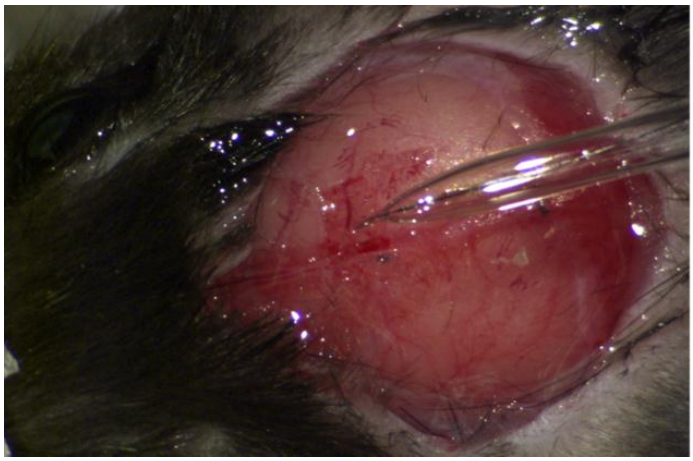

Figure 4: stimulating carbon electrode.

In order to avoid a strong susceptibility artefact induced by the metallic composition of the stimulating electrodes during fMRI acquisition, monopolar iridium wire were substituted by carbon electrode presenting the same electrical characteristics (Dunn et al., 2009).

5.4 - Local Field Potentials recordings

Population Spikes and Excitatory Post Synaptic Potentials

A Local Field Potential is an electrophysiological signal dominated by the electrical current flowing from all nearby dendritic synaptic activity within a volume of tissue. The current is produced by the summed synaptic current flowing across the local extracellular space. From these LFPs recordings in the hippocampus, we measured Excitatory Post

Synaptic Potentials (EPSP) and the Population Spikes (PS), and PS latencies (Figure 4). EPSPs are temporary depolarizations of postsynaptic membrane potential caused by the flow of positively charged ions into the postsynaptic cell and PS is a shift in electrical potential as a consequence of the movement of ions involved in the generation and propagation of action potentials. In the hippocampus, neurons are arranged in such a way that they all receive synaptic inputs and emit outputs in the same area. Because these neurons are in the same orientation, the extracellular signals from synaptic excitation add up to give a signal that can easily be recorded with an extracellular field electrode. This extracellular signal recorded from a population of neurons is a field potential.

Trisynaptic loop of the hippocampus

The trisynaptic loop of the hippocampus is a relay of synaptic transmission commonly used as a model. It is made up of three major cell groups: granule cells, CA3 pyramidal neurons, and CA1 pyramidal cells. The first synaptic transmission in the hippocampus occurs between the EC and the DG. The EC transmits its signals to the DG via axons known as the perforant path. These axons projects on the dendritic tree of the molecular layer of the DG. DG axons from the hilus then target pyramidal cells in CA3 (mossy cell fibers). CA3 then fires to CA1 via Schaffer collaterals which synapse in the subiculum where electrical signals are carried out from the hippocampus.

By measuring EPSPs and PSs within the hippocampus, we thus had access to the evolution of an initial input (electrical stimulation of the PP) through synaptic transmission (figure 5); the EPSPs and PSs representing respectively the input (presynaptic) and the output (postsynaptic).

To perform the electrophysiological experiments, the current amplitude, pulse duration, train duration, and stimulation frequency were delivered by a real-time operating system “MC stimulus STG 2004”.

Intensity/responses (I/O)

Once both electrodes were well positioned, an Intensity/Responses (called Input/Output or I/O) protocol was performed. It consisted in regularly increasing the intensity of stimulation of the PP (50uA, 200uA, 400uA, 800uA, 1000uA, 1200uA) while recording the responses in the DG for each stimulation. The EPSP observed in the molecular layer of the DG represents the input, and the PS in the hilus of the DG the output.

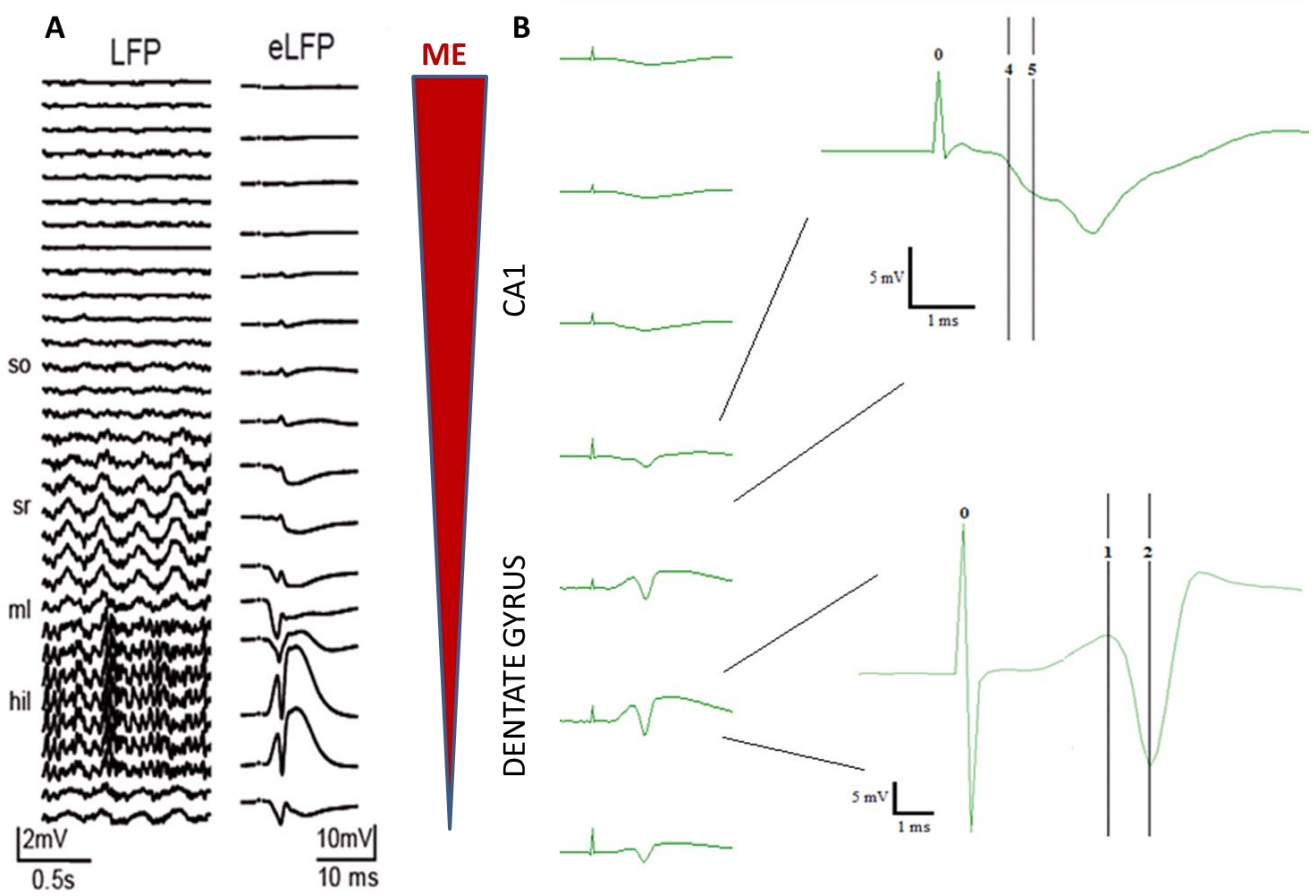

Figure 5: Local Field Recordings in the hippocampus.

A. Left, spontaneous activities are recorded all along the Multi Electrode. 32 LFPs are recorded every 50 µm. On the right, evoked LFPs are individualized from the spontaneous ones after recording. PSs are visible in the DG and EPSPs in the molecular layer.

B. After eLFP from the hilus and the molecular layer of the DG isolation, analysis are performed on « Spike 2 6.03 » software (CED, Cambridge, UK). Cursor 0 represents the artefact of the stimulation. The latency of appearance of the spike is calculated between cursors 0 and 2, the amplitude of the PS between cursors 1 and 2. The EPSP is measured by the steepest falling of the slope between cursors 4 and 5. Hil: hilus, ml: molecular layer, sr: stratum radiatum, so: stratum oriens, eLFP: evoked Local Field Potential.

5.5 - Set up of the fMRI stimulation protocols

Brief and long 10 hertz train protocols

As developed in introduction, the BOLD fMRI signal appears 2-3 seconds after the stimulation in rodents. We consequently needed a stimulation long enough to elicit this signal. A stimulation of 4 seconds that has previously shown to produce consistent results (Canals et al 2008) has been chosen. We needed to confirm its validity in mice in fMRI. In this purpose, we stimulated with a square pulse of 200 us in a 4 seconds train of stimulation at 5, 10 and 20 Hz. As described below, we got a more relevant response at 10 Hz, so that we kept this frequency of stimulation in the experiments.

Following the I/O protocol, it was possible to observe an intensity of stimulation when the amplitude of the response was maximal and not increasing with the increase of intensity. The answer was considered saturated. To avoid tissue damage, we arbitrarily decided to use in the 10 hertz protocol an intensity that was giving a response of half amplitude compared to the saturating amplitude. The used intensities were always comprised between 300 μA and 500 μA. Finally, the responses to this train of stimulation were recorded in the hippocampus through the ME.

At the end of the electrophysiological recordings, the ME was removed and the stimulating electrode was fixed with dental cement adhering to the skull without being moved.

The stimulation was here again delivered by a "MC stimulus STG 2004" and based on the electrophysiological recordings as described above.We used 2 different train of stimulation. We called "brief stimulation" the 4 seconds protocol designed in order to elicit an initiation of the BOLD fMRI signal. In order to study the maintenance of the BOLD signal in time, a "long stimulation" protocol was developed. Stimulation's duration from 12 to 60 seconds were tried. The more relevant images were got with 20 seconds of stimulation (data not shown). During fMRI acquisition, the brief stimulation protocol was a block design consisting of 10 periods of 4s stimulation epochs followed by resting epochs of 60s (11 min in total). The long stimulation protocol consisted in 5 periods of 20s stimulation epochs followed by resting epochs of 60s (6 min 40 s in total). These protocols were repeated 3 times per animal. The stimulation pulses were always biphasic and charge balanced, with the cathodal pulse leading the anodal pulse and pulse duration of 0.2 ms. The BOLD signal shown as result

of the brief stimulation is the average of these 30 stimulations. The BOLD signal shown as result of the long stimulation is the average of these 15 stimulations.

fMRI

For the MRI experiments, animals were placed in a custom-made animal holder with movable byte and ear bars and positioned fixed on the magnet chair. This allowed precise positioning of the animal with respect to the coil and the magnet and avoided movement artifacts. Animal body temperature was kept at physiological temperature using a water blanket. Temperature, heart rate and breathing rate were monitored throughout the scanning session.

Experiments were carried out in a horizontal 7 Tesla scanner with a 30 cm diameter bore (Biospec 70/30v, Bruker Medical, Ettlingen, Germany) (Figure 6). The system had a 675 mT/m actively shielded gradient coil (Bruker, BGA 12-S) of 11.4 cm inner diameter. Functional MRI was done in 12 coronal slices using a Gradient Echo Echo-Planar Imaging (GE-EPI) sequence with the following parameters: Field of View (FOV) 20 x 20mm, slice thickness 1mm, matrix 96 x 96, segments 1, Flip Angle (FA) 60°, Echo Time (TE) 15ms and Repetition Time (TR) 2000ms. Functional data were overlaid into high resolution anatomical images. T_2 weighted anatomical images were collected using a rapid acquisition relaxation enhanced sequence (RARE), applying the following parameters: FOV 20 x 20mm, 12 slices, slice thickness 1mm, matrix 192 x 192, Effective TE (TE_{eff}) 56ms, TR 2s and a RARE factor of 8.

Figure 6: 7 Tesla magnet used in funcional Magnetic Resonance Imaging experiments. Mice are placed in an adapted holder and then introduced inside the magnet for MRI and fMRI acquisition. The animal is hold in a still position. Breathing rate, heart rate as well as temperature are monitored. Mice can be anestetised by isoflurane directly inside or perfused by medetomidine from an external pump.

Functional MRI data were analyzed offline using our own software developed in MATLAB (Mathworks, Natick, MA, USA) and including the statistical parametric mapping packages (SPM8, SPM, London, UK). After linear detrending, temporal filtering (0.015-0.2 Hz) and spatial filtering (3x3 gaussian kernel of 1.5 sigma) of voxel time series, general linear model or cross-correlation analysis were applied with a simple boxcar model shifted forward in time typically by 2sec or a boxcar convolved with a gamma probability density function (MatLab), to account for the hemodynamic delay in the BOLD signal. Functional maps were generated from voxels that have a significant component for the model and are clustered together in space (Figure 7). Similar results were obtained with different analytical methods.

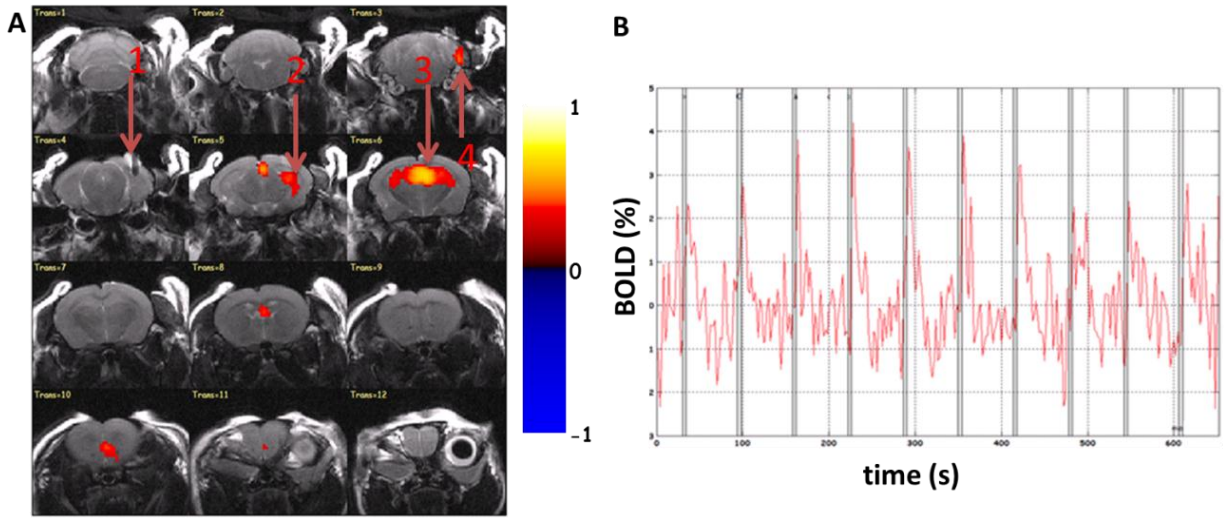

Figure 7: fMRI gives a visual appreciation of neuronal activity.

A. Example of BOLD fMRI map after statistical analysis. 12 slices are analyzed from the caudal to the rostral part of the brain. 1) Artefact due to the Iridium electrode in the Perforant Path, 2) BOLD signal in the ventral hippocampus, 3) BOLD signal in the dorsal hippocampus, 4) Light BOLD signal in the MEC. B. Exemple of BOLD signal time course during PP stimulation. The stimulation times appear in separated by 1 minute of rest. This pattern is repeted 10 times. The BOLD signal shown in A is the average of these 10 stimulations. The color code represents the correlation (R value) of the BOLD signal with the stimulation paradigm.

5.6 - Behavioral tests

Open field (OF)

Mice were placed in 30*30*30 cm acrylic glass boxes and monitored throughout a test session (30 min) using an overhead video tracking system (SMART, Panlab S.L., Barcelona, Spain) that recorded the position of the animal every 0.5 s. The footage is then analyzed by an automated tracking system. The area was divided in 2 zones in order to measure thygmotaxis, a behavior of the rodent to look for physical contact; in this case, the mouse will preferentially walk along the wall of the box. This parameter is a key indicator of the anxiety level (Denenberg 1969). This so called "periphery" consists in a band large as twice the body of the mouse, 5 cm, all around the box. This software provided measures, among others, of traveled distance, relative distance and time spent in each defined zone (Figure 8).

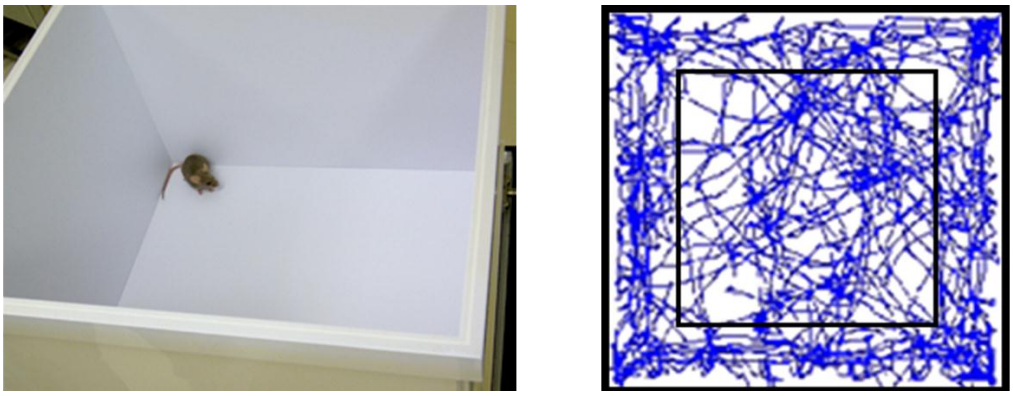

Figure 8: Open Field.

Each mouse is placed in the arena and allowed to freely move about for 30 minutes while being recorded by an overhead camera. The box is divided between a center and a peripheral area of two times the mouse body width. The tracking (in blue) is then analyzed by SMART (Panlab, Barcelona, Spain) tracking software to extract the relative time and distance passed in each zone.

Novel Object Recognition (NOR)

In the NOR memory task, mice were habituated to an open blue cylinder for 2 consecutive days (20 min/d). During training (third day), the mice explored for 20 min two

identical objects, and for testing (fourth day), the animals were presented for 10 min to one of the training objects and to a novel object. The familiar and the novel objects differed in shape, color, and texture and were located in the same positions in which the objects were located during the training session. The use of different objects as novel or familiar, as well as the relative position of the novel object, was balanced between genotypes. The objects consisted in a plastic spinning top and a halogen bulb, both presenting asperities of potential interests for the animal and easy to wash between each trial to avoid odor spreading and consequently bias on the exploration behavior. Time spent exploring the objects in both the training and testing sessions was measured with video-tracking system (SMART; Panlab Spain). The discrimination index (DI) was determined using the following formula: DI = 100 × (time exploring A − time exploring B) / (time exploring A + time exploring B) (Figure 9).

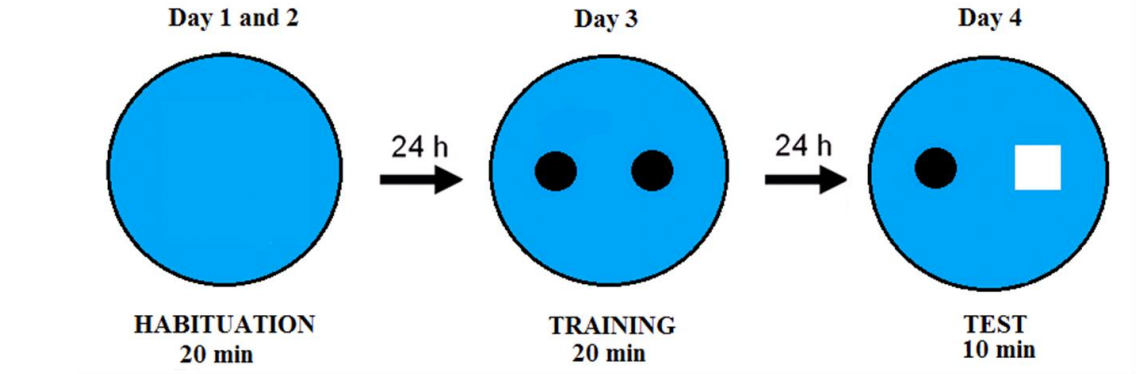

Figure 9: Novel Object Recognition protocol.

Mice were placed for 20 minutes at day in a clean circular area (bucket) during the first 2 days. The 3rd day, they were exposed 20 minutes to 2 identical objects equally splitted between groups. The last day, one of the object was substituted by an unknown one and the relative exploration time measured during 10 minutes.

5.7 - Statistical analysis

Student t-test is commonly applied to determine if two sets of data were significantly different from each other, when the data would follow a normal distribution. Statistical analyses were done using GraphPad Prism 5 software (GraphPad, La Jolla, USA). Alpha values were

considered statistically significant at $P < 0.05$ (*), $P<0.01$ (**) and $P<0.001$ (***), whereas analyses in which $P > 0.05$ were not referred. Means +/- SEM are presented in the figures.

fMRI images acquired were statistically analyzed as previously described.

6 - Results

6.1 - Behavioral results

It has been shown that Long Term Potentiation (LTP) was impaired in IP_3R2 KO mice in a study of in-vivo electrophysiology (Navarrete et al 2012). With the aim to characterize the behavioral phenotype of the IP_3R2 KO mice, we proceeded to a classical behavioral task based on learning and memory: the NOR task. To this purpose, we first had to control whether these mice were expressing a normal anxiety/exploratory behavior in the OF paradigm.

Open Field

Open-field experiments allow the evaluation of animal's basal activity and its evolution, in response to novelty or anxiogenic environment or genetic modification. It is used to determine general activity levels, gross locomotor activity, and exploration habits in rodent models. We tested general activity and anxiety-like phenotype in IP_3R2 KO mice. We investigated the general activity of IP_3R2 KO mice in an OF for 30 minutes. KO mice showed normal locomotor activity comparing to Wild Type (WT). A normal locomotion was evidenced in both measured parameters: distance and time spent in different zones (Figure 1).

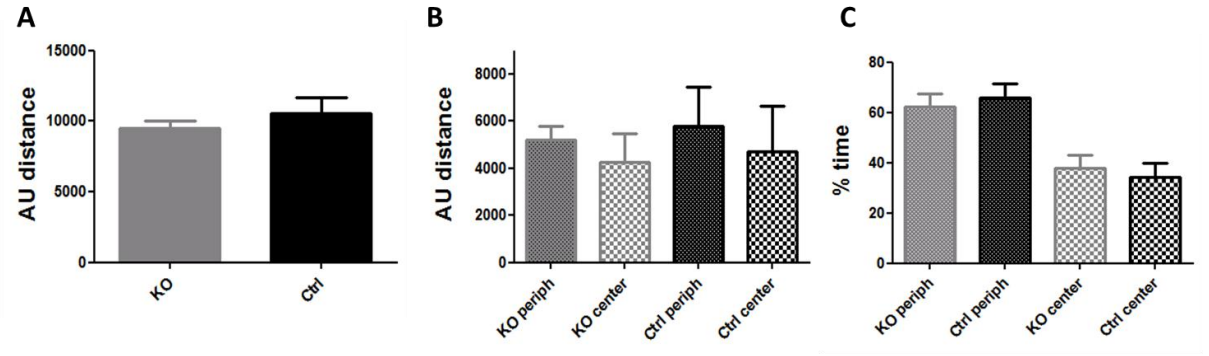

Figure 1: Open field locomotor activity.

WT animals appear in black and KO animals in grey. Mice were placed in an OF and monitored for 30 min using a videotracking system (SMART). A. Total traveled distance (p = 0,42), B. distance repartition by zone (center and periphery, respectively p = 0,54 and p = 0,36)and C. percentage of time spent in the zones were measured for the whole 30-min period (center and periphery, respectively p = 0,61 and p = 0,64). IP3R2 KO mice (n = 9) and WT mice (n = 9) traveled similar distances and spent the same time in the center and in the periphery of the arena. Both groups showed a similar exploratory behavior.

No significant changes in the total distance (t-test, p = 0.42) and the distances in periphery and center was found in either genotype (t-test, respectively p = 0.54 and p = 0.36). This analysis didn't detect any statistically significant differences in percentage of the time spent by IP_3R2 KO mice comparing to wild type in the center of the arena (t-test respectively, p = 0.61 and p = 0.65), a common measure of anxiety. In this anxiety and locomotion measuring task, the IP_3R2 KO mice present the same behavior than wild type mice.

Novel Object Recognition

Next, we examined the performance of IP_3R2 KO mice in a NOR memory task, a non-aversive memory task that relies on the natural exploratory behavior of mice. We assessed recognition memory retention 24 h after training. The experiments did not reveal significant differences between KO and wild type mice (p = 0.127). As expected, control and KO mice spent more time exploring the novel object during testing with a respective Differenciation Index of 0.26 and 0.18. Surprisingly, IP_3R2 *KO* mice spent more time exploring both novel and old object during training and testing *(*respectively p<0.0001 and p < 0.0001*)* despite a similar activity observed in the OF task. These results indicate that mutant mice have normal long-term recognition memory despite a longer exploration time that doesn't have yet clear explanations. No significant difference was observed in the preference between both objects (p = 0.38) (Figure 2).

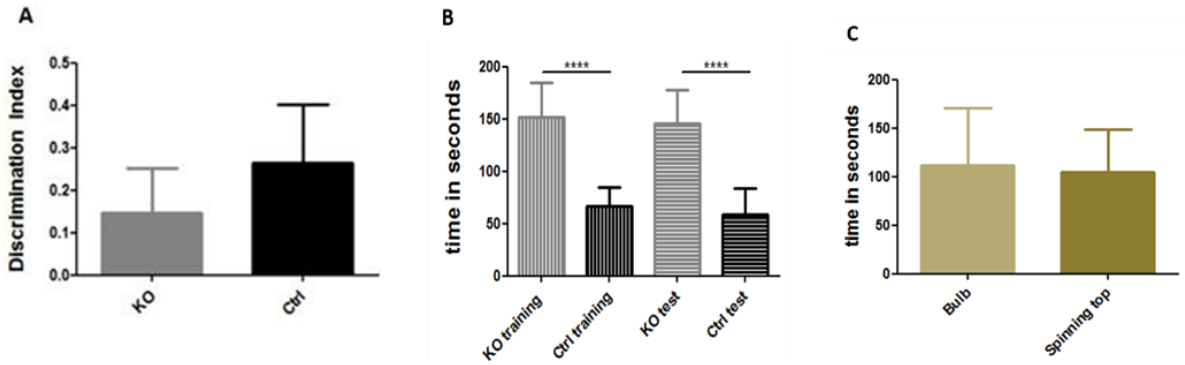

Figure 2: Novel Object Recognition.

WT animals appear in black and KO animals in grey. A. IP3R2 KO mice didn't show impaired long term memory for object recognition when tested 24 h after training (p = 0,127) B. IP3R2 KO mice express a largely significant level of exploration (p<0.0001 in training and test). In both group, n = 9. C. There were no preferences between the 2 objects used during the task (all mice pooled together n = 18, p=0,38).

6.2 - Set up of anesthesia and stimulation protocol

fMRI is usually used in combination with rats and more rarely with mice. Moreover, a brain-implanted electrode in mouse is a first in the fMRI field. Consequently, we needed to set up several parameters of the experiment, including the trial of different anesthetics.
It is important to notice that, in order to give a better idea of the set-up of fMRI images, figure 3 and 4 are presented with EPI instead of anatomical images. Moreover, because this kind of stimulation is a novelty, all these parameters have been studied on WT mice only and not on IP_3R2 KO animals, in order to set up a reproducible and reliable protocol but also to preserve the relative low number of animals available

Anesthesia

To anesthetize mice, we had the choice between few anesthetics commonly used in rodents' experiments: urethane, isoflurane and medetomidine. The mix ketamine/xylazine was immediately excluded as it needs to be reinforced every 45 minutes, which is not long enough for permit fMRI acquisition.

In rats, α-chloralose high doses cause convulsions and impaired LFPs (Huttunen et al 2008). In addition, it has a low analgesic potency; it should not be used for surgical procedures. Its side effects include hypothermia, tremor, respiratory failure and others. It is very toxic and as to be reserved for anesthesia without waking. For these reasons, α-chloralose anesthesia was also excluded.

Urethane has the advantage of relatively disrupt cardiovascular and respiratory physiological parameters. It can be used in rats and it causes a deep anesthesia with very good muscle relaxation. Because it presented the advantage to last all the experiment time with a single anesthesia and because it preserves the physiology (controlled empirically in the lab on rats), we started by trying urethane for the mice anesthesia. It presented a high mortality at the dose of 1.8g/kg in mice and a low BOLD fMRI signal at the dose of 1,7g/kg (data not shown). This, associated with a high rate of death during surgery or fMRI acquisition, pushed us to change anesthetic. We then switched to isoflurane that is commonly used but also present the advantage to be usable for both surgery and fMRI acquisition.

We didn't manage to get a coherent and stable response to PP stimulation in fMRI with isoflurane anesthesia (Figure 3).

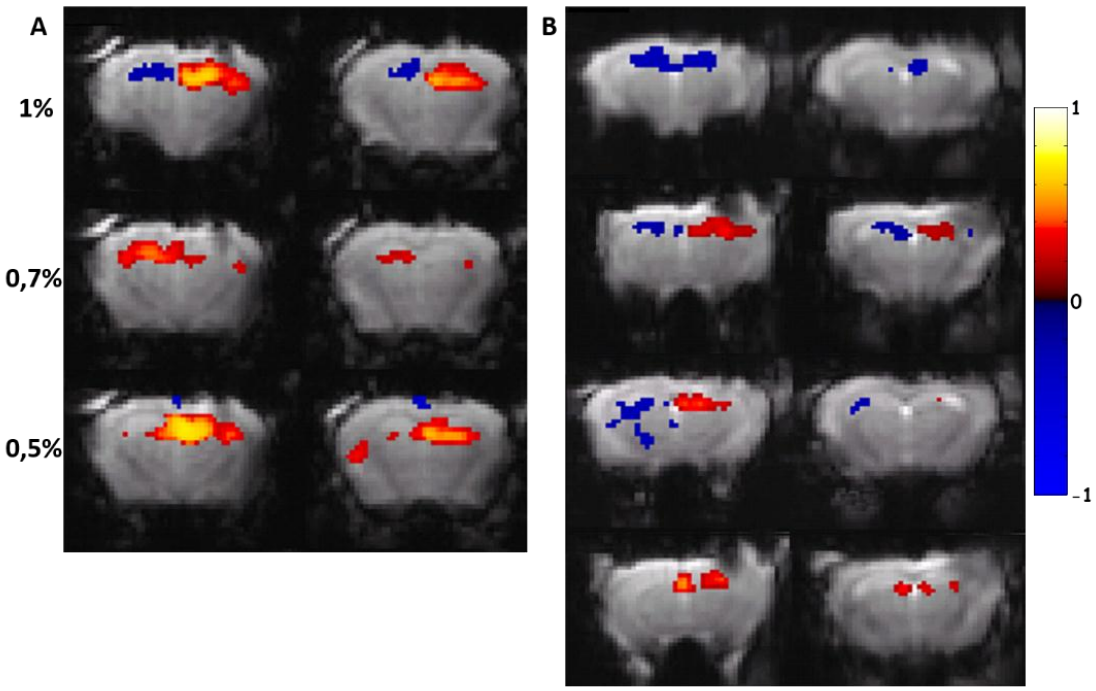

Figure 3: Unstable pattern of BOLD signal in isoflurane anesthetised mice.

A. BOLD signal in the hippocampus of a mouse at decreasing isoflurane levels indicated on the left, after a train of 4 seconds at 10 Hz stimulating the PP. B. BOLD signal at 0,7% of isoflurane in 4 different mice after a identical brief stimulation of the PP.

As shown in figure 3A, the BOLD signal dramatically changed within the same animal depending on isoflurane concentration, including expression of a negative BOLD signal. It indicates that mice are very sensitive to isoflurane concentration. As an example, 4 different BOLD maps from 4 different animals submitted to the same protocol in the same conditions, expressing 4 different BOLD patterns are shown in figure 4B. In conclusion, isoflurane resulted in a bimodal BOLD signal expression and so couldn't be used as a relevant anesthetic in our study.

Currently, since it is known that the BOLD response is highly dependent on CBF (Cohen et al 2002), most fMRI studies tend to avoid isoflurane in order to preserve functional-metabolic coupling (Ueki et al 1992). The α2-adrenergic receptor agonist dexmedetomidine, is now increasingly preferred due to the ease of implementation and, more importantly, because of its option to perform longitudinal experiments in the same animals (Pawela et al 2008, Weber et al 2006, Zhao et al 2008), as its effects can be easily reversed by using the competitive α2 antagonist Atipamezole. It has a sedative and anesthetic duration of about 90 minutes, that was long enough to perform fMRI studies. Similarly to α-chloralose

(Lindauer et al 1993), dexmedetomidine is however known to slightly reduce CBF, as measured by laser Doppler flowmetry in rats (Ganjoo et al 1998), but also to present much less side effects than α-chloralose.

Considering these parameters and our personal results, we finally managed to find a practical combination by using first an isoflurane anesthesia during surgery and then switch to dexmedetomidine for fMRI acquisition (see material and methods). It allowed performing surgery safely, to get reproductible results and a correct signal/ noise ratio that allows relevant images in fMRI.

fMRI protocols

Once the adapted anesthetic chosen, the next step was to optimize the stimulation protocol that was going to be used to stimulate the PP. Starting from empirical data got from the laboratory from previous studies on rats, we needed to adjust the length, frequency and intensity of the stimulation, as described in the material and methods. The intensity of stimulation chosen was depending on the electrophysiological results obtained during the first part of the experiment (previously described) and the pulse length was a standard one. The length of stimulation was chosen long enough to initiate the BOLD signal in the case of the brief stimulation. We used a long stimulation to study the maintenance of the BOLD signal in time but also because Ca^{2+}(i) signaling in astrocytes can be a relatively slow phenomenon, requiring several seconds. The crucial parameters were the length of the protocol and the frequency of stimulation. We tried different frequencies of electrical stimulation based on our own experience and literature: BOLD response under medetomidine sedation has been tested from1 to 18 Hz and was shown to be maximal in the range between 3 and 9 Hz in rats (Nair & Duong 2004, Zhao et al 2008). So we tested different frequencies from 3 to 20 Hz (Figure 4). Consecutively to a 3Hz stimulation of the PP, we couldn't get any significant BOLD responses in the hippocampus, as well as in case of 6 Hz stimulation. 10Hz was giving a nice BOLD signal in both hippocampus and 20 Hz was apparently too strong, generating responses in the right places but also in undesirable areas. It was moreover strong enough for generate artifacts due to brain movements as evidenced by the false positive BOLD response expressed as a tiny band above the brain. From other animals tested (data not shown), we finally concluded that 10Hz was the most adapted frequency in our case. It is also of a coherent scale, matching with the theta rhythm oscillations encountered in the hippocampus. It seemed to us that using 10Hz was a good compromised between getting a nice signal without artifacts, brain damages or eventual synapse saturation. The interval of time between 2 stimulations

was also tested. If 30 seconds are sufficient in rats to permit the BOLD signal to go down to the baseline and to stabilize, it appears that in the case of mice, a 1 minute separation was more adapted (data not shown).

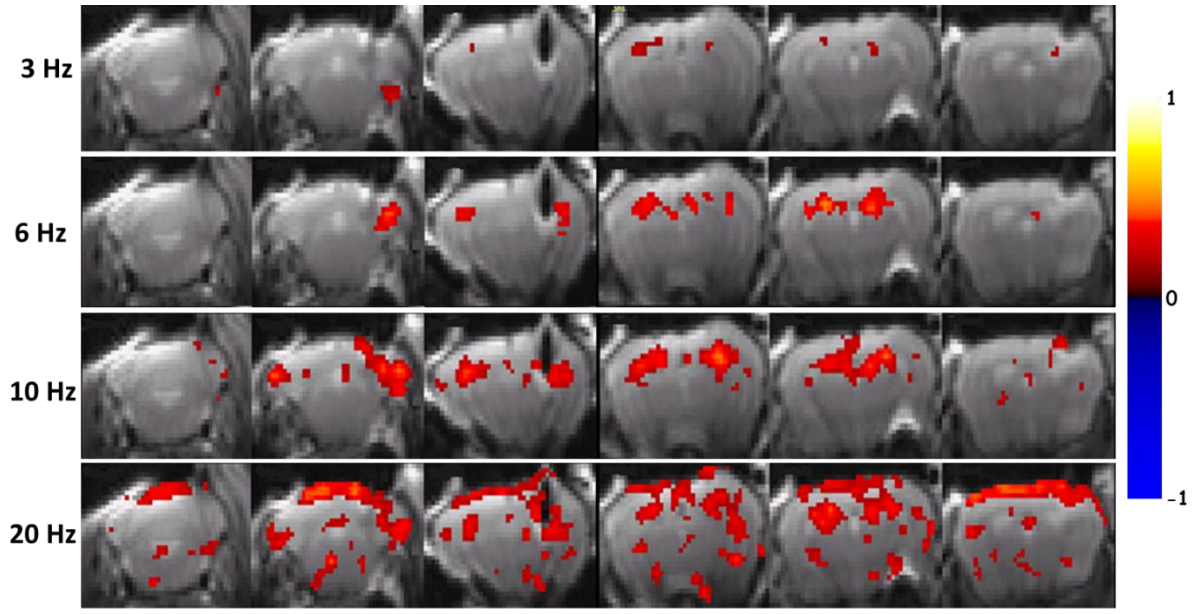

Figure 4: fMRI map of mouse brain after a left Perforant Pathway stimulation at 3, 6, 10 and 20 Hz.

The stimulation consists in 10 repetitions of 4 seconds of 200us pulses at 0,7mA at 3, 6, 10 and 20 Hz respectively from top left to bottom right. While the 3 and 6Hz stimulations show a very light BOLD signal in the hippocampus, the 10Hz stimulation presents a coherent activation in both the hippocamous and the EC. The 20Hz stimulation results in ectopic BOLD signal activations.

In order to confirm the validity of our protocol in terms of fMRI acquisition as well as anesthesia, we performed thalamo-cortical or cortico-cortical stimulation (figure 5) under dexmedetomidine anesthesia, at different intensities (3 to 20 Hz). The objective was to exclude any false positive signal. In this case, we used carbon electrode to reduce the artefact of the electrode. After the corpus callosum stimulation at 10Hz, we obtained a strong global cortical activation consistent with the stimulation of cortico-cortical axons. In the case of the Ventro-Posterior Medial and Ventro-Posterior Lateral nuclei of the thalamus stimulation at 20Hz, we observed a strong cortical activation in addition to the pre-cited nuclei.

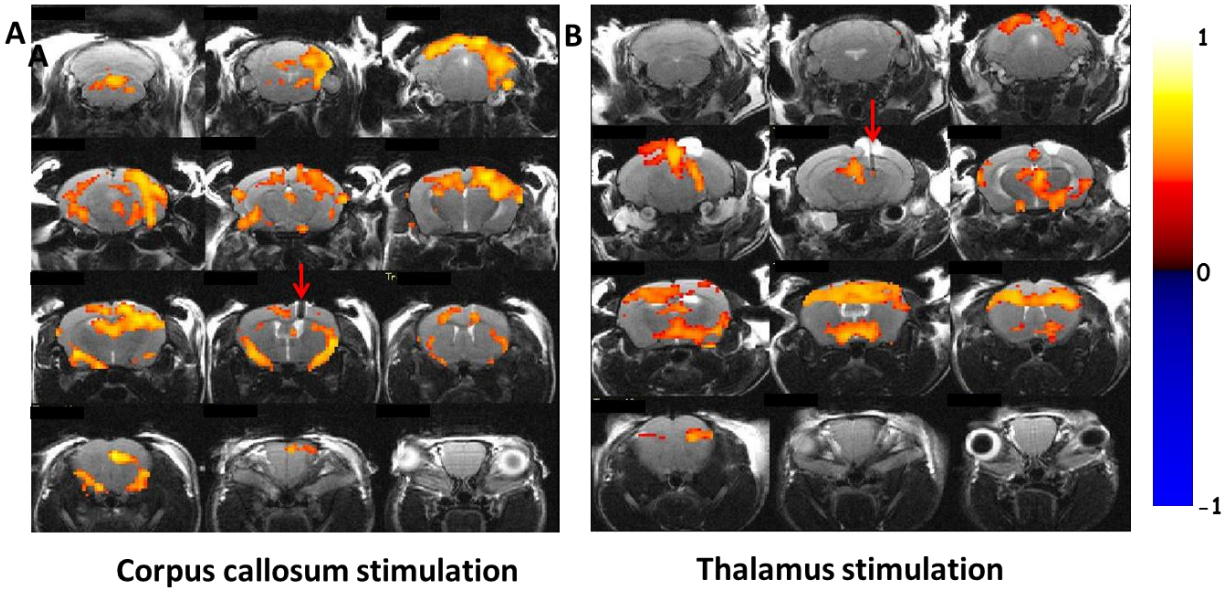

Figure 5: Corpus callosum and thalamo cortical stimulations with carbon electrodes.

A. BOLD fMRI map after statistical treatment. In this case, the Corpus Callosum (CC) (coord from bregma : AP -0,1mm; ML 0,9mm; DV 1,25mm) was stimulated by a carbon electrod (4 seconds, 10 Hz, 1mA). A large part of the cortex is activated, as the strong stimulation used contact a great number of axons. B. Pattern of BOLD signal during a VPM/VPL thalamic nucleus (AP -1,82mm; ML 1,5mm; DV 3,4mm) stimulation of 20 seconds, 20 Hz and 1mA. A strong somatosensory cortex activation can be observed, as well as other brain regions in contact with the thalamus. The red arrows indicate the positioning of the electrode

6.3 - Electrophysiology and BOLD fMRI signal

Electrophysiology

We first searched for the electrophysiological signature of WT animal comparing to IP_3R2 KO animals, by stimulating electrically the Perforant Path and recording LFPs in the DG. For this, we processed an Input-Output curve. The Excitatory Post Synaptic Potentials (EPSPs) are recorded in the molecular layer of the DG and the PS is recorded in the hilus. Every animal has a unique morphology and the electrodes present a relative qualitative positioning between two animals. So that we chose to stimulate in a range that could cover in

all cases the lowest to the highest response. The lowest intensity used here (0.2mA) is in general an intensity generating a very slight response at the contrary of the strongest one (1.2mA) that always corresponded to a saturating response. Another consequence of the lack of similarities between electrode positioning is consequent error bars. In order to compensate this approximation, a lot of animals were used and the regression curve was calculated to facilitate the comparison. Both groups of animals reach maximum PS amplitude of 15mV and maximum EPSP of about 4 mV/ms. For both genotypes, mice were not showing any PS at intensities lower than 0.2mA (0.05 mA tested) and once the threshold of stimulation for get an PS reached (0.2mA), the PS and EPSP get for KO and wild type were not different (Figure 6). At any intensity presented as an input to the DG, the transmission to the hilus and its relative output recording follows a classical I/O curve in WT animal as well as in IP_3R2 KO mice (Figure 7A). The regression curves present a similar slope (Wild Type: 5.83 and KO: 5.49 p =0.879) and Y interception (Wild Type 4.93 and 4.37 p=0.449) (Figure 7B). IP_3R2 KO mice do not present any deficit or enhancement of synaptic transmission between the molecular layer of the DG and the hilus (in other words at a monosynaptic level) regarding LFPs recordings. Based on an I/O protocol of increasing stimulation, the IP_3R2 KO mice have the same electrophysiological signature than wild type animals (Figures 6 and 7).

Brief stimulation of the Perforant Path and initiation of the BOLD signal

The animals were next submitted to the brief stimulation of 4 seconds at an intensity giving half the maximum PS amplitude got in the I/O protocol. This protocol was then performed during fMRI acquisition. From these data, the latency between the output (PS) and the stimulation but also the “power” of the input (EPSP) were analyzed and finally the strength of the output was measured through the amplitude of the PS. It is worthy to notice that LFPs recordings and fMRI acquisition belong to two different time scale. While the LFPs have a milliseconds (ms) precision, the BOLD signal is of the order of the second (s). For this reason, the EPSPs measured by LFPs are pooled together as an average, represented in a histogram. It gives a better representation of what is visualized on the BOLD maps.

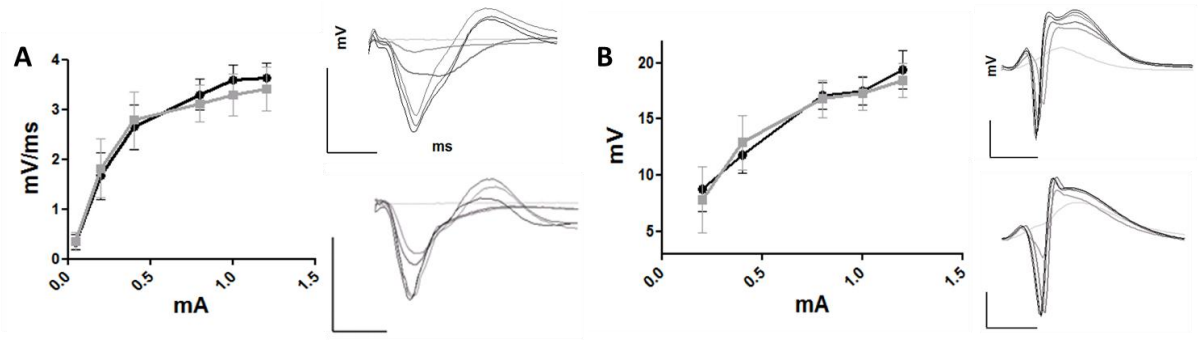

Figure 6: Electrophysiological signature of IP3R2 KO mice by Local Field Potentials (LFP) recordings in the hippocampus during a Perforant Path (PP) stimulation.

WT animals appear in black and KO animals in grey. A. Left, Relevant example of EPSPs recording in the DG during an intensity/response protocol (increasing intensities of 50, 200, 400, 800, 1000 and 1200 uA). Right, overlap of the successive EPSPs in WT (up) and KO (down). B. Left, Relevant example of PSs recording in the DG during an intensity/response protocol (increasing intensities of 200, 400, 800, 1000 and 1200 uA). Right, overlap of the successive PSs in WT (up) and KO (down).

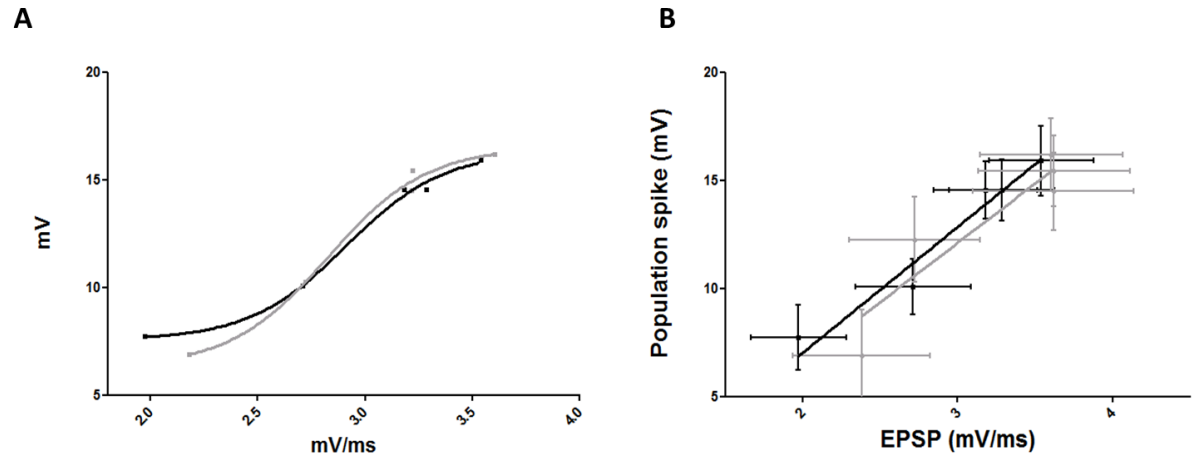

Figure 7: Input/Output profile of IP3R2 KO mice by Local Field Potentials recordings in the hippocampus during a Perforant Path (PP) stimulation.

WT animals appear in black and KO animals in grey. A. I/O curves of a relevant example of WT and KO animal (example from figure 6). B. I/O's regression curves of WT vs KO (n = 18 and n = 11, respectively). Slopes and elevations 5,83 and 5,49; 4,63 and 4,37, p = 0,879 and 0,449 respectively.

A certain number of axons from the EC and projecting to the molecular layer of the DG were electrically stimulated during the train. The EPSP caught from this LFP correspond to the "strenght" of the input to the hippocampus. As it is shown in figure 8, the axonal transmission is strictly similar between IP3R2 KO mice and their wild type. The EPSPs reaching the DG present the same profile and strength, as well as the same adaptation in time after repetitive inputs. The average of EPSPs measured is also similar in both genotypes (p = 0.58).

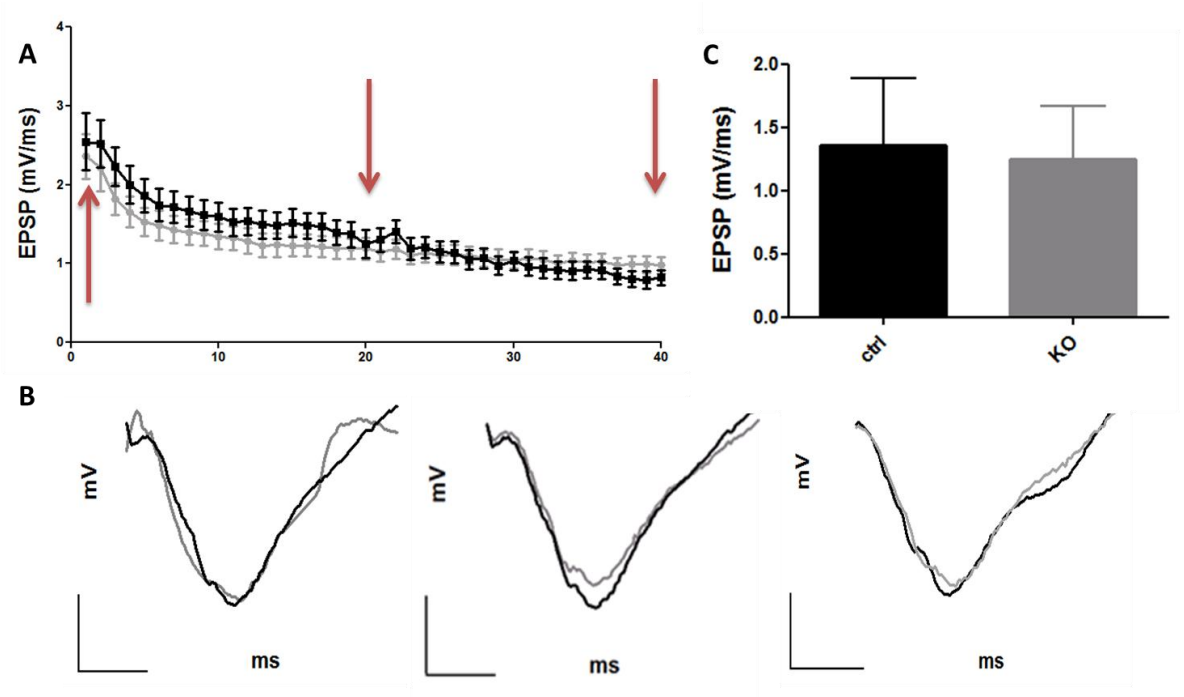

Figure 8: EPSPs slope in the DG during the brief stimulation of 4 seconds at 10hz

WT animals appear in black and KO animals in grey A. EPSPs behavior along the train of the brief stimulation (n = 18 for the WT and n = 11 for the KO). B. Relevant examples of an initial, intermediate and final EPSP, recorded at the respective red arrows C. Average of EPSP slope for each strain. (t-test p=0,579).

The PS measured in the hilus of the DG can be considered as the transmission of the initial stimulation after the first synapse. The PS behavior during the train is similar between groups although the PS in WT mice presents the tendency to superate the one in KO mice. In average, the output doesn't present significant difference (p = 0.19, Figure 9). The monosynaptic transmission is not significantly affected in IP3R2KO mice.

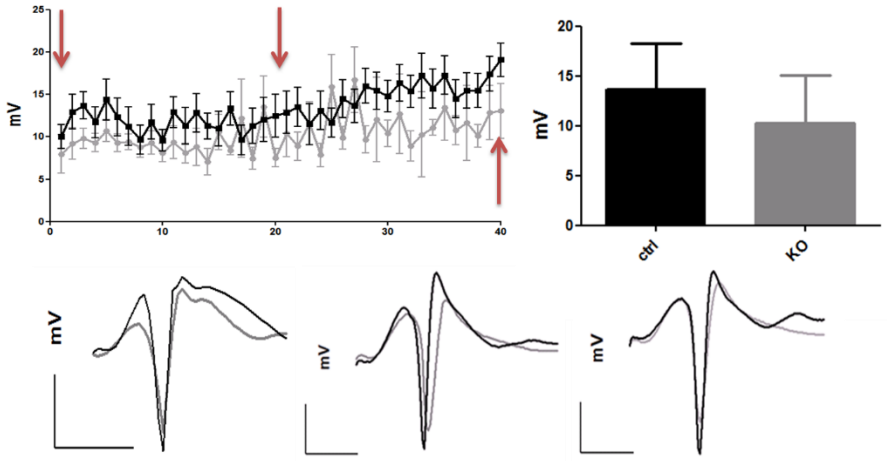

Figure 9: Population Spike amplitude in the DG during the brief stimulation of 4 seconds at 10hz.

WT animals appear in black and KO animals in grey A. PS behavior along the train of the brief stimulation (n = 18 for the WT and n = 11 for the KO). B. Relevant examples of an initial, intermediate and final PS, recorded at the respective red arrows C. Average of PS amplitude for each strain. (p=0,19).

No difference could be observed in the latency of appearance of the PS after a train of stimulation of the PP. Both group showed a similar pattern: the first spikes appear after 5,5ms, and then it increases slowly for 1 second until 6ms approximately. Confirming the PS recordings conclusions presented above, it seems that the lack of IP_3R2 receptor doesn't influence the transmission in a single synapse during a brief stimulation (Figure 10).

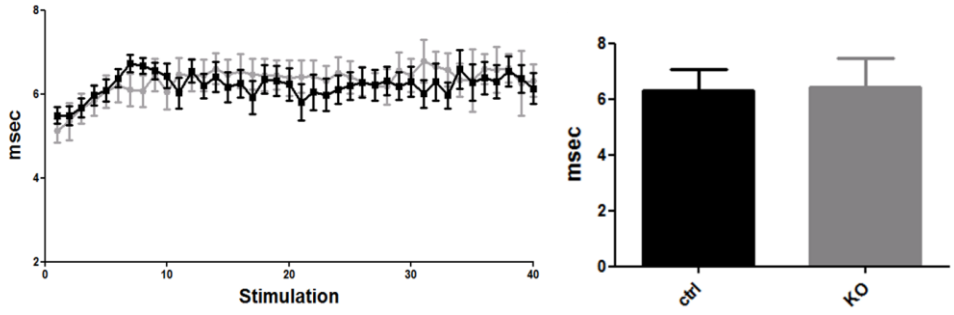

Figure 10: Population Spike latency in the DG during the brief stimulation of 4 seconds at 10hz.

WT animals appear in black and KO animals in grey A. PS latencies along the train of the brief stimulation (n = 18 for the WT and n = 11 for the KO). B. Average of PS latencies for each strain. (p=0,79).

The brief train of stimulation within the magnet for fMRI acquisition didn't give any significant differences between the IP_3R2 KO mice and their corresponding controls. As shown in figure 11A, PP stimulation with this protocol generates a nice BOLD response in the ipsilateral and contralateral hippocampus of both mice. Once the number of voxels activated measured in the restricted zone of the dorsal hippocampus, the activation in both groups is quantified (Figure 11B). No significant difference is observed. The same tendency is noticed in the intensity of BOLD signal, expressed in % of increase. The ipsilateral and contralateral hippocampi were activated in the same way in both groups, highlighting an identical neuronal activity due to the EC projections to the hippocampus and the intra-hippocampal communication.

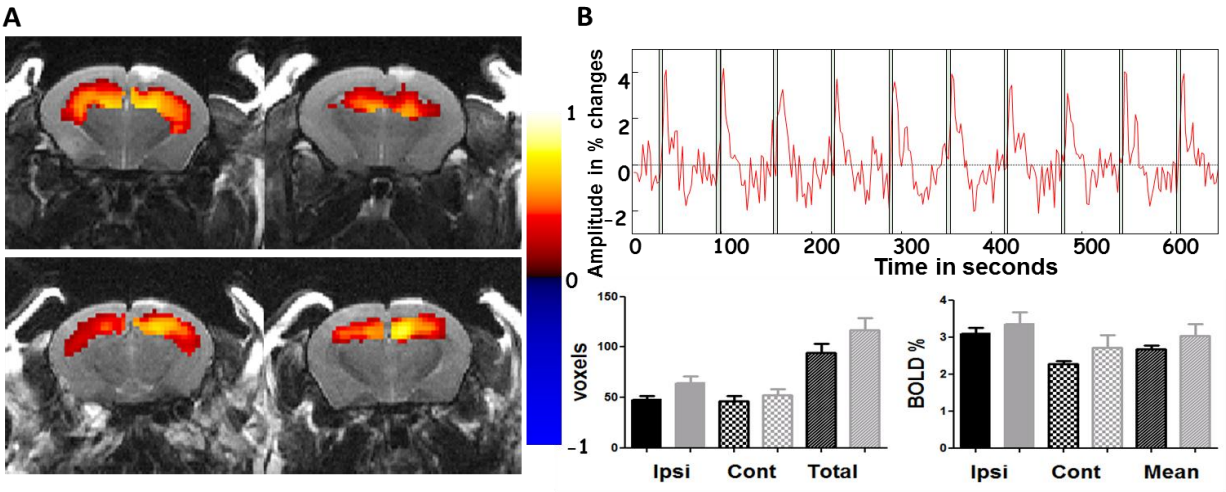

Figure 11: BOLD signal after a brief stimulation of the Perforant Path.

WT animals appear in black and KO animals in grey A. Relevant example of BOLD fMRI signal in the hippocampus in WT (up) and KO (down) after a 4 second stimulation of the PP at 10Hz. B. (up) Relevant example of a time course during a short stimulation. The stimulation periods are in blue. (Down) Left, Number of voxels activated during 4 seconds stimulation in the ipsilateral HP (ipsi), contralateral HP (contra) and in total ($p = 0.44$; $p = 0.14$ and $p = 0.23$ respectively); Right, BOLD activation during 4 seconds stimulation in the ipsilateral HP (ipsi), contralateral HP (contra) and in average ($p = 0.44$; $p = 0.14$ and $p = 0.23$ respectively) (WT n = 11; KO n = 9).

After raw data analysis in Matlab, the BOLD signals got were averaged for each single animal. All of them were then pooled together, in order to get a precise shape of the BOLD

signal occurring in the hippocampus. The graph (figure 12) presents the intensity of the BOLD signal all along the brief stimulation protocol, composed of 4 seconds of stimulation spaced by one minute, repeated 10 times in 3 different sessions. IP_3R2 KO mice show the same BOLD signal's shape than WT in this case of short stimulation. There is a slight variation around the baseline during the resting state that can be considered like noise or imperceptible movements of the brain during the acquisition. Once the stimulation occurred, the latency of the hyperemic response is about 2-3 seconds in both groups. Then, the BOLD signal increases for 4 seconds to reach a maximum at +/- 3%. In both groups, the hyperemic response goes back to the baseline after 12 volumes, or 24 seconds approximately. Surprisingly, the IP_3R2 KO mice present a BOLD signal after PP stimulation. This response is strictly similar to the WT animals (Figure 12).

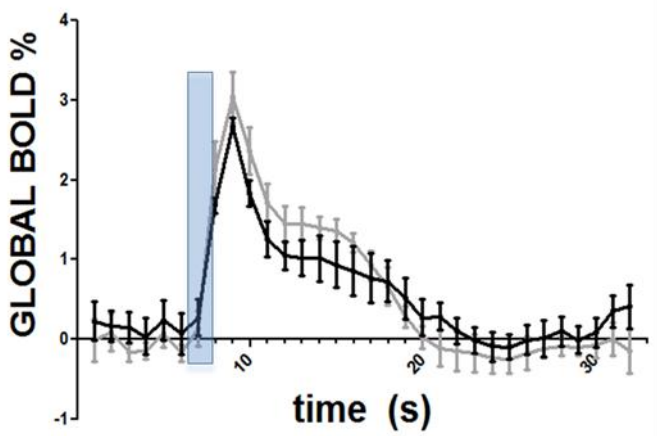

Figure 12: Global BOLD signal shape during the brief stimulation.

WT animals appear in black and KO animals in grey. The 4 seconds stimulation period appears in blue. It represents the average of 3 repetitions of 10 stimulations per animal (WT n = 11; KO n = 9).

Long stimulation of the Perforant Path and maintenance of the BOLD signal

In order to test the hypothetical role of IP_3 dependent astrocyte Ca^{2+}(i) signaling not only in the initiation of hyperemia but also in its maintenance, animals were submitted to a longer stimulation. The frequency and intensity of stimulation were kept but the duration was rise up to 20 seconds. The analyses were the same than in the case of the 4 seconds stimulation.

The PS amplitude in the DG increases regularly during the long stimulation, probably by potentiation, until 7 seconds of stimulation, to stabilize around 20/22 mV. Surprisingly, the IP_3R2 KO mice's PS amplitude decreases slowly from 12 seconds of stimulation until the end of the protocol, while the WT PS amplitude is stable until the end. Calculating the average of these PS, no significant difference appears but the tendency is obvious (Figure 13).

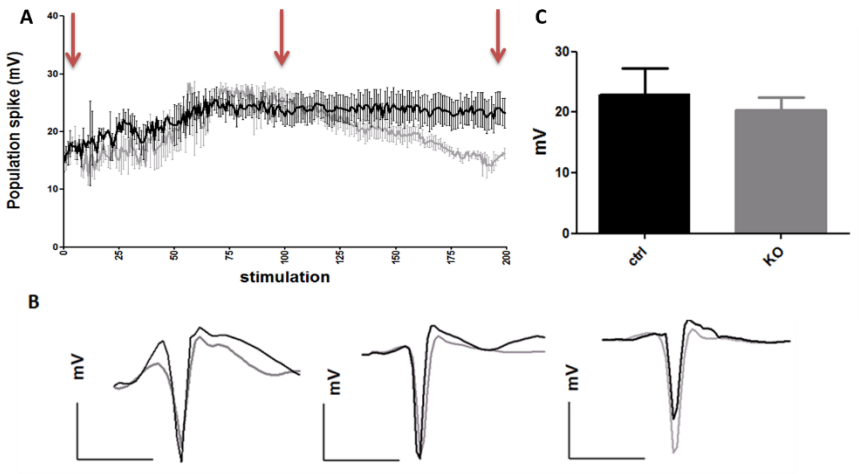

Figure 13: Population Spike amplitude in the DG during the long stimulation of 20 seconds at 10hz.

WT animals appear in black and KO animals in grey A. PS behavior along the train of the long stimulation (n = 5 for the WT and n = 3 for the KO). B. Relevant examples of an initial, intermediate and final PS, recorded at the respective red arrows C. Average of PS amplitude for each strain. (p=0,10).

Contrary to the PS amplitude in this 20 seconds stimulation protocol, the EPSPs slope in the DG in WT and IP_3R2 KO mice follow the same pattern, even after 12 seconds. There is also no difference in the average slope of these EPSPs. However, the same tendency can be observe; that is to say that IP_3R2 KO mice seem to express slightly lower EPSP slopes. In conclusion, it seems that IP_3R2 KO mice present a deficit of maintenance of the synaptic strength at the end of this protocol of 20 seconds of consecutive stimulation (Figure 14).

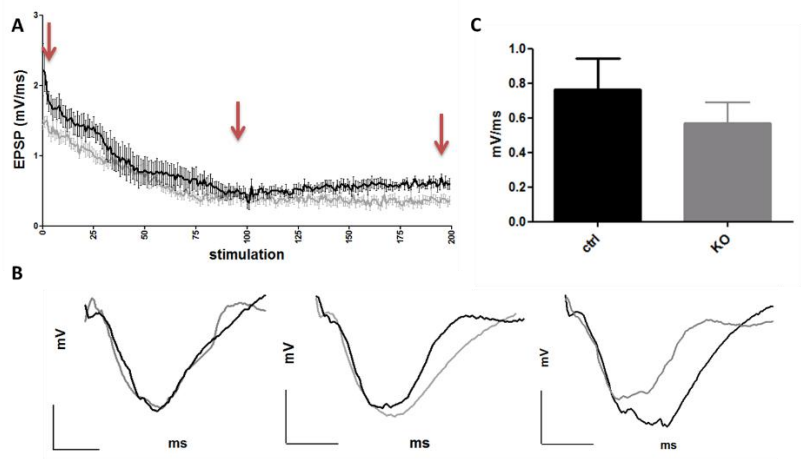

Figure 14: EPSPs slope in the DG during the long stimulation of 20 seconds at 10hz.

WT animals appear in black and KO animals in grey. A. EPSPs behavior along the train of the longstimulation (n = 5 for the WT and n = 3 for the KO). B. Relevant examples of an initial, intermediate and final EPSP, recorded at the respective red arrows C. Average of EPSP slope for each strain. (t-test p=0,156)

A slight deficit has been observed in the PS amplitude after 12 seconds of stimulation in the DG of IP_3R2 KO mice. When the latencies of these PS during the long stimulation of the PP were measured, nor difference neither tendency could be observed in these same mice. The latency, as it was for the short stimulation, is maintained around 5 ms during the first seconds of stimulation for increase slowly until the end, in both groups (Figure 15).

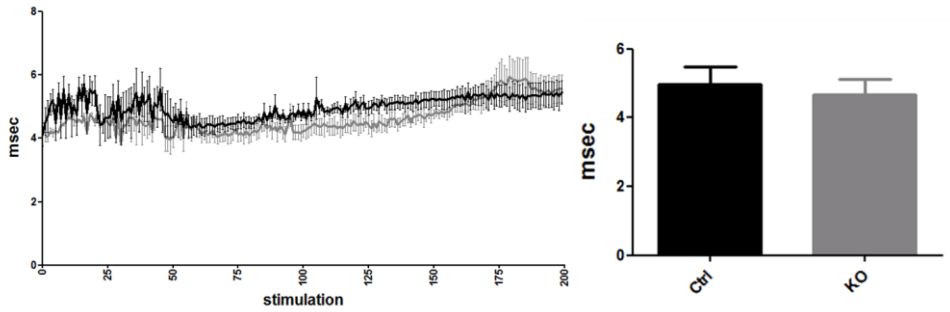

Figure 15: Population Spike latency in the DG during the long stimulation of 20 seconds at 10hz

WT animals appear in black and KO animals in grey. A. PS latencies along the train of the long stimulation (n = 5 for the WT and n = 3 for the KO). B. Average of PS latencies for each strain. (p=0,42).

In the case of the long stimulation, both groups of mice expressed a BOLD signaling pattern. A strong expression can be observed in the ipsi and contralateral hippocampi as well as in the EC. The intensity of the signal, express in % of increase from the baseline, and the volume (number of voxels) activated is identical in both groups (Figure 16).

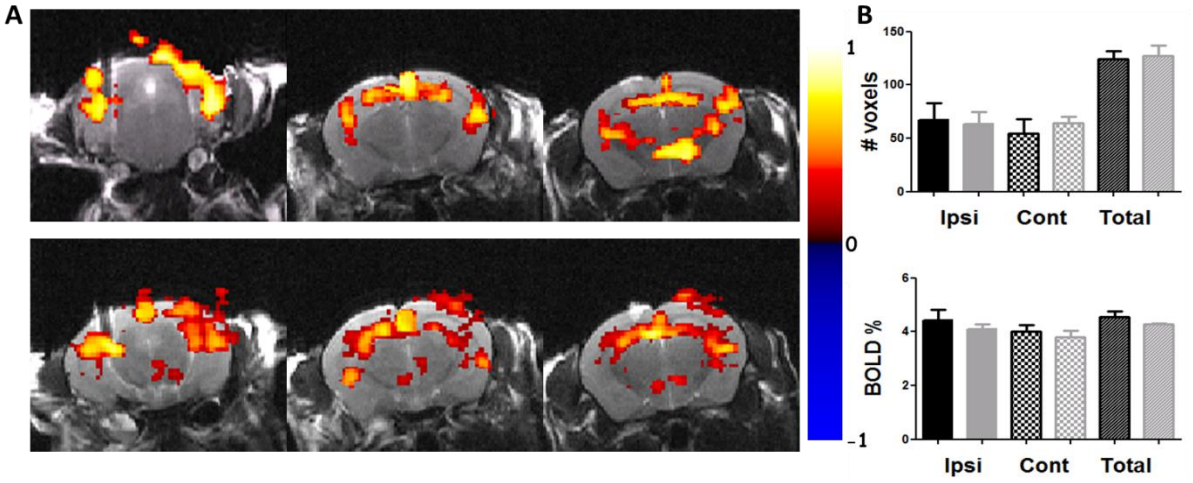

Figure 16: BOLD signal after a long stimulation of the Perforant Path.

WT animals appear in black and KO animals in grey. A. Relevant example of BOLD fMRI signal in the hippocampus in WT (up) and KO (down) after a 20 second stimulation of the PP at 10Hz. B. *Up*, Number of voxels activated during 20 seconds stimulation in the ipsilateral HP (ipsi), contralateral HP (contra) and in total ($p = 0.86$; $p = 0.56$ and $p = 0.84$ respectively); *Down*, BOLD activation during 20 seconds stimulation in the ipsilateral HP (ipsi), contralateral HP (contra) and in average ($p = 0.54$; $p = 0.46$ and $p = 0.29$ respectively) (WT n = 3; KO n = 3)

The BOLD signal‘s shape in the case of the 20 seconds stimulation doesn’t present differences between the WT and IP_3R2 KO mice (Figure 17). The BOLD signal appears 2-3 seconds after the stimulation and increases regularly until the end of the stimulation. It reaches a maximum of 4% in both groups of mice. Then the hyperemic response goes back to baseline after about 20 seconds. Even if we could observed a slightly different electrophysiological signature during the long stimulation, the BOLD signal of the IP_3R2 KO mice doesn’t reflect it, and follows the one of the WT. It puts in evidence that IP_3R2 dependent Ca^{2+}(i) signaling is not relevant for the maintenance of functional hyperemia in these conditions (Figure 17).

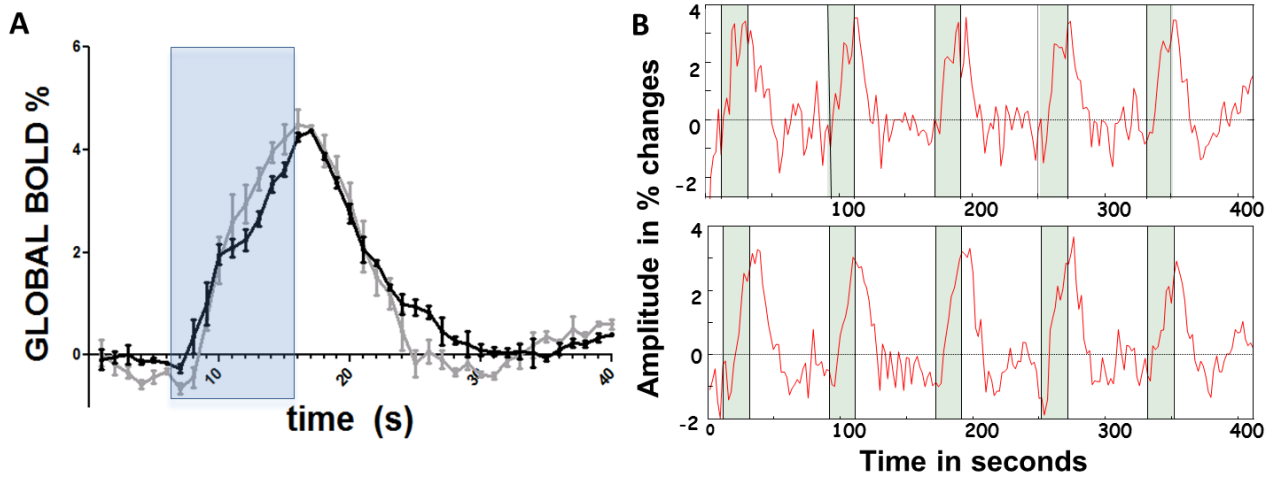

Figure 17: Global BOLD signal shape during the long stimulation.

WT animals appear in black and KO animals in grey. Global BOLD signal shape during 20 seconds stimulation, the stimulation period is in blue. It represents the average of 3 repetitions of 5 stimulations per animal (WT n = 3; KO n = 3). B. Relevant example of a time course during 20 seconds stimulation (Up, WT; Down, KO). The stimulation periods are in blue.

Local Field Potentials recordings in the CA1 region of the hippocampus

To deepen the observation that synaptic transmission seems to be impaired in IP_3R2 KO mice after a long stimulation, we looked the EPSP slope and the latency of its appearance in the CA1 region of the hippocampus. The stimulation's intensity was too weak to generate a PS in the subiculum, and anything was measurable.

Interestingly, by measuring the EPSP latency in CA1, a significant difference could be observed. Indeed, in the WT animals, the initial stimulations of PP reach the CA1 region after 14 ms. It increases slightly but regularly until a plateau around 16 ms. At the contrary, the IP_3R2 KO mice latency follow the WT one until 8-10 seconds but continue rising up until around 20 ms, at the end of the stimulation,. Pooling all the EPSPs latencies, the IP_3R2 KO one is significantly higher (16, 19 ms in WT against 18,68 ms in IP_3R2 KO mice, p = 0,0095) (Figure 18). This difference has to be put in parallel with the previously observed tendency that PS amplitude decreased after few seconds of stimulation in the hilus of the DG. It could underlie that the tendency of deficit of synaptic transmission observed in the DG after long PP stimulation is enhanced in the CA1 region, as a consequence of additional synapses passed.

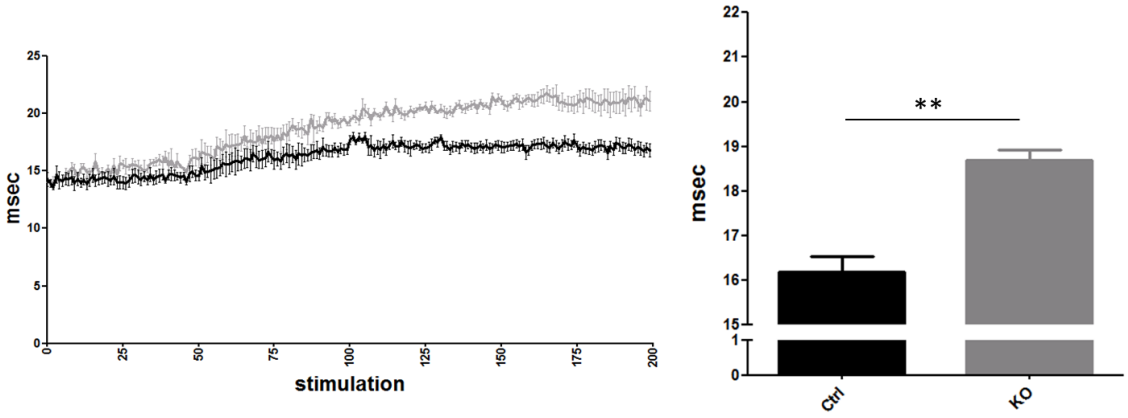

Figure 18: Population Spike latency during the long stimulation of 20 seconds at 10hz in the CA1 region of the hippocampus.

WT animals appear in black and KO animals in grey. A. PS latencies along the train of the long stimulation (n = 5 for the WT and n = 3 for the KO). B. Average of PS latencies for each strain. (p=0,009).

When the EPSP slope was measured in the CA1 region during long stimulation, we couldn't extract a significant difference because of huge error bars due to the low number of animals. Despite this, it appears that, even if IP_3R2 KO mice follow the same trend than WT mice, the average of EPSP's slope is slightly lower than the WT (WT at 0.84 mV/ms and KO at 0.59 mV/ms, p = 0.11) (Figure 19).

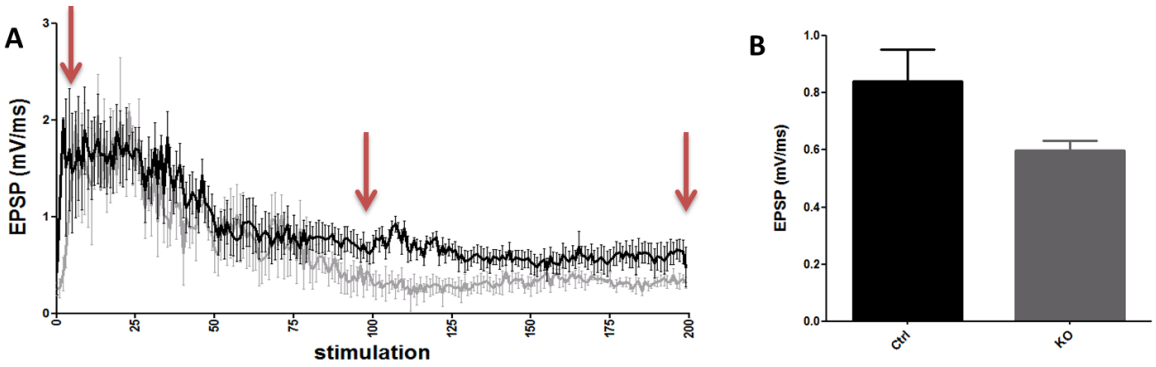

Figure 19: EPSPs slope during the long stimulation of 20 seconds at 10hz in the CA1 region of the hippocampus.

WT animals appear in black and KO animals in grey. A. EPSPs behavior along the train of the long stimulation (n = 5 for the WT and n = 3 for the KO). B. Average of EPSP slope for each strain. (t-test p=0,12).

Here again, at the beginning of the stimulation, IP_3R2 KO mice EPSPs are similar to the WT ones, but after 8-10 seconds, the IP_3R2 KO EPSPs look smaller than the WT ones, revealing a weaker input. The decay seems to be correlated with the tendency of impairment of synaptic transmission observed in IP_3R2 KO mice and described previously. IP_3R2 KO mice seem to present a deficit in the maintenance of synaptic strength at a single synapse. This deficit look increased throughout several synapses.

7 - Discussion

7.1 - fMRI set up

First of all, we perform for the first time, at our knowledge, fMRI on mice implanted with a brain electrode. We managed, in this study, to get reliable and reproductive images of BOLD signaling in mouse brain. As it has been previously exposed, we faced few critical problems among which the choice of isoflurane has been the most challenging. Despite these apparent positive BOLD reports of isoflurane as a gaseous anesthetic with the advantage of good control over anesthesia depth and fast recovery, it is known to be a suppressor of neuronal activity and a potent vasodilator. It is currently used for fMRI experiments on rats, but we got unstable results in mice, including a bimodal response in some cases at low level of anesthesia (0.5-0.75%). As a negative BOLD signal doesn't necessarily reflect a synaptic inhibition (Alvarez-Salvado et al 2014), we can suppose that isoflurane lead to changes in blood circulation. At other level currently used (1% or more), the BOLD responses was extremely low or null. Some past studies employed low levels of isoflurane to measure changes in CBV following hindpaw stimulation (Mueggler et al 2001), or BOLD change (Nair & Duong 2004). In these studies, electrical stimulation of the hindpaws ranged up to 6 mA, which is quite high but was required, most likely because isoflurane strongly suppresses neural activity. Isoflurane decrease the amplitudes of evoked potentials by 54% and increase CBF by 45% (Masamoto et al 2007). In our case, to avoid tissue damage, we couldn't reach this intensity of stimulation. Finally, it appears that isoflurane is unadapted to mice in fMRI studies in case of intra-cranial stimulation.

It is important to understand that the challenge of this kind of stimulation in mice comparing to rat, is that the metallic electrode creates an consequent artefact proportionally to the size of the brain. However, by using a stimulation point spaced from the region of interest (i.e. EC vs Hippocampus), we obtain BOLD signal in the hippocampus free of artefact. To reduce the artefact in the region of stimulation, we used a carbon electrode to stimulate the cortex (corpus callosum stimulation) or the thalamus (VPM/VPL stimulation). Here again, we got reliable and reproducible images of BOLD signaling.

In conclusion, intra-cranial stimulation permits a direct approach of a structure or a network, eluding the problem of potential physiological adaptations in case of poly synaptic stimulation, even more when different brain structures or nuclei are involved. This technic can be coupled with the advantages that mice present in research (mainly transgenesis). By

performing BOLD fMRI on mice with direct electrical brain stimulation, we open the way to several studies.

Our main objective was to study the hypothetical role of IP_3-Ca^{2+}(i) signaling in astrocytes using knockout mice for the subtypes 2 of IP_3 receptor. We first show that these mice do not present a deficit in a memory task. Secondly, we surprisingly discovered that these KO mice express a normal BOLD signal in fMRI, highlighting the irrelevance of IP_3 Ca^{2+}(i) signaling in astrocytes in both the initiation and the maintenance of functional hyperemia. Finally, and unexpectedly, Local Fields Potentials recordings in the hippocampus bring out that synaptic transmission strength is impaired in IP_3R2 KO mice, in case of a sustained stimulation.

7.2 - Neurovascular coupling

Astrocyte, and more particularly Ca^{2+}(i) signaling in astrocytes, is largely believed to be crucial in neurovascular coupling. It had been show by many groups that astrocytes are involved in this phenomenon linking neuronal activity to vasodilation. Due to their strategic location between synapses and vessels, they have been legitimately believed to be or the initiators or the relays of oxygen and glucose supplies to neurons.

It had been shown few years ago that blocking of glutamate receptors on astrocytes was largely decreasing functional hyperemia (Zonta et al 2003), and then that IP_3 injection in astrocytes leads to Ca^{2+}(i) rising and vasodilation of neighboring vessels (Metea & Newman 2006). However, a main caveat of these studies is that they have been mainly done *in vitro*, where the intrinsic vasoconstriction of vessels is largely modified even suppressed.

It was thus normal that the next step consisted in studying this mechanism *in vivo*, and IP_3R2 KO mice have been generated. It was expected a decrease more or less pronounced of vasodilation following sensitive or electrical stimulation. Surprisingly, we didn't observe any difference in the BOLD fMRI signal between KO mice and WT during 4 seconds stimulation. Considering that Ca^{2+}(i) releases in astrocyte occurs few seconds after the stimulation, it had also been proposed that IP_3 dependent Ca^{2+}(i) signaling in astrocytes was necessary for the maintenance rather than its initiation of functional hyperemia. We measured the BOLD fMRI response in case of a long stimulation of 20 seconds and here again, we didn't notice any

impairment in IP_3R2 KO mice. In both protocols, the number of voxels, representing the volume of tissue activated, the intensity of the BOLD signal and the shape of the hyperemic response were strictly similar between genotypes.

These results have to be put in parallel with two publications from other labs that went out at the same moment than our study. They show that "cerebral blood flow modulation by basal forebrain or whisker stimulation can occur independently of large cytosolic Ca2+ signaling in astrocytes" (Takata et al 2013) and that "*In vivo* stimulus-induced vasodilation occurs without IP_3 receptor activation and may precede astrocytic calcium increase" (Nizar et al 2013). In the first case, they use Laser Doppler flowmetry to measure CBF variations around the laser irradiated area at the surface of the brain after whisker of Meynert Nucleus electrical stimulation. These experiments showed that whisker stimulation-triggered hyperemia is also preserved in the absence of cytosolic Ca2+ elevations in astrocytes. In the second publication, they measure vessel diameter by 2-photon microscopy in the cortex after electrical paw stimulation. They demonstrated that *in vivo*, the onset of astrocytic Ca^{2+}(i) increases in response to a sensory stimulation can be delayed compared to the onset of arteriolar dilation, and thus excluding a role of IP_3R2 in the initiation of functional hyperemia. Therefore, we exclude the possibility that internal stores of Ca^{2+}(i) in astrocytes play a crucial role in vasodilation (by increasing inter astrocytic communication, by influencing intra astrocytic signaling or both phenomenon at the same time).

Our approach presents several advantages. First of all, we are using BOLD fMRI to understand the subjacent cellular mechanisms leading to vasodilation. fMRI is a fundamental tool to investigate human brain networks and the understanding of the underlying mechanisms is crucial to better applications inhuman medicine. At the same time, fMRI gives an access to a global view of the brain vasomotricity with a good spatial precision, when 2-photon microscopy and Laser Doppler Flowmetry focus on a spatially restricted area. This parameter is highly relevant considering that; functional hyperemia should not be considered at the scale of very localized area of the order of the hundreds of micrometers. Indeed, changes in vessel diameter occur in a crescent way along the vasculature to reach a maximum at the nutrients demanding area. Especially since the used stimulations in the previous studies are strong and thus, a considerable amount of neurons, synapses and astrocytes are engaged in the phenomenon. Furthermore, astrocytes, a supposed key player in this phenomenon, are known to communicate with each other and have the capacity to work as a syncytium, interconnecting a large volume of brain tissue. For all these reasons, fMRI appears to be a

more adapted tool to study neurovascular coupling in-vivo, as it allows a more global and spatially precise view of the physiological responses, of the order of the millimeter.

Secondly, in both studies, the authors used a polysynaptic stimulation, whether they are whisker or paw stimulation. By using this kind of stimulation, a physiological adaptation can be envisaged. Indeed, during the long whisker stimulation used by Takata *et al*., plenty of synapses are engaged and several structures are relaying the stimulus (notably the thalamus in case of somatosensory stimulation). A compensation mechanism could compensate the lack of Ca^{2+}(i) signaling in astrocytes. In our protocol, we used PP stimulation, thus depolarizing the long range axons directly targeting the hippocampus from the EC. Therefore, we got a response representing a direct and unbiased synaptic transmission. Finally, 90% of synapses in the hippocampus are enclosed by perisynaptic astrocytic processes (Patrushev et al 2013).It is so adapted to study neurovascular coupling.

Altogether, these results logically question the role of astrocyte in neurovascular coupling. It seems that Ca^{2+}(i) dependent pathways can be discarded to be the potential responsible of vasodilation following neuronal activities. Nevertheless, the role of astrocytes in this phenomenon cannot be definitively excluded for few reasons. First, IP_3 dependent Ca^{2+}(i) signaling is the main store of Ca^{2+}(i) in astrocyte but is not exclusive. A small amount of Ca^{2+}(i) is available apart from the endoplasmic reticulum and could be sufficient to trigger metabolic pathways leading to vasodilation. Secondly, Ca^{2+}(i) independent pathways exist within astrocytes and could be also responsible of vasodilation. Finally, the mice that have been used for these studies are constitutive knock out and do not present any phenotypic impairment. It cannot be excluded that they developed mechanisms of substitution to trigger vasodilation.

7.3 - Electrophysiology

It is now clearly established that astrocytes are a fully active part of the synapse (Araque et al 1999). The facts that they can uptake and release neurotransmitters, and also specific gliotransmitters, that astrocytes form a kind a syncytium and can communicate together at relatively long distances highlight their capacities to actively modulate synaptic

transmission, in some ways that starts to be established and others that remains poorly understood.

In addition to the fMRI studies in IP_3R2 KO mice, we also recorded LFPs in the hippocampus after Perforant Path stimulation. It has been show that LFPs are highly correlated with BOLD signal in fMRI (Canals et al 2009, Logothetis et al 2001) but the mechanisms underlying the fMRI signals are not fully understood, generating uncertainties about the quantitative neurophysiological translation of the recorded vascular signals. So, in order to compare the potential impairment of vasodilation, we recorded LFPs in the same protocol used in fMRI. As said above, we didn't find difference in functional hyperemia in IP_3R2 KO mice but, at the contrary, we found an unexpected deterioration of synaptic transmission strength in the hippocampus of these mice.

We didn't observe any differences in the KO mice comparing to WT when performing "single shot" protocols such as I/O, where the different inputs are separated in time by 30 seconds. We can suppose that the cytoplasmic available $Ca^{2+}(i)$ is sufficient to all the cellular pathways involved during a single synaptic transmission and intracellular stores of $Ca^{2+}(i)$ are not required during a punctual, time-limited input.

By performing the brief stimulation protocol, the amplitude of the PS in the DG was slightly, although not significant, lower in IP_3R2 KO mice than in WT mice while the latency of its appearance and the slope of the EPSPs were similar. When we performed the long stimulation protocol, we noticed a confirmation of this tendency. In the DG, after 12 seconds of sustained stimulation, the amplitude of PS in IP_3R2 KO mice abruptly collapse and EPSPs slopes smoothly decrease. To confirm it, we had a look at further synapses, in the CA1 region of the hippocampus. We couldn't measure any PS, but we observe a tendency of IP_3R2 KO mice EPSPs slopes to be once again, smaller that the respective WT. The latency of appearance of the EPSP in CA! was significantly longer in IP_3R2 KO mice. Altogether, these results go in the sense of an impairment of synaptic transmission in IP_3R2 KO mice. Unfortunately, we were restricted by the number of animals and we could observe mainly tendencies instead of significant differences. So far, it seems that the strength of synaptic transmission decrease in mice lacking IP_3 dependent $Ca^{2+}(i)$ signaling. This deterioration starts slowly at the first synapse but seems enhanced at each synapse crossed, as if this impairment was in a certain way "cumulative". It reveals the importance of $Ca^{2+}(i)$ signaling in astrocytes for synaptic transmission. For instance, in 1997, it has been showed that synaptic efficiency is enhanced by glial cells *in vitro*. Glial cells increased by 12-fold the action potential-independent quantal release (Pfrieger & Barres 1997). In more a recent paper, a

group shows that Astrocytic Ca(2+) waves mediate activation of extrasynaptic NMDA receptors in hippocampal neurons (Dong et al 2013). Finally, Ca^{2+}(i) increases in astrocytes have been shown to induce Ca^{2+}(i) responses in neighboring neurons (Bezzi et al 1998, Parpura et al 1994).

Another characteristic of this impairment that gives rise to question is the fact that this deterioration doesn't occur immediately, in the case of a brief stimulation, but after few seconds in the long stimulation. It has been suggested that some glio/neurotransmitters could pass the astrocytic membrane in undefined way Ca^{2+}(i) -independent (Hamilton & Attwell 2010). This, plus the fact that astrocytes possess other internal stores of Ca^{2+}(i) could explain why the synaptic transmission is maintained normal for few seconds. It could also let envisage that this slight decrease could be the consequence of a slow vanishing of some metabolites initially present that finally results in the decrease of the capacity of synaptic transmission. We could imagine that it could be the lack of Ca^{2+}(i) itself, or an indirect consequence of the lack of Ca^{2+}(i) , that leads to incapacity of the neurons to maintain a normal synaptic transmission (For example, a lot of ionic channels are Ca^{2+}(i) dependent). We didn't perform any complementary experiments to identify this(ese) defective metabolite(s) and thus we can only stipulate about it, based on the literature and already described pathways.

A possibility is that the role of IP_3 dependent Ca^{2+}(i) signaling in astrocytes is important in cellular Ca^{2+}(i) renewal. In our case, it might have been lacking for permiting endo- and exocytosis of gliotransmitters (Haydon 2001) to modulate synaptic activity (Araque et al 1999) in a long stimulation. During this stimulation, neuronal activity was too important to be sustained by the relatively small extra reticulum stores of Ca^{2+}(i) . It is known that the ER Ca^{2+}(i) is the main but not exclusive source of Ca^{2+}(i) in astrocytes (Patrushev et al 2013). Other explanation could be linked to the fact that astrocytes are also known to be organized in network (Bennett et al 2003, Giaume et al 2010) and to express long range calcium waves, whose functions are still unclear. This inter-astrocytes communication is slow (order of few um per second) and could be involved in a phenomenon with a large time and space scale, such as the long stimulation we used, including a thinner regulation of neurovascular coupling.

7.4 - Behavior

It has been recently shown that *in vivo* cholinergic activity evoked by sensory stimulation or electrical stimulation of the septal nucleus increases Ca2+ in hippocampal astrocytes and induces Long-term potentiation (LTP), a synaptic transmission representing the cellular basis of learning and memory (Navarrete et al 2012). It has been consequently proposed that astrocyte Ca2+ signal is necessary for cholinergic-induced synaptic plasticity, indicating that astrocytes are directly involved in brain storage information. It seemed necessary to process to *in vivo* experiment, to phenotypically characterize this impairment. We performed with IP_3R2 KO mice, devoted of intracellular Ca^{2+}(i) increases, the NOR task, a behavioral paradigm providing a measure of episodic and recognition memory. We didn't observe any significant impairment in KO mice comparing to WT animals. We therefore conclude that astrocyte Ca^{2+}(i) elevations are not relevant to this kind of memory with the protocol that we use. By the way, the mice presented a large increase in object exploration that was not seen in the classical test of exploratory behavior, the OF. We doubt, and it would have to be confirmed, that IP_3R2 KO mice present a visual deficit.

7.5 - Perspectives and conclusion

We showed (and it has been confirmed by parallel works from other teams) that IP_3 dependent Ca^{2+}(i) signaling in astrocytes, that constitute the main Ca^{2+}(i) signaling within these glial cells were not necessary to induce and maintain functional hyperemia. A major step in understanding the active role played by astrocytes in several brain functions has been achieved by demonstrating that Ca^{2+}(i) signaling is an important feature in astrocyte physiology and represents a form of cell excitability (Verkhratsky & Toescu 1998) but until now, nobody showed any important phenomenon occurring in these IP_3R2 KO mice as a consequence of the absence of huge Ca^{2+}(i) releases. In conclusion, our study gives rise to two main questions. What are the mechanisms and pathways involved in functional hyperemia if Ca^{2+}(i) signaling doesn't interfere in it? Do astrocytes really play the role they are assuming to play or do they have to be more simply considered as a relay of information? How would they

relay the information? It has been very recently shows that neuronal activity and the neurotransmitter glutamate evoke the release of messengers that dilate capillaries by actively relaxing pericytes (Hall et al 2014). And then, what are the roles and consequences of the Ca^{2+}(i) surges in astrocytes? To definitively exclude astrocytes Ca^{2+}(i) surges playing a role in functional hyperemia, it is conceivable to trigger Ca^{2+}(i) surges in astrocytes with optogenetic tool. Astrocytes can particularly express channelrhodopsin 2 under the promoter of Glial fibrillary acidic protein (GFAP), and can thus be activated (Perea et al 2014). Ca^{2+}(i) signaling can be follow at the same time than vessel dilation in the cortex by 2-photon imaging. Further, other potential roles of Ca^{2+}(i) signaling inastrocytes could be studied thanks to optogenetic tool.

8 - Conclusions

From the results presented in this work of PhD, we arrive to the conclusion that**:**

1) IP_3R2 KO mice do not present any impairment in BOLD fMRI expression after electrical Perforant Path stimulation, nor in the intensity of activation neither in the volume activated. The response is identical to Wild Type mice in time, space and amplitude.

2) IP3 dependent Ca^{2+}(i) signaling in astrocytes is not relevant for the initiation of functional hyperemia.

3) IP3 dependent Ca^{2+}(i) signaling in astrocytes is not relevant for the maintenance of functional hyperemia.

4) Moderate activation of the Perforant Pathway input to the hippocampus do not evidence any alteration in IP_3R2 KO mice

5) Astrocytic Ca^{2+}(i) signaling is playing a role in synaptic transmission in case of sustained stimulation. The synaptic transmission is deteriorated in the hippocampus of IP_3R2 KO.

6) IP_3R2 KO mice do not present a deficit in recognition memory.

Conclusiones

Con los resultados presentados en este trabajo de tesis doctoral, llegamos a las siguientes conclusiones:

1) Los ratones Knock-Out (KO) para IP_3R2 no presentan ninguna alteración en la respuesta fMRI BOLD tras la estimulación eléctrica del Tracto Perforante, ni en la intesidad de la activación ni en el volumen cerebral activado. La respuesta es idéntica a los ratones Wild-Type en tiempo, espacio y amplitud.

2) La señalización de $Ca^{2+}(i)$ dependiente de IP_3 en astrocitos no es relevante para la iniciación de una hiperemia funcional.

3) La señalización de $Ca^{2+}(i)$ dependiente de IP_3 en astrocitos no es relevante para el mantenimiento de una hiperemia funcional.

4) La activación moderada de las aferencias del Tracto Perforante al Hipocampo no evidencia ninguna alteración en los ratones KO para IP_3R2.

5) La señalización astrocítica de $Ca^{2+}(i)$ juega un papel en la transmisión sináptica en el caso de la estimulación mantenida. La transisión sináptica está deteriorada en el Hipocampo de los ratones KO para IP_3R2.

6) Los ratones KO para IP_3R2 no presentan ningún déficit en la memoria de reconocimiento.

9 - Bibliography

Adamczak JM, Farr TD, Seehafer JU, Kalthoff D, Hoehn M. 2010. High field BOLD response to forepaw stimulation in the mouse. *NeuroImage* 51: 704-12

Allbritton NL, Meyer T, Stryer L. 1992. Range of messenger action of calcium ion and inositol 1,4,5-trisphosphate. *Science (New York, N.Y.)* 258: 1812-5

Alvarez-Salvado E, Pallares V, Moreno A, Canals S. 2014. Functional MRI of long-term potentiation: imaging network plasticity. *Philosophical transactions of the Royal Society of London. Series B, Biological sciences* 369: 20130152

Ames A, 3rd, Wright RL, Kowada M, Thurston JM, Majno G. 1968. Cerebral ischemia. II. The no-reflow phenomenon. *Am J Pathol* 52: 437-53

Ances BM, Wilson DF, Greenberg JH, Detre JA. 2001. Dynamic changes in cerebral blood flow, O2 tension, and calculated cerebral metabolic rate of O2 during functional activation using oxygen phosphorescence quenching. *J Cereb Blood Flow Metab* 21: 511-6

Anderson CM, Nedergaard M. 2003. Astrocyte-mediated control of cerebral microcirculation. *Trends in neurosciences* 26: 340-4; author reply 44-5

Araque A, Parpura V, Sanzgiri RP, Haydon PG. 1999. Tripartite synapses: glia, the unacknowledged partner. *Trends in neurosciences* 22: 208-15

Attwell D, Buchan AM, Charpak S, Lauritzen M, Macvicar BA, Newman EA. 2010. Glial and neuronal control of brain blood flow. *Nature* 468: 232-43

Attwell D, Iadecola C. 2002. The neural basis of functional brain imaging signals. *Trends in neurosciences* 25: 621-5

Barres BA. 1991a. Glial ion channels. *Current opinion in neurobiology* 1: 354-9

Barres BA. 1991b. New roles for glia. *The Journal of neuroscience : the official journal of the Society for Neuroscience* 11: 3685-94

Bennett MV, Contreras JE, Bukauskas FF, Saez JC. 2003. New roles for astrocytes: gap junction hemichannels have something to communicate. *Trends in neurosciences* 26: 610-7

Bezzi P, Carmignoto G, Pasti L, Vesce S, Rossi D, et al. 1998. Prostaglandins stimulate calcium-dependent glutamate release in astrocytes. *Nature* 391: 281-5

Bundgaard M, Abbott NJ. 2008. All vertebrates started out with a glial blood-brain barrier 4-500 million years ago. *Glia* 56: 699-708

Burock MA, Buckner RL, Woldorff MG, Rosen BR, Dale AM. 1998. Randomized event-related experimental designs allow for extremely rapid presentation rates using functional MRI. *Neuroreport* 9: 3735-9

Canals S, Beyerlein M, Merkle H, Logothetis NK. 2009. Functional MRI evidence for LTP-induced neural network reorganization. *Curr Biol* 19: 398-403

Canals S, Beyerlein M, Murayama Y, Logothetis NK. 2008. Electric stimulation fMRI of the perforant pathway to the rat hippocampus. *Magn Reson Imaging* 26: 978-86

Cohen ER, Ugurbil K, Kim SG. 2002. Effect of basal conditions on the magnitude and dynamics of the blood oxygenation level-dependent fMRI response. *J Cereb Blood Flow Metab* 22: 1042-53

Cohen Z, Bonvento G, Lacombe P, Hamel E. 1996. Serotonin in the regulation of brain microcirculation. *Progress in neurobiology* 50: 335-62

Coles JA, Abbott NJ. 1996. Signalling from neurones to glial cells in invertebrates. *Trends in neurosciences* 19: 358-62

Cornell-Bell AH, Finkbeiner SM, Cooper MS, Smith SJ. 1990. Glutamate induces calcium waves in cultured astrocytes: long-range glial signaling. *Science (New York, N.Y.)* 247: 470-3

Denenberg VH. 1969. Open-field behavior in the rat: what does it mean? *Ann N Y Acad Sci* 159: 852-9

Dong L, Crosby ND, Winkelstein BA. 2013. Gabapentin alleviates facet-mediated pain in the rat through reduced neuronal hyperexcitability and astrocytic activation in the spinal cord. *J Pain* 14: 1564-72

Dunn JF, Tuor UI, Kmech J, Young NA, Henderson AK, et al. 2009. Functional brain mapping at 9.4T using a new MRI-compatible electrode chronically implanted in rats. *Magn Reson Med* 61: 222-8

Duong TQ, Kim DS, Ugurbil K, Kim SG. 2001. Localized cerebral blood flow response at submillimeter columnar resolution. *Proceedings of the National Academy of Sciences of the United States of America* 98: 10904-9

Fox RA, Henson PW. 1986. A general method for optimizing tissue discrimination in magnetic resonance imaging. *Med Phys* 13: 635-43

Frostig RD, Lieke EE, Ts'o DY, Grinvald A. 1990. Cortical functional architecture and local coupling between neuronal activity and the microcirculation revealed by in vivo high-resolution optical imaging of intrinsic signals. *Proceedings of the National Academy of Sciences of the United States of America* 87: 6082-6

Gandhi SP, Heeger DJ, Boynton GM. 1999. Spatial attention affects brain activity in human primary visual cortex. *Proceedings of the National Academy of Sciences of the United States of America* 96: 3314-9

Ganjoo P, Farber NE, Hudetz A, Smith JJ, Samso E, et al. 1998. In vivo effects of dexmedetomidine on laser-Doppler flow and pial arteriolar diameter. *Anesthesiology* 88: 429-39

Giaume C, Koulakoff A, Roux L, Holcman D, Rouach N. 2010. Astroglial networks: a step further in neuroglial and gliovascular interactions. *Nature reviews. Neuroscience* 11: 87-99

Gordon GR, Choi HB, Rungta RL, Ellis-Davies GC, MacVicar BA. 2008. Brain metabolism dictates the polarity of astrocyte control over arterioles. *Nature* 456: 745-9

Grinvald A, Slovin H, Vanzetta I. 2000. Non-invasive visualization of cortical columns by fMRI. *Nature neuroscience* 3: 105-7

Hall CN, Reynell C, Gesslein B, Hamilton NB, Mishra A, et al. 2014. Capillary pericytes regulate cerebral blood flow in health and disease. *Nature* 508: 55-60

Hamel E. 2004. Cholinergic modulation of the cortical microvascular bed. *Prog Brain Res* 145: 171-8

Hamilton NB, Attwell D. 2010. Do astrocytes really exocytose neurotransmitters? *Nature reviews. Neuroscience* 11: 227-38

Hara K, Harris RA. 2002. The anesthetic mechanism of urethane: the effects on neurotransmitter-gated ion channels. *Anesthesia and analgesia* 94: 313-8, table of contents

Harder DR, Alkayed NJ, Lange AR, Gebremedhin D, Roman RJ. 1998. Functional hyperemia in the brain: hypothesis for astrocyte-derived vasodilator metabolites. *Stroke* 29: 229-34

Harder DR, Roman RJ, Gebremedhin D. 2000. Molecular mechanisms controlling nutritive blood flow: role of cytochrome P450 enzymes. *Acta Physiol Scand* 168: 543-9

Harder DR, Zhang C, Gebremedhin D. 2002. Astrocytes function in matching blood flow to metabolic activity. *News Physiol Sci* 17: 27-31

Harel N, Ugurbil K, Uludag K, Yacoub E. 2006. Frontiers of brain mapping using MRI. *J Magn Reson Imaging* 23: 945-57

Haydon PG. 2001. GLIA: listening and talking to the synapse. *Nature reviews. Neuroscience* 2: 185-93

Herculano-Houzel S, Lent R. 2005. Isotropic fractionator: a simple, rapid method for the quantification of total cell and neuron numbers in the brain. *The Journal of neuroscience : the official journal of the Society for Neuroscience* 25: 2518-21

Hertz L, Zielke HR. 2004. Astrocytic control of glutamatergic activity: astrocytes as stars of the show. *Trends in neurosciences* 27: 735-43

Hofer T, Venance L, Giaume C. 2002. Control and plasticity of intercellular calcium waves in astrocytes: a modeling approach. *The Journal of neuroscience : the official journal of the Society for Neuroscience* 22: 4850-9

Hoge RD, Atkinson J, Gill B, Crelier GR, Marrett S, Pike GB. 1999. Linear coupling between cerebral blood flow and oxygen consumption in activated human cortex. *Proceedings of the National Academy of Sciences of the United States of America* 96: 9403-8

Holtzclaw LA, Pandhit S, Bare DJ, Mignery GA, Russell JT. 2002. Astrocytes in adult rat brain express type 2 inositol 1,4,5-trisphosphate receptors. *Glia* 39: 69-84

Huttunen JK, Grohn O, Penttonen M. 2008. Coupling between simultaneously recorded BOLD response and neuronal activity in the rat somatosensory cortex. *NeuroImage* 39: 775-85

Iadecola C. 2004. Neurovascular regulation in the normal brain and in Alzheimer's disease. *Nature reviews. Neuroscience* 5: 347-60

Iadecola C, Arneric SP, Baker HD, Callaway J, Reis DJ. 1990. Maintenance of local cerebral blood flow after acute neuronal death: possible role of non-neuronal cells. *Neuroscience* 35: 559-75

Iadecola C, Gorelick PB. 2004. Hypertension, angiotensin, and stroke: beyond blood pressure. *Stroke* 35: 348-50

Iadecola C, Reis DJ. 1990. Continuous monitoring of cerebrocortical blood flow during stimulation of the cerebellar fastigial nucleus: a study by laser-Doppler flowmetry. *J Cereb Blood Flow Metab* 10: 608-17

Kellman P, Gelderen P, de Zwart JA, Duyn JH. 2003. Method for functional MRI mapping of nonlinear response. *NeuroImage* 19: 190-9

Koehler RC, Roman RJ, Harder DR. 2009. Astrocytes and the regulation of cerebral blood flow. *Trends in neurosciences* 32: 160-9

Krimer LS, Muly EC, 3rd, Williams GV, Goldman-Rakic PS. 1998. Dopaminergic regulation of cerebral cortical microcirculation. *Nature neuroscience* 1: 286-9

Lauritzen M. 2005. Reading vascular changes in brain imaging: is dendritic calcium the key? *Nature reviews. Neuroscience* 6: 77-85

Li B, Freeman RD. 2007. High-resolution neurometabolic coupling in the lateral geniculate nucleus. *The Journal of neuroscience : the official journal of the Society for Neuroscience* 27: 10223-9

Lindauer U, Villringer A, Dirnagl U. 1993. Characterization of CBF response to somatosensory stimulation: model and influence of anesthetics. *Am J Physiol* 264: H1223-8

Logothetis NK, Pauls J, Augath M, Trinath T, Oeltermann A. 2001. Neurophysiological investigation of the basis of the fMRI signal. *Nature* 412: 150-7

Logothetis NK, Wandell BA. 2004. Interpreting the BOLD signal. *Annu Rev Physiol* 66: 735-69

Magistretti PJ, Pellerin L. 1999. Cellular mechanisms of brain energy metabolism and their relevance to functional brain imaging. *Philosophical transactions of the Royal Society of London. Series B, Biological sciences* 354: 1155-63

Mandeville JB, Marota JJ, Ayata C, Moskowitz MA, Weisskoff RM, Rosen BR. 1999. MRI measurement of the temporal evolution of relative CMRO(2) during rat forepaw stimulation. *Magn Reson Med* 42: 944-51

Masamoto K, Kim T, Fukuda M, Wang P, Kim SG. 2007. Relationship between neural, vascular, and BOLD signals in isoflurane-anesthetized rat somatosensory cortex. *Cereb Cortex* 17: 942-50

Mathiesen C, Caesar K, Akgoren N, Lauritzen M. 1998. Modification of activity-dependent increases of cerebral blood flow by excitatory synaptic activity and spikes in rat cerebellar cortex. *J Physiol* 512 (Pt 2): 555-66

Mathiesen C, Caesar K, Lauritzen M. 2000. Temporal coupling between neuronal activity and blood flow in rat cerebellar cortex as indicated by field potential analysis. *J Physiol* 523 Pt 1: 235-46

Matthew E, Nordahl T, Schut L, King AC, Cohen R. 1993. Metabolic and cognitive changes in hereditary ataxia. *J Neurol Sci* 119: 134-40

Mennerick S, Zorumski CF. 1994. Glial contributions to excitatory neurotransmission in cultured hippocampal cells. *Nature* 368: 59-62

Metea MR, Newman EA. 2006. Glial cells dilate and constrict blood vessels: a mechanism of neurovascular coupling. *The Journal of neuroscience : the official journal of the Society for Neuroscience* 26: 2862-70

Moreno A, Jego P, de la Cruz F, Canals S. 2013. Neurophysiological, metabolic and cellular compartments that drive neurovascular coupling and neuroimaging signals. *Frontiers in neuroenergetics* 5: 3

Mueggler T, Baumann D, Rausch M, Rudin M. 2001. Bicuculline-induced brain activation in mice detected by functional magnetic resonance imaging. *Magn Reson Med* 46: 292-8

Mulligan SJ, MacVicar BA. 2004. Calcium transients in astrocyte endfeet cause cerebrovascular constrictions. *Nature* 431: 195-9

Nair G, Duong TQ. 2004. Echo-planar BOLD fMRI of mice on a narrow-bore 9.4 T magnet. *Magn Reson Med* 52: 430-4

Navarrete M, Perea G, Fernandez de Sevilla D, Gomez-Gonzalo M, Nunez A, et al. 2012. Astrocytes mediate in vivo cholinergic-induced synaptic plasticity. *PLoS biology* 10: e1001259

Newman E, Reichenbach A. 1996. The Muller cell: a functional element of the retina. *Trends in neurosciences* 19: 307-12

Nicholls D, Attwell D. 1990. The release and uptake of excitatory amino acids. *Trends in pharmacological sciences* 11: 462-8

Nizar K, Uhlirova H, Tian P, Saisan PA, Cheng Q, et al. 2013. In vivo stimulus-induced vasodilation occurs without IP3 receptor activation and may precede astrocytic calcium increase. *The Journal of neuroscience : the official journal of the Society for Neuroscience* 33: 8411-22

Oberheim NA, Goldman SA, Nedergaard M. 2012. Heterogeneity of astrocytic form and function. *Methods in molecular biology (Clifton, N.J.)* 814: 23-45

Offenhauser N, Thomsen K, Caesar K, Lauritzen M. 2005. Activity-induced tissue oxygenation changes in rat cerebellar cortex: interplay of postsynaptic activation and blood flow. *J Physiol* 565: 279-94

Ogawa S, Lee TM, Kay AR, Tank DW. 1990. Brain magnetic resonance imaging with contrast dependent on blood oxygenation. *Proceedings of the National Academy of Sciences of the United States of America* 87: 9868-72

Pakkenberg B, Gundersen HJ. 1988. Total number of neurons and glial cells in human brain nuclei estimated by the disector and the fractionator. *Journal of microscopy* 150: 1-20

Parkes LM, Schwarzbach JV, Bouts AA, Deckers RH, Pullens P, et al. 2005. Quantifying the spatial resolution of the gradient echo and spin echo BOLD response at 3 Tesla. *Magn Reson Med* 54: 1465-72

Parpura V, Basarsky TA, Liu F, Jeftinija K, Jeftinija S, Haydon PG. 1994. Glutamate-mediated astrocyte-neuron signalling. *Nature* 369: 744-7

Patrushev I, Gavrilov N, Turlapov V, Semyanov A. 2013. Subcellular location of astrocytic calcium stores favors extrasynaptic neuron-astrocyte communication. *Cell calcium* 54: 343-9

Pawela CP, Biswal BB, Cho YR, Kao DS, Li R, et al. 2008. Resting-state functional connectivity of the rat brain. *Magn Reson Med* 59: 1021-9

Pawlik G, Rackl A, Bing RJ. 1981. Quantitative capillary topography and blood flow in the cerebral cortex of cats: an in vivo microscopic study. *Brain research* 208: 35-58

Pellerin L, Magistretti PJ. 2004. Neuroenergetics: calling upon astrocytes to satisfy hungry neurons. *Neuroscientist* 10: 53-62

Perea G, Yang A, Boyden ES, Sur M. 2014. Optogenetic astrocyte activation modulates response selectivity of visual cortex neurons in vivo. *Nature communications* 5: 3262

Petravicz J, Fiacco TA, McCarthy KD. 2008. Loss of IP3 receptor-dependent Ca2+ increases in hippocampal astrocytes does not affect baseline CA1 pyramidal neuron synaptic activity. *The Journal of neuroscience : the official journal of the Society for Neuroscience* 28: 4967-73

Petzold GC, Murthy VN. 2011. Role of astrocytes in neurovascular coupling. *Neuron* 71: 782-97

Pfrieger FW, Barres BA. 1996. New views on synapse-glia interactions. *Current opinion in neurobiology* 6: 615-21

Pfrieger FW, Barres BA. 1997. Synaptic efficacy enhanced by glial cells in vitro. *Science (New York, N.Y.)* 277: 1684-7

Porter JT, McCarthy KD. 1997. Astrocytic neurotransmitter receptors in situ and in vivo. *Progress in neurobiology* 51: 439-55

Raichle ME, Hartman BK, Eichling JO, Sharpe LG. 1975. Central noradrenergic regulation of cerebral blood flow and vascular permeability. *Proceedings of the National Academy of Sciences of the United States of America* 72: 3726-30

Raichle ME, Mintun MA. 2006. Brain work and brain imaging. *Annu Rev Neurosci* 29: 449-76

Rancillac A, Rossier J, Guille M, Tong XK, Geoffroy H, et al. 2006. Glutamatergic Control of Microvascular Tone by Distinct GABA Neurons in the Cerebellum. *The Journal of neuroscience : the official journal of the Society for Neuroscience* 26: 6997-7006

Rauch A, Rainer G, Logothetis NK. 2008. The effect of a serotonin-induced dissociation between spiking and perisynaptic activity on BOLD functional MRI. *Proceedings of the National Academy of Sciences of the United States of America* 105: 6759-64

Roy CS, Sherrington CS. 1890. On the Regulation of the Blood-supply of the Brain. *J Physiol* 11: 85-158 17

Schummers J, Yu H, Sur M. 2008. Tuned responses of astrocytes and their influence on hemodynamic signals in the visual cortex. *Science (New York, N.Y.)* 320: 1638-43

Sheth SA, Nemoto M, Guiou M, Walker M, Pouratian N, Toga AW. 2004. Linear and nonlinear relationships between neuronal activity, oxygen metabolism, and hemodynamic responses. *Neuron* 42: 347-55

Shi Y, Liu X, Gebremedhin D, Falck JR, Harder DR, Koehler RC. 2008. Interaction of mechanisms involving epoxyeicosatrienoic acids, adenosine receptors, and metabotropic glutamate receptors in neurovascular coupling in rat whisker barrel cortex. *J Cereb Blood Flow Metab* 28: 111-25

Shmuel A, Yacoub E, Chaimow D, Logothetis NK, Ugurbil K. 2007. Spatio-temporal point-spread function of fMRI signal in human gray matter at 7 Tesla. *NeuroImage* 35: 539-52

Takata N, Mishima T, Hisatsune C, Nagai T, Ebisui E, et al. 2011. Astrocyte calcium signaling transforms cholinergic modulation to cortical plasticity in vivo. *The Journal of neuroscience : the official journal of the Society for Neuroscience* 31: 18155-65

Takata N, Nagai T, Ozawa K, Oe Y, Mikoshiba K, Hirase H. 2013. Cerebral blood flow modulation by Basal forebrain or whisker stimulation can occur independently of large cytosolic Ca2+ signaling in astrocytes. *PLoS One* 8: e66525

Temel Y, Visser-Vandewalle V, van der Wolf M, Spincemaille GH, Desbonnet L, et al. 2004. Monopolar versus bipolar high frequency stimulation in the rat subthalamic nucleus: differences in histological damage. *Neurosci Lett* 367: 92-6

Thompson PM, Sowell ER, Gogtay N, Giedd JN, Vidal CN, et al. 2005. Structural MRI and brain development. *Int Rev Neurobiol* 67: 285-323

Thomsen K, Offenhauser N, Lauritzen M. 2004. Principal neuron spiking: neither necessary nor sufficient for cerebral blood flow in rat cerebellum. *J Physiol* 560: 181-9

Tsacopoulos M, Magistretti PJ. 1996. Metabolic coupling between glia and neurons. *The Journal of neuroscience : the official journal of the Society for Neuroscience* 16: 877-85

Ueki M, Mies G, Hossmann KA. 1992. Effect of alpha-chloralose, halothane, pentobarbital and nitrous oxide anesthesia on metabolic coupling in somatosensory cortex of rat. *Acta Anaesthesiol Scand* 36: 318-22

Uludag K, Dubowitz DJ, Yoder EJ, Restom K, Liu TT, Buxton RB. 2004. Coupling of cerebral blood flow and oxygen consumption during physiological activation and deactivation measured with fMRI. *NeuroImage* 23: 148-55

Vanzetta I, Slovin H, Omer DB, Grinvald A. 2004. Columnar resolution of blood volume and oximetry functional maps in the behaving monkey; implications for FMRI. *Neuron* 42: 843-54

Ventura R, Harris KM. 1999. Three-dimensional relationships between hippocampal synapses and astrocytes. *The Journal of neuroscience : the official journal of the Society for Neuroscience* 19: 6897-906

Verkhratsky A, Kettenmann H. 1996. Calcium signalling in glial cells. *Trends in neurosciences* 19: 346-52

Verkhratsky A, Toescu EC. 1998. Calcium and neuronal ageing. *Trends in neurosciences* 21: 2-7

Viswanathan A, Freeman RD. 2007. Neurometabolic coupling in cerebral cortex reflects synaptic more than spiking activity. *Nature neuroscience* 10: 1308-12

Wang X, Takano T, Nedergaard M. 2009. Astrocytic calcium signaling: mechanism and implications for functional brain imaging. *Methods in molecular biology (Clifton, N.J.)* 489: 93-109

Weber R, Ramos-Cabrer P, Wiedermann D, van Camp N, Hoehn M. 2006. A fully noninvasive and robust experimental protocol for longitudinal fMRI studies in the rat. *NeuroImage* 29: 1303-10

Yacoub E, Shmuel A, Logothetis N, Ugurbil K. 2007. Robust detection of ocular dominance columns in humans using Hahn Spin Echo BOLD functional MRI at 7 Tesla. *NeuroImage* 37: 1161-77

Yoshor D, Ghose GM, Bosking WH, Sun P, Maunsell JH. 2007. Spatial attention does not strongly modulate neuronal responses in early human visual cortex. *The Journal of neuroscience : the official journal of the Society for Neuroscience* 27: 13205-9

Zhao F, Zhao T, Zhou L, Wu Q, Hu X. 2008. BOLD study of stimulation-induced neural activity and resting-state connectivity in medetomidine-sedated rat. *NeuroImage* 39: 248-60

Zonta M, Angulo MC, Gobbo S, Rosengarten B, Hossmann KA, et al. 2003. Neuron-to-astrocyte signaling is central to the dynamic control of brain microcirculation. *Nature neuroscience* 6: 43-50

10 - Annex

frontiers in
NEUROENERGETICS

MINI REVIEW ARTICLE
published: 28 March 2013
doi: 10.3389/fnene.2013.00003

Neurophysiological, metabolic and cellular compartments that drive neurovascular coupling and neuroimaging signals

Andrea Moreno[1], Pierrick Jego[1], Feliberto de la Cruz[2] and Santiago Canals[1]*

[1] *Instituto de Neurociencias, Consejo Superior de Investigaciones Científicas, Universidad Miguel Hernández, San Juan de Alicante, Spain*
[2] *Centro de Estudios Avanzados de Cuba, Ministerio de Ciencia Tecnología y Medio Ambiente, Habana, Cuba*

Edited by:
Sebastian Cerdan, Instituto de Investigaciones Biomedicas Alberto Sols, Spain

Reviewed by:
Sebastian Cerdan, Instituto de Investigaciones Biomedicas Alberto Sols, Spain
Tiago B. Rodrigues, Cambridge Research Institute and University of Cambridge, UK

***Correspondence:**
Santiago Canals, Instituto de Neurociencias, Consejo Superior de Investigaciones Científicas, Universidad Miguel Hernández, Campus de San Juan, Avenida Ramón y Cajal, s/n, 03550 San Juan de Alicante, Spain.
e-mail: scanals@umh.es

Complete understanding of the mechanisms that coordinate work and energy supply of the brain, the so called neurovascular coupling, is fundamental to interpreting brain energetics and their influence on neuronal coding strategies, but also to interpreting signals obtained from brain imaging techniques such as functional magnetic resonance imaging. Interactions between neuronal activity and cerebral blood flow regulation are largely compartmentalized. First, there exists a functional compartmentalization in which glutamatergic peri-synaptic activity and its electrophysiological events occur in close proximity to vascular responses. Second, the metabolic processes that fuel peri-synaptic activity are partially segregated between glycolytic and oxidative compartments. Finally, there is cellular segregation between astrocytic and neuronal compartments, which has potentially important implications on neurovascular coupling. Experimental data is progressively showing a tight interaction between the products of energy consumption and neurotransmission-driven signaling molecules that regulate blood flow. Here, we review some of these issues in light of recent findings with special attention to the neuron-glia interplay on the generation of neuroimaging signals.

Keywords: neurovascular coupling, fMRI, neurophysiology, astrocytes, glycolysis

INTRODUCTION

By the end of the nineteenth century, two scientists provided the first evidence in support of coordination between brain work and energy supply. Mosso (1881), on measuring brain pulsations over the right prefrontal cortex in a subject with abnormally thinned skull, reported increased pulsations when the subject performed a mathematical task. In 1890, Sherrington, using a more direct approach, showed that stimulation of the sensory nerves, or the medulla oblongata, produced an increase in brain blood pressure (Roy and Sherrington, 1890). This hemodynamic response that accompanies brain activation was later found to also exist in pathological situations such as ischemia (Ames et al., 1968). This vascular response was interpreted as a compensatory mechanism that fuels the brain either during increased energy expenditure or during restriction of metabolic substrate delivery.

Brain energy is mainly used for restoring the resting membrane potential of activated neurons (Ames, 2000; Attwell and Laughlin, 2001). It is well established that the metabolic processes that fuel energy consumption are distributed in different cell types (neurons and glia) and subcellular compartments with predominantly either glycolytic or oxidative metabolisms. This segregation allows a functional compartmentalization of energy expenditure and is critical in understanding the mechanisms that coordinate brain work and energy supply, the so called neurovascular coupling. As such, is also fundamental in interpreting the signals obtained from brain imaging techniques as functional magnetic resonance imaging (fMRI).

Functional MRI based on blood oxygen level-dependent (BOLD) signal is the principal neuroimaging technique for basic and clinical research in humans. It is based on the paramagnetic nature of deoxygenated hemoglobin (Pauling and Coryell, 1936) and the overcompensation of blood supply in response to brain activation that produces a net increase in oxygenated hemoglobin (Fox and Raichle, 1986). This is accompanied by an enhancement of the MRI signal (Ogawa and Lee, 1990; Ogawa et al., 1990).While the physical origin of the signal is clear, both the triggering mechanisms and its relation to neuronal activity are still controversial.

NEUROPHYSIOLOGY

An important matter for neuroimaging is to understand which aspects of neuronal work are reflected in increased cerebral blood flow (CBF). Experiments simultaneously combining fMRI and electrophysiological recordings in the primary visual cortex of anesthetized monkeys showed that the imaging signal evoked by visual stimulation maximally correlates with the local field potential (LFP), an aggregate measure of synaptic and active dendritic currents (Logothetis et al., 2001). Although the correlation of the BOLD signal was only slightly higher toward LFP compared with spiking activity (multiunit and single unit activity), the LFP signal was the only predictor of the hemodynamic response when long stimulation protocols that habituate spiking activity were used. Consistent with these findings were studies in the rat cerebellar cortex which convincingly showed that local CBF can indeed be dissociated from spiking activity while

strongly correlated with LFPs (Mathiesen et al., 1998, 2000; Thomsen et al., 2004).

Based on the above results, it has been argued that neuroimaging signals reflect the local processing of incoming neuronal activity to a particular area, rather than the output message being sent in outgoing efferent neuronal activity. Recent support of this view comes from combined fMRI-electrophysiology experiments, demonstrating that local synaptic plasticity modulates the amplitude of the BOLD signal (Canals et al., 2009). In anesthetized rats, the dentate gyrus was activated with electrical microstimulation of the perforant pathway, while simultaneously recording electrophysiological and high resolution fMRI signals (**Figures 1** and **2**). Of note, in the hippocampus, the axial organization of the cellular elements, with a rather precise alignment of dendritic trees and somas, minimizes the cancellation of current sources form the LFP generators and facilitates the neurophysiological interpretation of the electrically-evoked field potentials, such as synaptic currents reflected in the excitatory post-synaptic potential (EPSP) and spiking activity in the population spike. Using this preparation, we showed that the glutamate-evoked post-synaptic currents were a precise predictor of BOLD signal amplitude, better than either the population spike or the electrical current used for stimulation (Canals et al., 2008, 2009). This result has recently been confirmed in experiments combining electrophysiological recordings with hippocampal CBF measurements based on Laser-Doppler flowmetry (Hamadate et al., 2011). Interestingly, the extension of the functional maps correlated better with the spiking activity than the EPSP recorded in the dentate gyrus (Canals et al., 2009). This result indicated, perhaps not surprisingly, that while the local BOLD signal follows the synaptic input, the output (spiking) activity of a particular region predicts the activity propagation in the network connected to that region (**Figures 1** and **2E**).

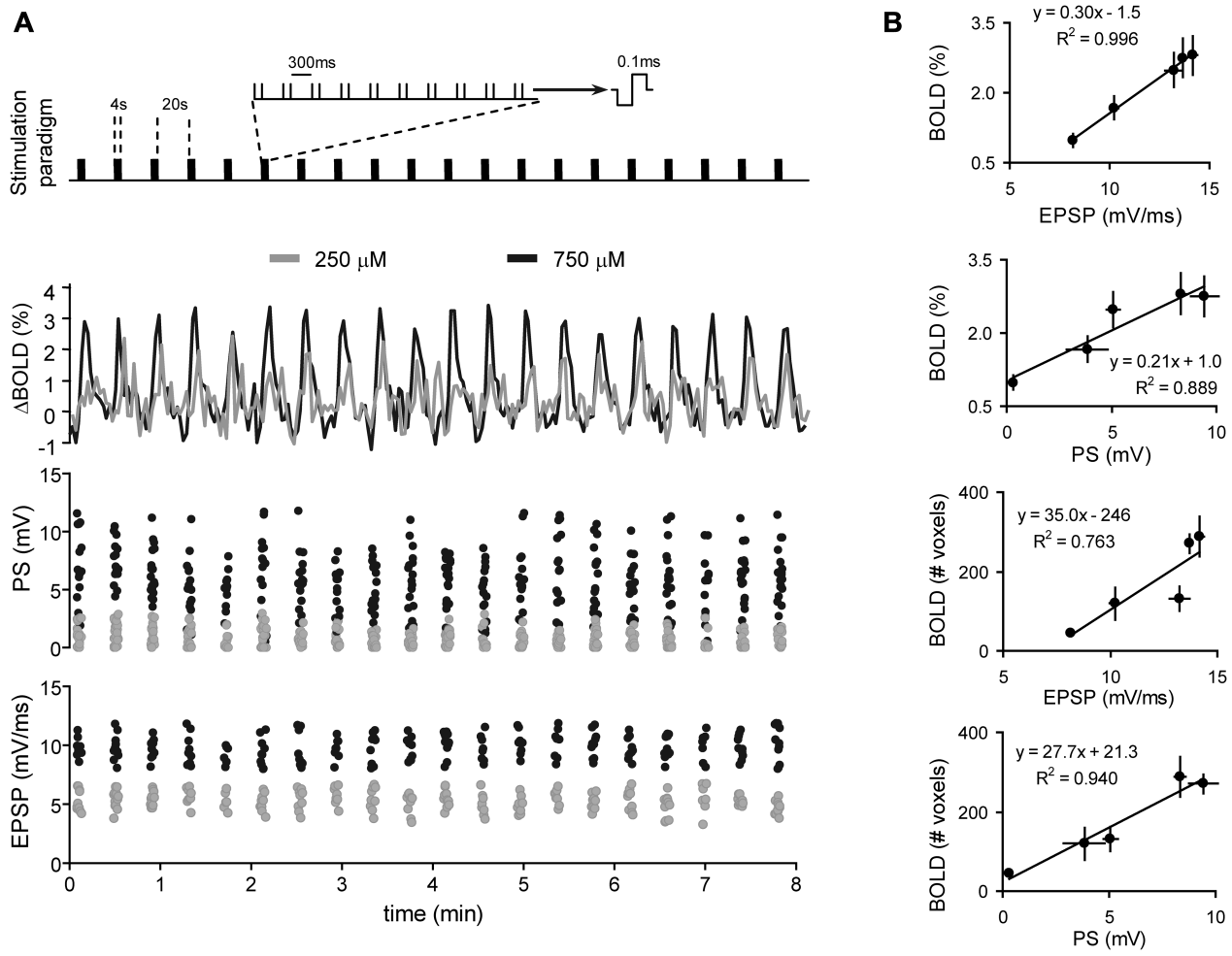

FIGURE 1 | Correlation of BOLD and electrophysiological signals. (A) Simultaneous recordings of BOLD (middle panel) and electrophysiological signals (PS and EPSP; lower two panels, respectively) during a typical block-design protocol of electric-stimulation fMRI (upper panel). Two stimulation intensities in one animal are shown. **(B)** The amplitude of the BOLD signal in the dentate gyrus (%, two upper panels) or the volume of brain activated during perforant path stimulation (#, number of activated voxels, two lower panels) is plotted against the EPSP in the dentate gyrus or the corresponding PS. BOLD, EPSP and PS represent the mean ± SEM of all hemodynamic, synaptic and spiking responses, respectively, during a complete experiment ($n = 5$ experiments, collected in four different animals). Data is fitted with linear regression. Adapted with permission from Canals et al. (2009).

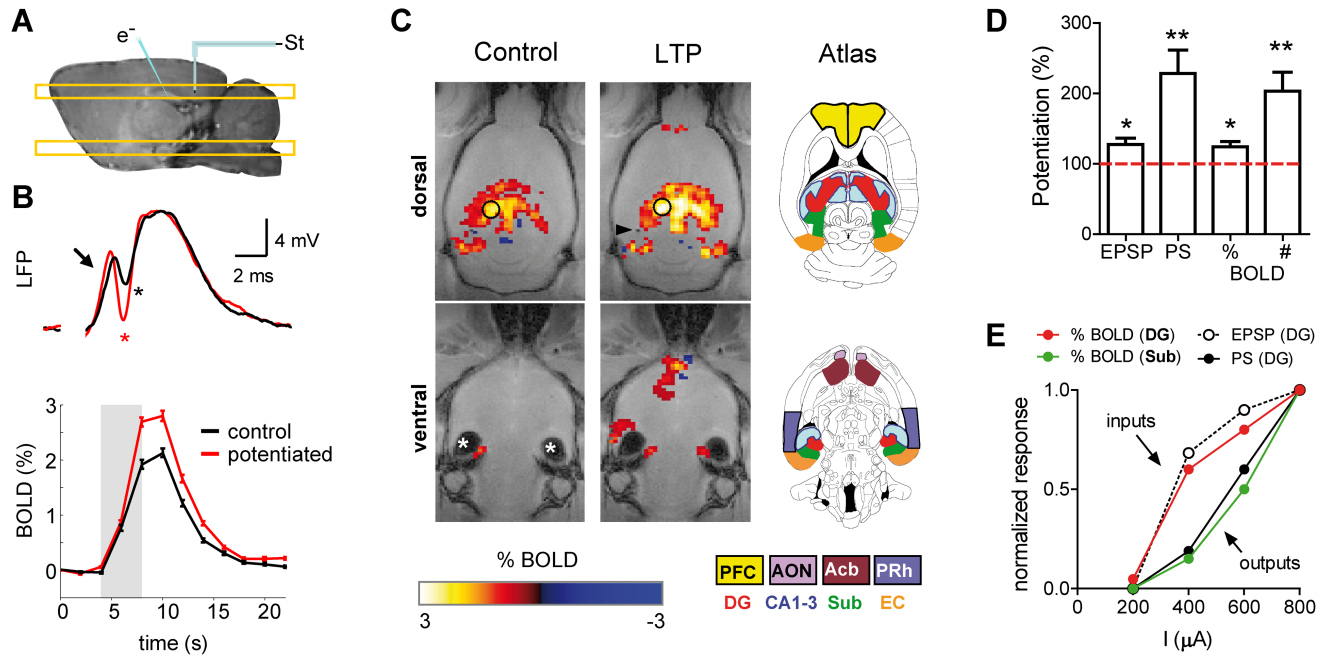

FIGURE 2 | Potentiation of the synaptic strength is accompanied by enhancement of the BOLD-fMRI signal. (A) Schematic representation of the experimental preparation. The placement of the stimulating and recording electrodes is shown on a sagital T1-weighted image acquired with manganese-enhanced MRI. The location of the dorsal and ventral MRI slices shown in **(C)** is also illustrated. **(B)** LFP (upper panel) and BOLD signal time course (lower panel) recorded in the dentate gyrus during perforant pathway stimulation, before (black) and after (red) induction of long-term potentiation (LTP) of the synaptic strength. Arrow points toward the EPSP and asterisks mark the PS. **(C)** Functional maps thresholded and overlaid on horizontal FLASH anatomical scans, showing brain active areas during perforant path stimulation before (control) and after synaptic potentiation (LTP). New structures are recruited after LTP. Asterisks "*" mark image artifacts due to the ear channel. The color-coded scale represents positive and negative BOLD response in percent change from baseline. The position of the tip of the stimulation electrode is marked by the black arrowhead. The inset drawings, modified from the Paxinos and Watson rat brain atlas (Paxinos and Watson, 2007), delineate different regions of interest. **(D)** Quantification of EPSP, PS and the amplitude of the BOLD signal (%) in the dentate gyrus, and the total number of activated fMRI voxels in the brain (#). **(E)** Electrophysiological and fMRI responses to different stimulation intensities measured in the dentate gyrus and the subiculum. Synaptic input (EPSP) and local BOLD signal amplitude in the dentate evolve together and diverge from the spiking output (PS) and its propagation to the subiculum. PFC, prefrontal cortex; AON, anterior olfactory nucleus; Acb, accumbens; PRh, perirhinal cortex; DG, dentate gyrus; Sub, subiculum; EC, entorhinal cortex. **(A–D)** adapted with permission from Canals et al. (2009).

It must be noted, however, that the local synaptic input of a volume of tissue relevant for the spatial resolution of fMRI (2–3 mm in human studies and 0.2–0.5 mm in small animal studies) is also contributed to by synaptic currents driven by recurrent spiking activity. Therefore, input and output activities are somehow mixed to some extent. What is the relative contribution to the BOLD signal of the synaptic inputs driven by recurrent spiking activity? In hippocampal preparations, when the strength of the synapses in the dentate gyrus was experimentally increased by means of a tetanic stimulation of the perforant pathway (long-term potentiation, LTP), the BOLD signal concomitantly increased (Canals et al., 2009). Both, the EPSP and BOLD signal potentiations were of comparable magnitude and two to three times smaller than the spike potentiation. The dissociated evolution of the spiking activity vs. the BOLD signal and EPSP becomes even clearer in the small proportion of experiments in which, as originally described by Bliss and Lomo (1973), the tetanization of the perforant pathway is followed by an increase in the spiking probability without changing the EPSP (EPSP-to-spike or E-S potentiation). In these cases of increased tissue excitability, the local BOLD signal evoked by perforant path stimulation remains almost unaffected, like the EPSP, while the population spike amplitude increases two- to threefold (Benito et al., unpublished results). These results indicate that the effect of extrinsic synaptic inputs on the hyperemic response in the hippocampus outweigh the effect of synapses on recurrent axon collaterals, and suggest the intriguing possibility that not all glutamatergic synapses are equally suited to initiate a vascular response.

In summary, the above observations indicate that between the electrophysiological events constituting neuronal computations, glutamate evoked synaptic currents critically contribute to neuroimaging signals. It is intuitively appealing that the supply of energy substrates could be coupled to the process that, as mentioned earlier, consumes most of the energy used for neuronal signaling (Ames, 2000; Attwell and Laughlin, 2001). However, the nature of the coupling mechanisms is under intense debate.

METABOLISM vs. NEUROTRANSMISSION

Two major concepts have been put forward to mechanistically explain the coupling between neuronal activity and hyperemia. A classical view supports a feed-back mechanism in which the

byproducts of energy expenditure act as signaling molecules to increase blood supply and restore energy buffers. In a more recent view, a feed-forward mechanism controlled by neurotransmitter-mediated signaling has a major role in CBF regulation. While neurotransmitter signaling is intrinsically correlated with energy consumption, the feed-forward model maintains that a causal link with CBF regulation only exists for the first. A large body of recent experimental data, mainly from *in vitro* preparations (see below), is shifting the field in favor of the feed-forward model (Attwell et al., 2010; Petzold and Murthy, 2011). Both models, however, are mutually non-exclusive and may coexist in specific physiological states.

METABOLIC FEED-BACK MECHANISM

Initial observations challenging the feed-back model came from studies showing that experimental manipulations of metabolic substrates such as O_2 (Mintun et al., 2001; Lindauer et al., 2010) or glucose (Powers et al., 1996) *in vivo* have little effect on CBF regulation. However, other metabolic byproducts such as adenosine can regulate CBF, linking the action of the Na^+/K^+ ATPase pump to local vasodilatation. Extracellular adenosine acting on A_{2A} receptors in vascular smooth muscle inhibits the arteriolar vasoconstriction mediated by the arachidonic acid (AA) metabolite 20-hydroxy-eicosatetraenoic acid (20-HETE; Gordon et al., 2008). This vasodilatory effect has been demonstrated in the cortex (Ko et al., 1990) and the cerebellum (Li and Iadecola, 1994) following neuronal stimulation. Adenosine effects on CBF regulation mediated by A_{2B} receptors have also been reported and involve interaction with Ca^{2+} signaling in astrocytes and probably AA metabolism (Shi et al., 2008). A caveat in interpreting the source of extracellular adenosine is that ATP used as a gliotransmitter is also hydrolyzed to adenosine by extracellular ectonucleotidases (Latini and Pedata, 2001). Therefore, depending on its origin, adenosine will couple CBF to energy consumption or neuronal signaling through glio-transmission. An additional unsolved question of adenosine-mediated functional hyperemia is the concomitant synaptic depressing effect that adenosine may exert on pre- and post-synaptic A_1 receptors (Greene and Haas, 1991), to which it binds with highest affinity (Fredholm et al., 2001). The dual effect of adenosine may help maintain a safety energy level for neuronal integrity under conditions of transient energy limitations such as ischemia (Dunwiddie and Masino, 2001; Canals et al., 2008), but it may interfere with neuronal computations in physiological conditions. The functional compartmentalization of adenosine release may constitute a solution to this potential problem (Pelligrino et al., 2011).

One key energy metabolite in the brain which reinforces the feed-back model of neurovascular coupling is lactate. Important work on the special role of glycolysis in brain energy production provided the concept that glycolytic increase during brain activation (Raichle and Mintun, 2006) results from the uptake of synaptically-released glutamate into astrocytes together with Na^+ (Magistretti and Pellerin, 1999; Pellerin and Magistretti, 2004). In the astrocyte, glutamate is converted into glutamine and the excess Na^+ is released to the extracellular space, both processes consuming ATP (Erecinska and Silver, 1994). Refilling of the energy buffer seems to critically depend on glycolysis (Raichle and Mintun, 2006), and glycolysis is linked to blood flow modulation through lactate. Accordingly, it has been convincingly shown that CBF response to an increase in neuronal activity is modulated by changes in the plasma lactate/pyruvate ratio in experimental animals (Ido et al., 2001, 2004) and humans (Mintun et al., 2004; Vlassenko et al., 2006). Accordingly, it has been recently shown that lactate indeed modulates the BOLD fMRI signal in the early visual cortex of non-human primates (von Pfostl et al., 2012). These results and others (Kasischke et al., 2004) support a direct metabolic (glycolytic) effect on CBF regulation and identify astrocytes as important players in the generation of neuroimaging signals.

Glutamate recycling is not the only mechanism linking astrocytes to functional hyperemia (see below), nor is metabolic compartmentalization of glycolytic enzymes restricted to astrocytes. Of potential functional (and imaging) relevance is also the discovery of glycolytic enzymes in the post-synaptic density of glutamatergic synapses (Wu et al., 1997) and GABA receptors (Laschet et al., 2004), potentially linking post-synaptic activations, glycolysis, and neuroimaging signals.

NEUROTRANSMITTER-MEDIATED FEED-FORWARD SIGNALING

The feed-forward model is mainly represented by nitric oxide (NO) and AA metabolites released from neurons and glial cells as a consequence of glutamatergic neurotransmission. While vasoactive peptides and GABA (γ-aminobutyric acid) released by interneurons have been shown to contribute to the functional hyperemia in some systems (Cauli et al., 2004; Kocharyan et al., 2008), and therefore contribute to the feed-forward neurovascular coupling mechanism, the experimental evidence accumulated to date is less abundant (Lauritzen et al., 2012).

Synaptically-released glutamate acting on NMDA receptors increases post-synaptic Ca^{2+} levels and activates neuronal NO synthase (nNOS), which translates into NO release. NO mediates vasodilation in the brain, as repeatedly demonstrated in slice and *in vivo* preparations (Busija et al., 2007). It has to be noted, however, that NO contribution to blood flow regulation presents regional differences in the brain (Sokoloff et al., 1977). In the cortex (but not the cerebellum), while NO is required for functional hyperemia, it does not directly mediate the neuron-to-vessel signaling (Lindauer et al., 1999). Its role in the cortex has been suggested to be the modulation of the AA metabolic pathways in astrocytes (Attwell et al., 2010). There is strong evidence supporting blood flow regulation through the production and release of AA metabolites in response to synaptic glutamate. The supported mechanisms start with an mGluR-dependent increase in the astrocytic $[Ca^{2+}]i$ that activates phospholipase A_2 and releases AA from membrane phospholipids. Subsequently, AA metabolites with vasodilatory activity, such as prostaglandins and epoxyeicosatrienoic acids, are produced and released. Interestingly, vasoconstrictions induced by increases in astrocytic $[Ca^{2+}]i$ have also been reported *in vitro* (Mulligan and MacVicar, 2004; Metea and Newman, 2006) and are also mediated by the AA metabolite 20-HETE (Behm et al., 2009). This conflicting result was elegantly explained by demonstrating that the metabolic state of the tissue ultimately determines the sign of the astrocytic control over vascular responses (Gordon et al., 2008), with decreasing O_2 concentrations favoring the production

of vasodilatory responses. This interaction may therefore reflect the combination of feed-back and feed-forward mechanisms of blood flow regulation. Although conceptually attractive, it must be noted that the above *in vitro* results are challenged by previous (Mintun et al., 2001) and recent (Lindauer et al., 2010) studies showing no effect of O_2 concentration on CBF regulation *in vivo* (see above).

A tight interaction between feed-back and feed-forward mechanism of neurovascular coupling starts to be clear as their respective counterparts are found to be closely related in the biochemical pathways supporting functional hyperemia. For example, the vasodilatory effect of adenosine at A_{2A} receptors is coupled to AA signaling pathway by interfering with 20-HETE vasoconstriction, a mechanism that also mediates part of the NO vasodilatory effect (Roman, 2002). Furthermore, the mechanism linking lactate to vasodilation involves the inhibition of the prostaglandin transporter, increasing the extracellular concentration of PGE2 released from astrocytes and potentiating vasodilation (Gordon et al., 2008). The vasodilatory effects of glutamate on astrocytes is reduced by blocking glutamate uptake (Raichle, 1998; Bernardinelli et al., 2004), suggesting a metabolic contribution to the signaling effect. Therefore, activity-driven energy expenditure and neuronal or astrocytic-initiated signaling seem to be the two ends of the same rope. This may explain why inhibitory cocktails combining antagonists for the different pathways (AA, NO, adenosine) do not show additive blocking of functional hyperemia (Koehler et al., 2006).

An additional level of interaction arises when considering that NO and AA have also been involved in the mechanism that strengthens synaptic currents after LTP induction and learning (Schuman and Madison, 1991; Hardingham and Fox, 2006; DeCostanzo et al., 2010; Dachtler et al., 2011), protocols shown to increase the hyperemic response (Canals et al., 2009; Hamadate et al., 2011). An intriguing possibility then is that the same set of molecules acting on converging signaling pathways is coordinating the strength of synaptic currents and energy consumption with the level of local blood supply. Whether a long-lasting increase in synaptic efficacy is accompanied by a similarly-lasting enhancement of neurovascular coupling efficacy is an important yet unsolved question, with potentially relevant implications on neuroimaging signal interpretation.

ASTROCYTES

In light of the reviewed results and their strategic location between synapses and blood vessels, astrocytes have often been regarded as key players in the neurovascular coupling (Ramón y Cajal, 1899). Astrocytes seem to be the compartment where many of the biochemical processes that determine the magnitude and direction of the vascular response to neuronal activation take place. Increases in astrocytic $[Ca^{2+}]$i linked to AA metabolism is the principal mechanism thought to contribute to hyperemia. However, Ca^{2+} fluctuation in astrocytes not only occurs in response to neuronal activity (i.e., spontaneous events may also trigger astrocytic Ca^{2+} waves; Perea and Araque, 2005; Wang et al., 2009). Therefore, it has been suggested that a significant contribution to the neuroimaging signals may arise from the activation of astrocytes independently of neuronal signaling (Wang et al., 2009). Nevertheless, a number of issues regarding Ca^{2+}-mediated astrocyte-dependent neurovascular coupling still need to be clarified before a quantitative contribution of astrocytes to neuroimaging signals can be ascertained. First, functional hyperemia occurs less than 2 sec after the onset of the stimulation, whereas astrocytic Ca^{2+} elevation is slower, typically delayed by more than 2–3 sec (Wang et al., 2006; Schummers et al., 2008). Based on this finding it was suggested that the astrocyte-Ca^{2+} response might be more important for sustaining the vasodilation during prolonged activation rather than as an initiating signal (Koehler et al., 2009), an argument that has recently found some experimental support in simultaneous fMRI and fiber-optic Ca^{2+} recordings in rat neocortex (Schulz et al., 2012). Second, and more importantly, neither spontaneous nor evoked $[Ca^{2+}]$i increases in astrocytes are affected by ionotropic glutamate receptor antagonists such us CNQX (6-cyano-7-nitroquinoxaline-2,3-dione) and APV [(2R)-amino-5-phosphonovaleric acid; Takano et al., 2006; Thrane et al., 2012]. This pharmacological manipulation, however, eliminates both post-synaptic electrophysiological activity and the coupled vascular response.

CONCLUDING REMARKS

Interactions between neuronal activity and CBF are largely compartmentalized. First, a functional compartmentalization that situates glutamatergic peri-synaptic activity and its electrophysiological events exists in close proximity to vascular coupling. Whether all glutamatergic synapses are equally suited for neurovascular coupling is an interesting yet unsolved question. In this direction, it is also important to acknowledge that heterogeneity in coupling mechanisms between different brain regions has already been reported and requires further attention. Second, the metabolic processes fueling peri-synaptic activity are partially segregated in glycolytic vs. oxidative compartments, with lactate production in response to increased neuronal activity as a key metabolite for energy supply, but also vascular coupling. A distinction between feed-back (metabolic) and feed-forward (signaling) mechanisms appears diffuse, since both mechanisms closely interact in the mediating biochemical pathways. An important issue to be clarified is whether a constant metabolic baseline and a constant neurovascular coupling efficiency can be assumed across brain states and synaptic plasticity. The quantitative value of neuroimaging signals may otherwise be affected by fluctuations in the reference baseline. Finally, a third level of segregation occurs at the cellular level, with astrocytic and neuronal compartments involved in vascular coupling through different but converging signaling pathways (NO, AA, adenosine, lactate/pyruvate ratio). Still, the actual relevance of astrocytes to neuroimaging signals needs to be clarified.

ACKNOWLEDGMENTS

The work is Santiago Canals lab is supported by grants of the Spanish Ministry of Science and Innovation BFU2009-09938 and PIM2010ERN-00679 (part of the coordinated ERA-Net NEURON project TRANSALC). Pierrick Jego has been supported by the "Symbad" Marie Curie ITN program and Feliberto de la Cruz was supported by a fellowship from CSIC-CITMA.

REFERENCES

Ames, A. III. (2000). CNS energy metabolism as related to function. *Brain Res. Brain Res. Rev.* 34, 42–68.

Ames, A. III, Wright, R. L., Kowada, M., Thurston, J. M., and Majno, G. (1968). Cerebral ischemia. II. The no-reflow phenomenon. *Am. J. Pathol.* 52, 437–453.

Attwell, D., Buchan, A. M., Charpak, S., Lauritzen, M., Macvicar, B. A., and Newman, E. A. (2010). Glial and neuronal control of brain blood flow. *Nature* 468, 232–243.

Attwell, D., and Laughlin, S. B. (2001). An energy budget for signaling in the grey matter of the brain. *J. Cereb. Blood Flow Metab.* 21, 1133–1145.

Behm, D. J., Ogbonna, A., Wu, C., Burns-Kurtis, C. L., and Douglas, S. A. (2009). Epoxyeicosatrienoic acids function as selective, endogenous antagonists of native thromboxane receptors: identification of a novel mechanism of vasodilation. *J. Pharmacol. Exp. Ther.* 328, 231–239.

Bernardinelli, Y., Magistretti, P. J., and Chatton, J. Y. (2004). Astrocytes generate Na+-mediated metabolic waves. *Proc. Natl. Acad. Sci. U.S.A.* 101, 14937–14942.

Bliss, T. V., and Lomo, T. (1973). Long-lasting potentiation of synaptic transmission in the dentate area of the anaesthetized rabbit following stimulation of the perforant path. *J. Physiol.* 232, 331–356.

Busija, D. W., Bari, F., Domoki, F., and Louis, T. (2007). Mechanisms involved in the cerebrovascular dilator effects of *N*-methyl-D-aspartate in cerebral cortex. *Brain Res. Rev.* 56, 89–100.

Canals, S., Beyerlein, M., Keller, A. L., Murayama, Y., and Logothetis, N. K. (2008). Magnetic resonance imaging of cortical connectivity in vivo. *Neuroimage* 40, 458–472.

Canals, S., Beyerlein, M., Merkle, H., and Logothetis, N. K. (2009). Functional MRI evidence for LTP-induced neural network reorganization. *Curr. Biol.* 19, 398–403.

Cauli, B., Tong, X. K., Rancillac, A., Serluca, N., Lambolez, B., Rossier, J., et al. (2004). Cortical GABA interneurons in neurovascular coupling: relays for subcortical vasoactive pathways. *J. Neurosci.* 24, 8940–8949.

Dachtler, J., Hardingham, N. R., Glazewski, S., Wright, N. F., Blain, E. J., and Fox, K. (2011). Experience-dependent plasticity acts via GluR1 and a novel neuronal nitric oxide synthase-dependent synaptic mechanism in adult cortex. *J. Neurosci.* 31, 11220–11230.

DeCostanzo, A. J., Voloshyna, I., Rosen, Z. B., Feinmark, S. J., and Siegelbaum, S. A. (2010). 12-Lipoxygenase regulates hippocampal long-term potentiation by modulating L-type Ca2+ channels. *J. Neurosci.* 30, 1822–1831.

Dunwiddie, T. V., and Masino, S. A. (2001). The role and regulation of adenosine in the central nervous system. *Annu. Rev. Neurosci.* 24, 31–55.

Erecinska, M., and Silver, I. A. (1994). Ions and energy in mammalian brain. *Prog. Neurobiol.* 43, 37–71.

Fox, P. T., and Raichle, M. E. (1986). Focal physiological uncoupling of cerebral blood flow and oxidative metabolism during somatosensory stimulation in human subjects. *Proc. Natl. Acad. Sci. U.S.A.* 83, 1140–1144.

Fredholm, B. B., Ap, I. J., Jacobson, K. A., Klotz, K. N., and Linden, J. (2001). International Union of Pharmacology. XXV. Nomenclature and classification of adenosine receptors. *Pharmacol. Rev.* 53, 527–552.

Gordon, G. R., Choi, H. B., Rungta, R. L., Ellis-Davies, G. C., and Macvicar, B. A. (2008). Brain metabolism dictates the polarity of astrocyte control over arterioles. *Nature* 456, 745–749.

Greene, R. W., and Haas, H. L. (1991). The electrophysiology of adenosine in the mammalian central nervous system. *Prog. Neurobiol.* 36, 329–341.

Hamadate, N., Yamaguchi, T., Sugawara, A., Tsujimatsu, A., Izumi, T., Yoshida, T., et al. (2011). Regulation of cerebral blood flow in the hippocampus by neuronal activation through the perforant path: relationship between hippocampal blood flow and neuronal plasticity. *Brain Res.* 1415, 1–7.

Hardingham, N., and Fox, K. (2006). The role of nitric oxide and GluR1 in presynaptic and postsynaptic components of neocortical potentiation. *J. Neurosci.* 26, 7395–7404.

Ido, Y., Chang, K., and Williamson, J. R. (2004). NADH augments blood flow in physiologically activated retina and visual cortex. *Proc. Natl. Acad. Sci. U.S.A.* 101, 653–658.

Ido, Y., Chang, K., Woolsey, T. A., and Williamson, J. R. (2001). NADH: sensor of blood flow need in brain, muscle, and other tissues. *FASEB J.* 15, 1419–1421.

Kasischke, K. A., Vishwasrao, H. D., Fisher, P. J., Zipfel, W. R., and Webb, W. W. (2004). Neural activity triggers neuronal oxidative metabolism followed by astrocytic glycolysis. *Science* 305, 99–103.

Ko, K. R., Ngai, A. C., and Winn, H. R. (1990). Role of adenosine in regulation of regional cerebral blood flow in sensory cortex. *Am . J. Physiol.* 259, H1703–H1708.

Kocharyan, A., Fernandes, P., Tong, X. K., Vaucher, E., and Hamel, E. (2008). Specific subtypes of cortical GABA interneurons contribute to the neurovascular coupling response to basal forebrain stimulation. *J. Cereb. Blood Flow Metab.* 28, 221–231.

Koehler, R. C., Gebremedhin, D., and Harder, D. R. (2006). Role of astrocytes in cerebrovascular regulation. *J. Appl. Physiol.* 100, 307–317.

Koehler, R. C., Roman, R. J., and Harder, D. R. (2009). Astrocytes and the regulation of cerebral blood flow. *Trends Neurosci.* 32, 160–169.

Laschet, J. J., Minier, F., Kurcewicz, I., Bureau, M. H., Trottier, S., Jeanneteau, F., et al. (2004). Glyceraldehyde-3-phosphate dehydrogenase is a GABAA receptor kinase linking glycolysis to neuronal inhibition. *J. Neurosci.* 24, 7614–7622.

Latini, S., and Pedata, F. (2001). Adenosine in the central nervous system: release mechanisms and extracellular concentrations. *J. Neurochem.* 79, 463–484.

Lauritzen, M., Mathiesen, C., Schaefer, K., and Thomsen, K. J. (2012). Neuronal inhibition and excitation, and the dichotomic control of brain hemodynamic and oxygen responses. *Neuroimage* 62, 1040–1050.

Li, J., and Iadecola, C. (1994). Nitric oxide and adenosine mediate vasodilation during functional activation in cerebellar cortex. *Neuropharmacology* 33, 1453–1461.

Lindauer, U., Leithner, C., Kaasch, H., Rohrer, B., Foddis, M., Fuchtemeier, M., et al. (2010). Neurovascular coupling in rat brain operates independent of hemoglobin deoxygenation. *J. Cereb. Blood Flow Metab.* 30, 757–768.

Lindauer, U., Megow, D., Matsuda, H., and Dirnagl, U. (1999). Nitric oxide: a modulator, but not a mediator, of neurovascular coupling in rat somatosensory cortex. *Am. J. Physiol.* 277, H799–H811.

Logothetis, N. K., Pauls, J., Augath, M., Trinath, T., and Oeltermann, A. (2001). Neurophysiological investigation of the basis of the fMRI signal. *Nature* 412, 150–157.

Magistretti, P. J., and Pellerin, L. (1999). Cellular mechanisms of brain energy metabolism and their relevance to functional brain imaging. *Philos. Trans. R. Soc. Lond. B Biol. Sci.* 354, 1155–1163.

Mathiesen, C., Caesar, K., Akgoren, N., and Lauritzen, M. (1998). Modification of activity-dependent increases of cerebral blood flow by excitatory synaptic activity and spikes in rat cerebellar cortex. *J. Physiol.* 512(Pt 2), 555–566.

Mathiesen, C., Caesar, K., and Lauritzen, M. (2000). Temporal coupling between neuronal activity and blood flow in rat cerebellar cortex as indicated by field potential analysis. *J. Physiol.* 523(Pt 1), 235–246.

Metea, M. R., and Newman, E. A. (2006). Glial cells dilate and constrict blood vessels: a mechanism of neurovascular coupling. *J. Neurosci.* 26, 2862–2870.

Mintun, M. A., Lundstrom, B. N., Snyder, A. Z., Vlassenko, A. G., Shulman, G. L., and Raichle, M. E. (2001). Blood flow and oxygen delivery to human brain during functional activity: theoretical modeling and experimental data. *Proc. Natl. Acad. Sci. U.S.A.* 98, 6859–6864.

Mintun, M. A., Vlassenko, A. G., Rundle, M. M., and Raichle, M. E. (2004). Increased lactate/pyruvate ratio augments blood flow in physiologically activated human brain. *Proc. Natl. Acad. Sci. U.S.A.* 101, 659–664.

Mosso, A. (1881). *Ueber den Kreislauf des Blutes im menschlichen Gehirn.* Leipzig: Veit.

Mulligan, S. J., and MacVicar, B. A. (2004). Calcium transients in astrocyte endfeet cause cerebrovascular constrictions. *Nature* 431, 195–199.

Ogawa, S., and Lee, T. M. (1990). Magnetic resonance imaging of blood vessels at high fields: in vivo and in vitro measurements and image simulation. *Magn. Reson. Med.* 16, 9–18.

Ogawa, S., Lee, T. M., Kay, A. R., and Tank, D. W. (1990). Brain magnetic resonance imaging with contrast dependent on blood oxygenation. *Proc. Natl. Acad. Sci. U.S.A.* 87, 9868–9872.

Pauling, L., and Coryell, C. D. (1936). The Magnetic properties and structure of hemoglobin, oxyhemoglobin and carbonmonoxyhemoglobin. *Proc. Natl. Acad. Sci. U.S.A.* 22, 210–216.

Paxinos, G., and Watson, C. (2007). *The Rat Brain in Stereotaxic Coordinates.* Amsterdam: Elsevier.

Pellerin, L., and Magistretti, P. J. (2004). Neuroenergetics: calling upon astrocytes to satisfy hungry neurons. *Neuroscientist* 10, 53–62.

Pelligrino, D. A., Vetri, F., and Xu, H. L. (2011). Purinergic mechanisms in gliovascular coupling. *Semin. Cell Dev. Biol* . 22, 229–236.

Perea, G., and Araque, A. (2005). Synaptic regulation of the astrocyte calcium signal. *J. Neural. Transm.* 112, 127–135.

Petzold, G. C., and Murthy, V. N. (2011). Role of astrocytes in neurovascular coupling. *Neuron* 71, 782–797.

Powers, W. J., Hirsch, I. B., and Cryer, P. E. (1996). Effect of stepped hypoglycemia on regional cerebral blood flow response to physiological brain activation. *Am. J. Physiol.* 270, H554–H559.

Raichle, M. E. (1998). Behind the scenes of functional brain imaging: a historical and physiological perspective. *Proc. Natl. Acad. Sci. U.S.A.* 95, 765–772.

Raichle, M. E., and Mintun, M. A. (2006). Brain work and brain imaging. *Annu. Rev. Neurosci.* 29, 449–476.

Ramón y Cajal, S. (1899). *Textura del sistema nervioso del hombre y de los vertebrados : estudios sobre el plan estructural y composición histológica de los centros nerviosos adicionados de consideraciones fisiológicas fundadas en los nuevos descubrimientos.* Madrid: N. Moya.

Roman, R. J. (2002). P-450 metabolites of arachidonic acid in the control of cardiovascular function. *Physiol. Rev.* 82, 131–185.

Roy, C. S., and Sherrington, C. S. (1890). On the regulation of the blood-supply of the brain. *J. Physiol.* 11, 85–158.

Schulz, K., Sydekum, E., Krueppel, R., Engelbrecht, C. J., Schlegel, F., Schroter, A., et al. (2012). Simultaneous BOLD fMRI and fiber-optic calcium recording in rat neocortex. *Nat. Methods* 9, 597–602.

Schuman, E. M., and Madison, D. V. (1991). A requirement for the intercellular messenger nitric oxide in long-term potentiation. *Science* 254, 1503–1506.

Schummers, J., Yu, H., and Sur, M. (2008). Tuned responses of astrocytes and their influence on hemodynamic signals in the visual cortex. *Science* 320, 1638–1643.

Shi, Y., Liu, X., Gebremedhin, D., Falck, J. R., Harder, D. R., and Koehler, R. C. (2008). Interaction of mechanisms involving epoxyeicosatrienoic acids, adenosine receptors, and metabotropic glutamate receptors in neurovascular coupling in rat whisker barrel cortex. *J. Cereb. Blood Flow Metab.* 28, 111–125.

Sokoloff, L., Reivich, M., Kennedy, C., Des Rosiers, M. H., Patlak, C. S., Pettigrew, K. D., et al. (1977). The [14C]deoxyglucose method for the measurement of local cerebral glucose utilization: theory, procedure, and normal values in the conscious and anesthetized albino rat. *J. Neurochem.* 28, 897–916.

Takano, T., Tian, G. F., Peng, W., Lou, N., Libionka, W., Han, X., et al. (2006). Astrocyte-mediated control of cerebral blood flow. *Nat. Neurosci.* 9, 260–267.

Thomsen, K., Offenhauser, N., and Lauritzen, M. (2004). Principal neuron spiking: neither necessary nor sufficient for cerebral blood flow in rat cerebellum. *J. Physiol.* 560, 181–189.

Thrane, A. S., Rangroo Thrane, V., Zeppenfeld, D., Lou, N., Xu, Q., Nagelhus, E. A., et al. (2012). General anesthesia selectively disrupts astrocyte calcium signaling in the awake mouse cortex. *Proc. Natl. Acad. Sci. U.S.A.* 109, 18974–18979.

Vlassenko, A. G., Rundle, M. M., Raichle, M. E., and Mintun, M. A. (2006). Regulation of blood flow in activated human brain by cytosolic NADH/NAD+ ratio. *Proc. Natl. Acad. Sci. U.S.A.* 103, 1964–1969.

von Pfostl, V., Li, J., Zaldivar, D., Goense, J., Zhang, X., Serr, N., et al. (2012). Effects of lactate on the early visual cortex of non-human primates, investigated by pharmaco-MRI and neurochemical analysis. *Neuroimage* 61, 98–105.

Wang, X., Lou, N., Xu, Q., Tian, G. F., Peng, W. G., Han, X., et al. (2006). Astrocytic Ca^{2+} signaling evoked by sensory stimulation in vivo. *Nat. Neurosci.* 9, 816–823.

Wang, X., Takano, T., and Nedergaard, M. (2009). Astrocytic calcium signaling: mechanism and implications for functional brain imaging. *Methods Mol. Biol.* 489, 93–109.

Wu, K., Aoki, C., Elste, A., Rogalski-Wilk, A. A., and Siekevitz, P. (1997). The synthesis of ATP by glycolytic enzymes in the postsynaptic density and the effect of endogenously generated nitric oxide. *Proc. Natl. Acad. Sci. U.S.A.* 94, 13273–13278.

Conflict of Interest Statement: The authors declare that the research was conducted in the absence of any commercial or financial relationships that could be construed as a potential conflict of interest.

Received: 14 February 2013; accepted: 13 March 2013; published online: 28 March 2013.

Citation: Moreno A, Jego P, de la Cruz F and Canals S (2013) Neurophysiological, metabolic and cellular compartments that drive neurovascular coupling and neuroimaging signals. Front. Neuroenergetics ***5****:3. doi: 10.3389/fnene.2013.00003*